Università degli studi di Roma “Tor Vergata”


Facoltà di Scienze Matematiche, Fisiche e Naturali

Dottorato di Ricerca in Astronomia

XIX ciclo (2003-2006)

# SELF-CONSISTENT DISTANCE SCALES FOR POPULATION II VARIABLES

*Marcella Di Criscienzo*

*Coordinator:*

PROF. R. BUONANNO

*Supervisors:*

PROF. R. BUONANNO

PROF.SSA F. CAPUTO

DOTT.SSA M. MARCONI

*Vedere il mondo in un granello di sabbia*
*e il cielo in un fiore di campo*
*tenere l'infinito nel palmo della tua mano*
*e l'eternitá in un ora.*

(William Blake)

Dedico questa tesi a:

Mamma e Papá

Sarocchia

Giuliana

Marcella & Vincenzo

Massimo

Filippina Caputo

Massimo Capaccioli

Roberto Buonanno

che mi aiutarono a trovare la strada,

e a Tommaso

che su questa strada ha viaggiato con me

per quasi tutto il tempo

# Contents

# List of Figures

# List of Tables

# The scientific project

My PhD thesis is a part of a larger project, dealing with GRAPES (GRoup for Advancement of Pulsation and Evolution Studies) operating since 1995 and involving several researchers around the world and with the main scope to make homogenous studies on pulsating variable stars from both pulsation and evolution points of view. Note that in the previous decades these two theories have been developed independently and frequently using different and not updated physical parameters. In particular, my research activity has been mainly devoted to the study of Population II variables in globular clusters and similar metal-poor stellar fields.

Radially pulsating stars, whether they are Population I or Population II stars, are of great relevance in several fields of modern astrophysics. In particular, RR Lyrae variables are widely used, via the calibration of their absolute visual magnitude $M_V(RR)$ in terms of the iron-to-hydrogen content [Fe/H], as standard candles for distance determination in the Local Group. On the other hand, since the absolute magnitude of the globular cluster main-sequence turnoff is the classical "clock" to estimate the age of these ancient stellar systems, one easily understands the relevance of an accurate RR Lyrae distance scale for cosmological studies.

On the basis of updated nonlinear pulsation models including a nonlocal time-dependent treatment of convection, I have produced a new theoretical scenario for RR Lyrae stars with different chemical composition, typical of Galactic globular clusters ($0.0001 < Z < 0.006$). All the computed models have been trasformed both in the Johnson-Cousins and in the sloan photometric bands, and relevant relations connecting pulsation observables, such as the period and the amplitude of the oscillation, to the intrinsic stellar parameters have been derived and applied to the Galactic globular cluster samples. The dependence of theoretical predictions on the adopted efficiency of convection has also been investi-

gated in detail.

The same nonlinear convective code used for RR Lyrae stars has been extended to Population II Cepheids (BL Herculis stars in particular) and combined with an updated evolutionary scenario to obtain syntietic models of this class of stars; in particular, pulsational relations providing distance estimates for those globular clusters which have a blue HB and, as a consequence, very small number of RR Lyrae are observed. It is worth mentioning that a comparison between the distances obtained for RR Lyrae stars and the ones for Population II variables has shown a good agreement, supporting, in such a way, the reliability of the adopted theoretical scenario.

Moreover, RR Lyrae distances have been used to calibrate a secondary distance indicator, *i.e.* the Globular Cluster Luminosity Function (GCLF) in external galaxies. I have used various calibrations of the $M_V(RR)$-[Fe/H] relation (including the theoretical one based on the pulsation models) and several globular cluster samples to calculated the turnover magnitude of the Galactic GCLF, which is the first step to use this method. The application to external galaxies has shown that the turnover magnitude of metal poor clusters is in excellent agreement with the value of both Galactic and M31 ones, as inferred by an RR Lyrae distance scale referenced to the same LMC fiducial distance.

The thesis is organized as follows:

- in **chapter 1** the observational properties of Population II variables belonging to globular clusters and similar metal poor field, are described;
- in **chapter 2** I give same remarks on pulsation theory and I describe shortly, the non linear and convective hydrodynamical code used to obtain pulsational models of Population II variables;
- in **chapter 3** I describe the new models of RR Lyrae stars and BL Herculis computed during the last three years and the derived relations connecting pulsation observables and intrinsic stellar parameters are presented;
- in **chapter 4** I compare pulsational models with observations of similar variables observed in Galactic globular clusters. Different methods, based on the calculated relations are derived, to obtain individual distance moduli of these type of stars. A comparison between the distances calculated with RR Lyrae and Population II

Cepheids is performed in order to demonstrate the self-consistency of the adopted theoretical scenario.

- Finally, in **chapter 5** I present the results obtained calibrating the Globular Cluster Luminosity Function on RR Lyrae stars;

- a small chapter containing the summary of principal results, close this work.

Refereed publications accepted and submitted during this PhD project.

1. Marconi, M., Caputo, F., **Di Criscienzo, M.**, Castellani, M.
   RR Lyrae Stars in Galactic Globular Clusters. II. A Theoretical Approach to Variables in M3
   2003, ApJ, 596.

2. Ripepi, V., Monelli, M., dall'Ora, M., Bono, G., Corsi, C., Caputo, F., Pulone, L., Testa, V., Andreuzzi, G., Buonanno, R., Marconi, G., Marconi, M., **Di Criscienzo, M.**, Storm, J., degl'Innocenti, S.
   UBVI Time-series Photometry of the Old LMC Globular Cluster Reticulum
   2004, CoAst, 145, 24

3. **Di Criscienzo, M.**, Marconi, M., Caputo, F.
   RR Lyrae Stars in Galactic Globular Clusters. III. Pulsational Predictions for Metal Content Z=0.0001 to Z=0.006
   2004, ApJ,612.

4. Marconi, M., Cignoni, M.,**Di Criscienzo, M.**; Castelli, F., Ripepi, V., Musella, I., Ruoppo, A.,
   Predicted properties of RR Lyrae stars in the SDSS photometric system
   2006, MNRAS, 371, 1503

5. **Di Criscienzo, M.**, Marconi, M., Musella, I., Caputo, F.
   RR Lyrae besed calibration of Globular Cluster Luminosity Function
   2006, MNRAS, 365,1357

6. Marconi, M. & **Di Criscienzo, M.**
   Updated pulsational models of BL Herculis stars
   A&A, in press (astro-ph/0701256)

7. **Di Criscienzo, M.**, Caputo, F., Marconi, M., Cassisi, S.
   Synthetic properties of bright metal-poor variables. II BL Her stars
   A&A, submitted.

8. Bono, G., Caputo,F., **Di Criscienzo, M.**
   RR Lyrae stars in Galactic globular clusters. VI. The Period-Amplitude relation
   MNRAS, submitted

9. Ripepi, V., Greco, C., Clementini, G.,**Di Criscienzo, M.**, Dall'Ora, M., Marconi, M., Musella, I.
   Discovery of new variable stars in Globular Cluster NGC 2419
   in advanced state of preparation.

# 1

# Population II variables

When we look up at the night sky, it is easy to imagine that the stars are unchanging. Apart from twinkling due to the effects of our atmosphere, stars appear fixed and constant to the untrained eye. Careful observations, some even done with the naked eye, show that some stars do in fact appear to change in brightness over time. Some exhibit periodic behaviour, brightening quickly then diminishing in brightness slowly only to repeat themselves. Some of these changes take place over several days while others occur in a matter of hours or many months. Other stars exhibit a once-off dramatic change in brightness by orders of magnitude before fading away to obscurity. All of these are examples of what are termed "variable" stars. A variable star is simply one whose brightness (or other physical property such as radius or spectral type) changes over time. In this context pulsating variables are of extremly importance.

Pulsating variable stars are intrinsic variables as their variation in brightness is due to a physical change within the star. In the case of pulsating variables this is due to the periodic expansion and contraction of the surface layers of the stars. This means that the star actually increases and decreases in size periodically. The different types of pulsating variables are distinguished by their periods of pulsation and the shapes of their light curves. These properties, in turn, are a function of the mass and evolutionary stage of a given star. SX Phoenicis (SX Phoe), $\delta$ Scuti, RR Lyrae, BL Herculis (BL Her), Anomalous Cepheids

***Table 1.1:*** *Main properties of pulsating stars.*

| type | P (days) | Mv (mag) | Av (mag) | Spectral Type | Population Type | Evolutionary Phase |
|---|---|---|---|---|---|---|
| SX Phoe | $\leq 0.1$ | 2-3 | $\leq 0.5$ | A-F | II | Main Sequence (MS) |
| $\delta$ Scuti | $\leq$0.5 | 2-3 | $\leq$1.5 | A-F | I | MS |
| RR Lyrae | 0.3-1 | $0.0 - 1$ | $\leq$2 | A2-F2 | II | Horizontal Branch (HB) |
| BL Her | 1-10 | $-$1-0 | $\leq$1.5 | F2-G6 | II | post-HB |
| AC | 0.3-2 | $-$2-0 | $\leq$1.5 | A-F | ? | massive HB |
| W Vir | 10-50 | $-3$ - $-1$ | $\leq$1.5 | F2-G6 | II | post-HB |
| CC | 1-100 | $-7$ - 2 | $\leq$1.5 | F6-K2 | I | blue loop |

(AC), W Virginis (W Vir), Classical Chepheids (CC) are examples of the large variety of different pulsating stars that are nowadays observed and studied. The variable classes have typical pulsation periods, magnitudes, spectral types and evolutionary state (see Table 1.1) and they are located in well-defined regions of Color-Magnitude diagram (CMD) called Instability Strip (IS, see Fig. 1.1). All these stars are thought to owe their instability to a common physical mechanism (partial ionizated zone in the envelope); the details are discussed in the next chapter.

The study of pulsating variables is of great importance to astronomers. In fact, the analysis of light curves provides vital information about the interior processes in stars. In particular, Population II variable stars (RR Lyrae, BL Her, W Vir and AC) play a major role in our understanding of the properties of old stellar populations as well as in the definition of the cosmic distance scale. Among them, RR Lyrae stars are definitively the most abundant and the ones currently used as tracers of the dynamical and chemical properties of old stellar populations and as standard candles to establish the globular cluster distance scale (see e.g. Cacciari & Clementini 2003). Moreover they can be adopted to calibrate secondary distance indicators such as the globular cluster luminosity function (see e.g. Di Criscienzo et al. 2006).

In the next, I will focuse my attention on RR Lyrae stars and Population II Cepheids because these stars are the argument of this PhD work. In this chapter, I will remind to the reader the main properties of these stars giving particular attention to those belonging to globular clusters.

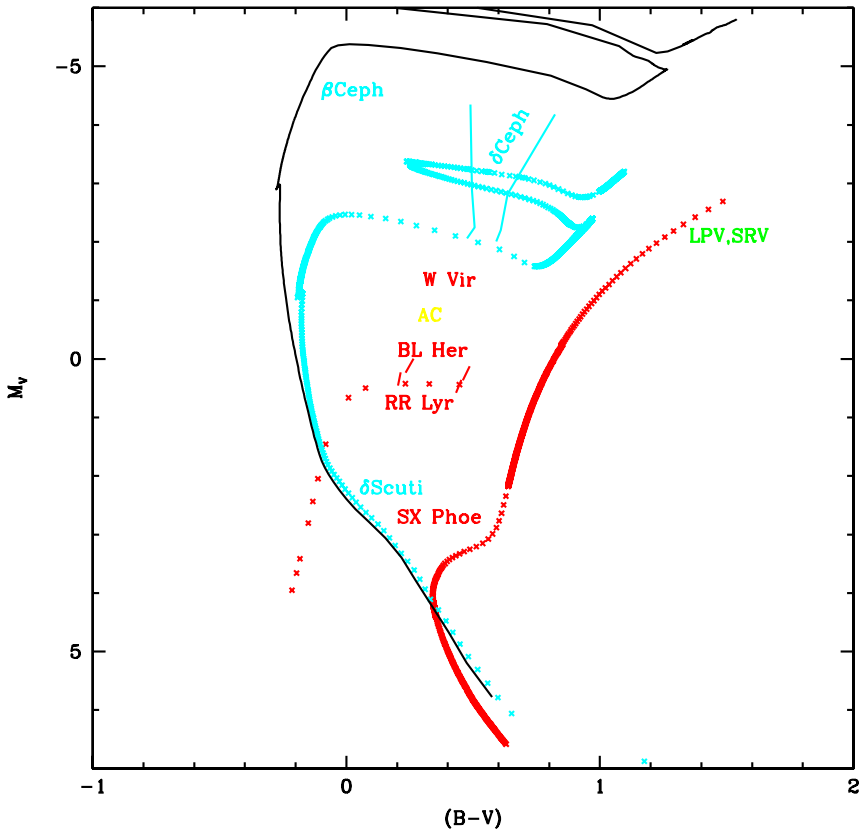


***Figure 1.1:*** *Position in Color-Magnitude diagram of different type of radial pulsating variables.*

## 1.1 RR Lyrae stars

The study of RR Lyrae stars is a century old. In the closing decade of nineteenth century, as astronomers subjected the globular clusters (GC) to increasingly close scrutiny, they discovered the first of the short period variable stars today known as RR Lyrae stars. In the course of the last hundred years, the number of the RR Lyraes has increased so much that, in representative, they outnumber known members of any other well defined class of variable. Directly or indirectly, investigations of RR Lyrae stars have contributed to almost every branch of modern astronomy:

1. RR Lyrae stars have been used as tracers of the chemical and dynamical properties of old stellar populations within our and nearby galaxies;

2. RR Lyrae have been used as standard candles, indicating the distances to globular clusters, to the center of Galaxy and to neighboring Local Group systems; moreover

***Table 1.2:*** *Main physical properties of RR Lyrae stars (Smith, 1985)*

| | |
|---|---|
| Pulsation period | P=0.2-0.85 days |
| Mean V magnitude | $< M_V >$=0.6 $\pm$ 0.2 mag |
| Mean effective temperature | $< T_{eff} >$=6000$-$7400 K |
| Mean gravity | <log g>=2.5 - 3.0 |
| Metallicity | [Fe/H]=0.0 - $-$2.5 dex |
| Mass | M=0.6 - 0.8 $M_\odot$ |
| Radius | R=4 - 6 $R_\odot$ |
| Luminosity | L=40 $L_\odot$ |

they can be adopted to calibrate secondary distance indicators such as the globular cluster luminosity function;

3. RR Lyrae stars have served as test objects for understanding theories of the evolution of low mass stars including the radial pulsation phase.

In recent years, the great technological progress, which has allowed to observe these stars in farther and farther far stellar system, have helped to make the study of RR Lyrae stars a particularly active field and one which seems likely to continue to grow in the next future. In this context, this thesis helps to give some light on problems, both from the theroretical and the empirical point of view, which still afflict this research theme.

### 1.1.1 Observational properties

The most relevant properties of RR Lyrae stars are reported in Table 1.2.
Bailey in his paper on $\omega$ Cen (1902) divided these stars (at that time called "cluster type variables") into two classes: types ab stars (RR$_{ab}$) characterized by "saw-tooth" light curves with steep rise and less steep decline and types c stars (RR$_c$) which have almost sinusoidal light curve variations. These two classes occupy two separate portions of the amplitude-period diagram (the so called Bayley diagram), as one can see in the upper panel of Fig. 1.2, where RR$_{ab}$ have amplitudes which decrease when the period increases and the RR$_c$ have smaller and non correlated period and amplitude. The theory of pulsation (see next chapter) has identified these two classes with two different pulsational modes: RR$_{ab}$ pulsate in the fundamenal mode, while RR$_c$ stars are first overtone pulsators.

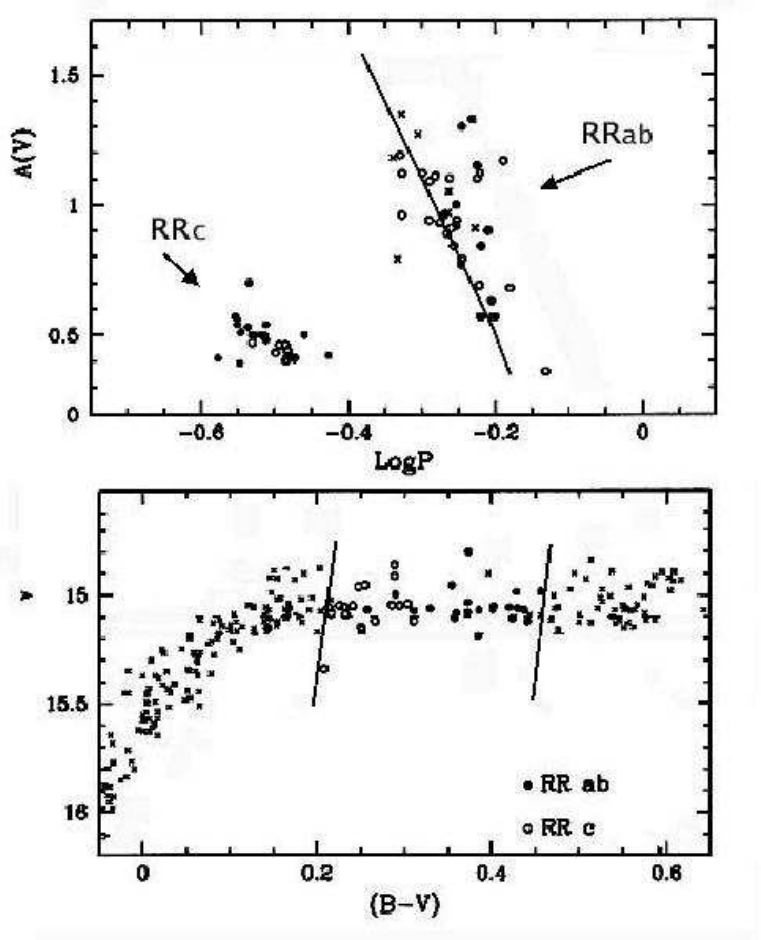


***Figure 1.2:*** *Upper panel: Bailey's diagram for the RR Lyrae stars in M15. Lower panel: the same stars in the CM diagram. Filled and open circles depict $RR_{ab}$ and $RR_c$ stars respectively. The two solid lines display the predicted edges of the IS, which hosts RR Lyrae stars. Figure from Caputo et al. (1999)*

Talking about the metallicity of RR Lyrae stars, as one can see in Table 1.2, this type of stars shows a wide range of chemical compositions, particulary in the photospheric abudances of the elements heavier than helium. These large spread in metal abundance depends on the enviroment in which we observe these stars. The RR Lyrae found in the Galactic halo can be very deficent in heavy elements and usually have $-1 \geq$ [Fe/H] $\geq -2.5$. Many RR Lyrae stars belonging to the old disk population of the Galaxy and some (but not all) of those found in the Galactic bulge are only modestly deficent in metals relative the Sun. Some may be as metal-rich as the the Sun and others perhaps even supermetallic.

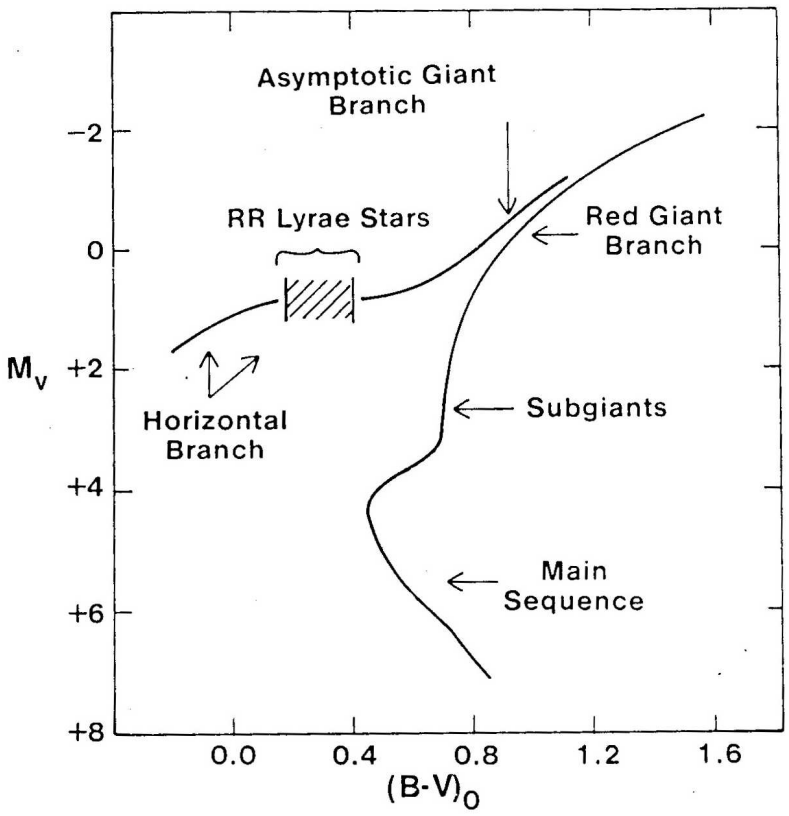


***Figure 1.3:*** *A schematic CMD for a typical globular cluster. The principal sequences are labelled. RR Lyrae stars are HB stars which happen to be located where the instability strip intersects the horizontal branch.*

### 1.1.2 Evolutionary properties

RR Lyrae are low-mass stars in the core helium burning stage of their evolution. This places them on the horizontal branch in the HR diagram (see Fig.1.3). As just stressed, not all HB stars are RR lyrae stars but only those within a well defined instability strip are pulsationally unstable. At the level of the HB, at luminosity near 40 $L_{\odot}$, the blue (BE) and the red edge (RE) of the instabilty strip lie near (B-V)$\sim$0.18 and 0.40 mag , respectively, which correspond to effective temperature of about 7400 K and 6000 K.

The evolution of low mass stars has been reviewed many times (Iben 1971, Renzini 1977, Castellani 1985; Caputo 1985) and only a brief sketch is needed here. A typical RR Lyrae star is thought to begin as a main sequence star with mass near 0.8 $M_{\odot}$. The exact evolutionary course is dependent upon its chemical composition, and perhaps upon other properties as well.

Like other low mass stars, the progenitors of RR Lyrae stars spend most of their energy-

producing lifetime on the main sequence, fusing hydrogen to helium in its core. After a long period of time, about 10 Gyr, hydrogen is exhausted in the core and the star climbs the red giant branch, burning hydrogen to helium in a shell surronding a helium core. Temperatures in the helium core are not yet high enough for fusion of helium core atoms to form still heavier elements, and the inert core collapses, becoming electron degenerate. At the tip of the red giant branch the core temperature becomes high enought to initiate helium fusion. In a so called "helium flash" phenomenon, helium burning is ignited in the electron degenerate core via the triple $\alpha$ process. This removes the core degeneracy and the star proceeds to the zero-age horiontal branch (ZAHB) and the core helium burning stage. It is in this evolutionary phase that, if the star falls within the bounds of the instability strip in the HR diagram, it pulsates as an RR Lyrae star. RR Lyrae are giant stars at this point, with a radius 4-6 times that of the Sun, but both their radii and luminosities are much reduced from what they were at the tip of the red giant branch.

The location of a star on the ZAHB depends (at least) on its total mass, core mass, and chemical composition. Stars in a single globular cluster are believed to have all started out on the main sequence with closely similar chemical compositions. Moreover, when they reach the ZAHB they are also expected to have similar core masses. Thus, in a canonical evolutionary theory, the color sequence along the horizontal branch implies a mass sequence among the horizontal branch stars. Because the horizontal branch lifetime is short compared to the age of the cluster, stars which are found at any one time on the horizontal branch are believed to have had nearly identical main sequence masses. Thus the spread in color among horizontal branch stars implied that different horizontal branch stars have experienced different amounts of mass loss before reaching the ZAHB, with losses of 0.1 $M_{\odot}$ being typical.

After about $10^8$ years, the central helium is depleted. As the core helium exhaustion approches, the star leaves the HB, it swells and cools once again, ascending the asymptotic red giant (AGB) branch and deriving energy from a hydrogen burning shell and a helium burning shell. Then approaching the Hayashi track the star loses all its envelope during the Thermal Pulsing phase and crosses the CMD towards high temperatures to start its cooling phase as a white dwarf.

### 1.1.3 RR Lyrae as standard candles

Today is well known that the absolute magnitude of RR Lyrae stars depends in first approximation by metallicity. Usually, V band luminosity is calibrated as a linear function of the metallicity [Fe/H]:

$$M_V(RR) = a + b[Fe/H] \tag{1.1}$$

This relation is very important because, if we know the metallicity, we can determine the absolute magnitude. Unfortunatly, no general agrement has still been reached both on the slope and on the zero point of this relation. Indeed, recent evaluations for $a$ cover an interval of about 0.3 mag, while the values of the slope $b$ range from $\sim$ 0.13 to 0.30 dex$^{-1}$ (see Cacciari & Clementini, 2003 and Section 5.1 for an outline of the most recent calibrations).Moreover and even more importantly, theoretical calibrations of relation 1.1 supply magnitudes that are systematically brighter than empirical calibrations, revealing the existence of poorly-known systematic effect.
For the sake of the following discussion, here I briefly summarize the basic ingredients which are needed for a reliable "theoretical route":

1. trustworthy HB models computed with the most recent updating of the relevant physics;

2. synthetic HB simulations (SHB) in order to estimate the evolutionary effects and the role of different HB populations;n

3. realistic bolometric corrections and color-temperature transformations;

4. appropriate scaling between the metallicity $Z$ and the iron-to-hydrogen content [Fe/H].

Such a "shopping list" should help the common reader to understand the main reasons for the rather different theoretical predictions on the $M_V$(RR)-[Fe/H] relation, as presented in the recent literature (see Caputo et al. 2000 and references therein).
It is known that, due to somehow different input physics, current updated HB models still provide slightly different luminosity values (see, e.g., Castellani 2003). Moreover, different bolometric corrections, as well as different assumptions concerning the value of

the overabundance of $\alpha$-elements with respect to iron, are used by the various researchers. Furthermore, in order to account for the luminosity of actual (evolved) pulsators, the zero age horizontal branch (ZAHB) luminosity at the RR Lyrae instability strip is artificially increased, by a fixed quantity or as a function of metallicity, instead of making use of SHB results.

Eventually, we notice that as evidenced in Castellani, Chieffi & Pulone (1992), Caputo et al. (2000) and Bono et al. (2005), the $M_V$-[Fe/H] relation is not strictly linear, but there is a change of slope at [Fe/H] $\sim -1.5$. A quadratic curve seems to be more appropriate to fit the data.

### 1.1.4 RR Lyrae in Globular Clusters

Since 1900 the number of RR Lyrae stars known to belong to globular clusters is exceeded by the number of known field representatives of that species, nevertheless the globular cluster RR Lyrae stars continue to play a vital role in the study of stellar variability. This is due, not only as the convenience of observations (many cluster RR Lyraes can be recorded on a single CCD frame) but also to the fact that RR Lyrae within any single globular cluster display a unique homogenity. In fact the stars within any given globular cluster can be regarded as essentially coeval and, except for the anomalous cluster $\omega$ Centauri, they appear to share a common value of [Fe/H]. These circumstances have helped to make globular clusters particularly important testing grounds for the theory of evolution of low mass stars.

Before proceeding I want to remember the reader that a recent summary of RR Lyrae in globular clusters has been given by Clement et al. (2001). Their survey of the literature reveled that the total number of recognized RR Lyrae stars is $\sim$ 1800. The number of RR Lyrae stars differs widely from one cluster to another. In NGC 5272 (M3) 260 RR Lyrae are known (Contreras et al. 2005), whereas in a number of other well-searched clusters no RR Lyrae stars have been found. The number of RR Lyrae stars known in a globular cluster is not always a good indicator of how likely it is that an evolved star in that cluster becomes a RR Lyrae. That is because there is a considerable range in the total number of evolved stars among the globular clusters. Following Kukarkin (1973), Suntzeff et al. 1991 normalized the observed number of RR Lyrae star by total cluster luminosity, de-

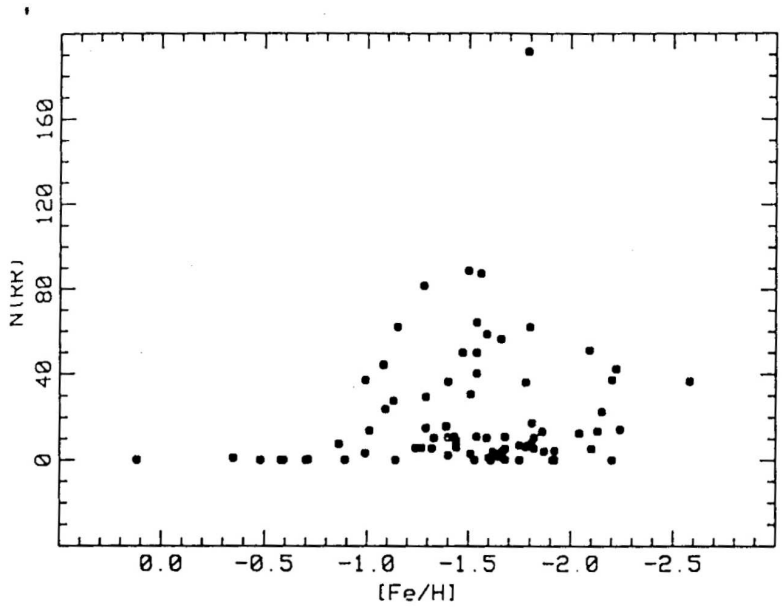


***Figure 1.4:*** *N(RR), as indicator of richness in RR Lyrae stars, is plotted against [Fe/H] for globular clusters of the Galaxy (Stuntzeff et al. 1991).*

riving the quantity N(RR), the number of RR Lyrae stars which a globular cluster would have if it were a cluster with $M_V$=−7.5 mag.

A plot of N(RR) versus [Fe/H] is shown in Fig. 1.4. Note that the value of N(RR) is small for metal rich cluster and lower again for the most metal deficient ones. Note also that, below [Fe/H]=-0.8, clusters of the same [Fe/H] may have different values of N(RR). The broad trend of Fig. 1.4 is explicable in terms of the correlation of metallicity with the horizontal branch type, the so called first parameter governing the distribution of stars on the HB. Metal rich clusters have horizontal branches which lie to the red side of the instability strip in the CMD; as a consequence N(RR) is near zero for these clusters. As one proceeds to metal poor clusters, the distribution of stars on the horizontal branch becomes bluer, populating the instability strip with RR Lyrae and increasing the value of N(RR). For the most metal deficient cluster, the horizontal branch stars lie mainly to the blue side of the instability strip, and the value of N(RR) decreases again.

But it is clear from Fig. 1.4 that such correlation of N(RR) with metallicity cannot be the whole story. At the same value of [Fe/H] there can be a wide range in observed values of N(RR). Sandage and Wildey (1967) and van den Berg (1967) were among the first to

point out that the HB morphology is not a function of the [Fe/H] value alone and that different globular clusters can have horizontal branches with very different color distributions. This is the so called **second parameter problem**. At least one further parameter, besides [Fe/H], determines the HB morphology, but there is no consensus on what actually the second parameter is. The helium abundance, the relative abundance of CNO elements whith respect to iron, stellar rotation and age have all been suggested but today is not clear yet which is the most important one.

Another debated problem concerning the RR Lyrae in globular clusters, is the so called **Oosterhoff dichotomy**.

In 1939, Oosterhoff drew attention to a dichotomy of properties for the RR Lyrae in a sample of five Galactic GC. Three of these clusters ($\omega$ Cen, M15 and M53) had mean periods, $< P_{ab} >$, near 0.64 days for their RR$_{ab}$ variables and for these clusters RR$_c$ variables accounted for more than 40 percent of the total of known RR Lyraes. In contrast, the other two clusters (M3 and M5) had ab-type RR Lyraes with a mean period near 0.55 days and in these cluster RR$_c$ variables made up less than 20 percent of the total RR Lyrae population. Subsequent analysis soon confirmed the dichotomy and now, clusters like M3 are called Oosterhoff I-type (OoI) while clusters as M15 are Oosterhoff II-type (OoII). These works have also highlighted that OoI and OoII GGCs show also a dichotomy in the metal content, having OoI clusters a metallicty higher than OoII. The dichotomy in the mean periods of ab pulsators has been explained with a difference in luminosities: indeed, from the equation of pulsation($P\rho^{1/2} = Q$), longer periods imply higher luminosity, the other parameter being fixed. This explanation is known as the Sandage's "period shift effect" (Sandage 1990). The main problem with this interpretation is that it is at odds with some predictions of evolutionary theories and with chemical enrichment models: indeed, to have higher luminosities, OoII clusters should have higher helium abundance than OoI clusters, therefore showing an anticorrelation between helium and metals (Gratton, Tornambé & Ortolani 1986).

Another explanation was proposed by Van Albada & Baker (1973) and supported by Caputo et al. 1982. These authors assumed the existence of a hysteresis mechanism in the IS, with the mode of pulsations in the H zone* (see Fig. 1.5) depending on the evolu-

*As you can see in detail in the Chapter 3, the outer edges of IS are FO-blu edge on the hot side and F-red edge on the cool side, while the F-IS and FO-IS intersect in a zone (H zone) where both the two

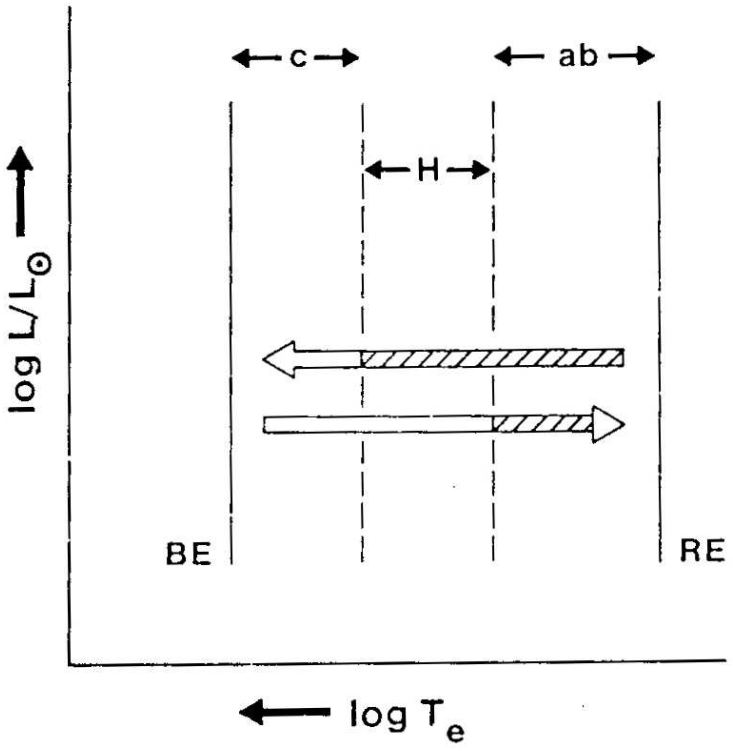


***Figure 1.5:*** *Van Albada and Beker's (1973) proposed mechanism to explain the Oosterhoff mechanism (see text).*

tionary path in the IS. In this model, $RR_{ab}$ stars that enter the H zone from the red side, save their pulsation mode until they reach the FBE; conversly, $RR_c$ stars that enter the H zone from the blue side keep the pulsating first overtone mode until they reach the FORE. Therefore, if the H zone is populated mainly by $RR_{ab}$ stars, and since the period is a strong function of the temperature, $< Pab >$ will be shorter and the cluster will be an OoI type; on the other hand, if the OR zone is populated mainly by $RR_c$ stars, $< Pab >$ will be longer and the cluster will be an OoII type. At the present time, the Oosterhoff dichotomy seems to be a phenomenon connected only with the Galaxy, since other galaxies in the Local Group show intermediate properties between the two Oosterhoff types (as in dwarf spheroidals, Mateo 1998; Dall'Ora et al. 2003), or a continuum in the RR Lyrae pulsation properties as in the Large Magellanic Cloud (Smith 1995 and reference therein).

pulsation mode are possible.

## 1.2 Population II Cepheids

### 1.2.1 Present status of knowledge

Other classes of radial pulsators are actually observed in globular clusters and similar metal-poor stellar fields. In the current nomenclature, they are named Population II Cepheids (P2Cs) and Anomalous Cepheids (ACs): the former ones, with periods $P$ from $\sim 1$ to $\sim 25$ days, are observed in Globular Clusters with few RR Lyrae stars and blue HB, while the latters, with $\sim 0.3 \leq$ P $\leq \sim 2$ days, are observed in the majority of the Local Group dwarf galaxies which have been surveyed for variable stars. These two classes are both brighter but either less massive (P2Cs) or more massive (ACs) than RR Lyrae stars with similar metal content.

Marconi, Fiorentino & Caputo (2004), Caputo et al. (2004) and Fiorentino et al. (2006) have discussed the pulsation and evolution properties of ACs and they have showed that they originate from $Z \leq 0.0004$ central He-burning models more massive than $\sim 1.3\ M_{\odot}$ which evolve through the pulsation region at luminosity and effective temperature which increase, on average, as the mass increases. Given the basic equation for radial pulsation, the effect of the higher luminosity is in part balanced by the larger mass and temperature and consequently these bright variables show periods that are not significantly longer than those typical of RR Lyrae stars.

As for the P2Cs, which are often separated into BL Her stars ($\log P < 1$) and W Vir stars ($\log P > 1$), previous investigations (see, e.g., Gingold 1985; Bono et al. 1997a; Caputo 1998; Wallerstein & Cox 1984; Harris 1985; Wallerstein 1990, 2002) have already suggested that they originate from hot, low-mass stellar structures which started the main central He-burning phase in the blue side of the RR Lyrae gap and now evolve toward the Asymptotic Giant Branch crossing the pulsation region with the luminosity and the effective temperature that increases and decreases, respectively, with decreasing the mass: for this reason, these bright low-mass pulsators should reach periods of several days.

On the observational side, Nemec, Nemec & Lutz (1994) derived metal dependent Period-Luminosity ($PL$) relations in various photometric bands, suggesting that observed P2Cs pulsate either in the fundamental and in the first-overtone mode and that the slopes of the $PL$ relations are significantly different for the two modes. On the other hand, on the

basis of a sample of P2Cs identified in the OGLE-II variable star catalogue for the Galactic bulge fields, Kubiack & Udalsky (2003) found that all the observed stars, which have periods from $\sim$ 0.7 to about 10 days, follow the same $PL$ relation. Similar results are derived by Pritzl et al. (2003) and Matsunaga et al. (2006) for P2Cs in Galactic globular clusters. Furthermore, these last two investigations support the hypothesis that the same $PL$ relation holds for BL Her and W Vir stars, without an increasing in the slope for periods longer than $P \sim 10$ days, as earlier suggested by McNamara (1995).

From the theoretical point of view, the pulsation models by Buchler & Moskalik (1992) and Buchler & Buchler (1994), as based on a linear and nonlinear radiative analysis, showed that the blue edge for first-overtone pulsation was very close ($\leq$ 100 K) to the fundamental one, producing a very narrow region of FO-only pulsation. More recently, Bono, Caputo & Santolamazza (1997) computed nonlinear convective models, finding a good agreement between the predicted and the observed boundaries of the P2C instability strip and suggesting that the observed variables are pulsating in the fundamental mode with a typical mass of $\sim$ 0.52-0.59$M_{\odot}$. However, the Bono, Caputo & Santolamazza (1997) nonlinear convective models, although able to provide reliable information also on the red edge of pulsation region, were limited to a quite restricted range of stellar parameters and adopted an old input physics (see Bono & Stellingwerf 1994 for details). For this reason, following our program dealing with a homogeneous study of the radially pulsating stars with various chemical composition, mass and luminosity, in the present work I will discuss the results of updated pulsation models with mass 0.50-0.65$M_{\odot}$ and luminosity $\log L/L_{\odot}$ =1.81-2.41 in order to build a sound theoretical scenario for the analysis of the P2Cs. In particular, I will derive the predicted relations connecting evolutionary and pulsation properties for BL Her stars (section 3.2) and I will verify their use as distance indicators (Section 4.2).

# 2

# Some remarks on the pulsation theory and the computational methods

*Till now I have focused my attention on observational properties of Population II variables and RR Lyrae in particular. I have also marked the main characteristics of the variables belonging to globular clusters and to other silmilar metal-poor fields. Because one of the main gols of this work is to study these stars from the theoretical point of view, this chapter is thought to give the reader some remarks on pulsation theory. I will also describe shortly the non linear and convective pulsational code used to perform this type of investigation.*

## 2.1 The pulsation cycle: observations

The variation in luminosity of a pulsating star is affected by changes both in radius (R) and in effective temperature ($T_e$). Fig. 2.1 shows that the light amplitude of a pulsating star is a strong function of wavelenght. The star is bluer at the phase of maximum luminosity than at the minimum and the amplitude in B (at about 4400 A) exceeds that in V (about 5500 A ), while both the B and V amplitudes are much higher than the near infrared one (typical in the K band about 2.2 $\mu$m). This dependency can be understood if the star is considered

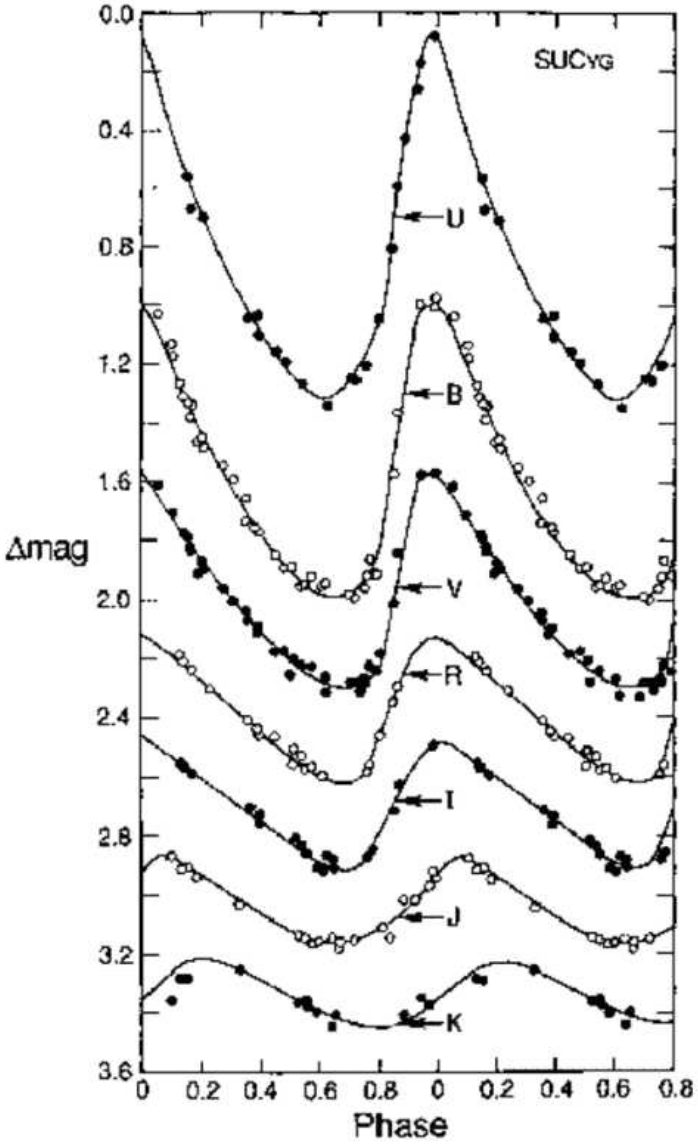


***Figure 2.1:*** *A typical light-curve of a pulsating stars in various photometric bands*

as a blackbody radiator. Visible wavelenghts fall near the peak of the Planck function for a radial pulsator as a consequence visible (as well as bolometric) fluxes scales as $R^2Te^4$. On the other hand the K passband lies on the Raleight-Jeans tail of the Planck function and the K-band flux scales as $R^2T_e^{1.6}$. As a consequence of these scaling relations, the luminosity changes in B and V filters mainly reflect the changes in effective temperature of the star during the pulsatin cycle, whereas the near infrared magnitude variation is more dependent upon the changes in radius.

As shown in Fig.2.2, the pulsation of a pulsating variable star induces a periodic variation

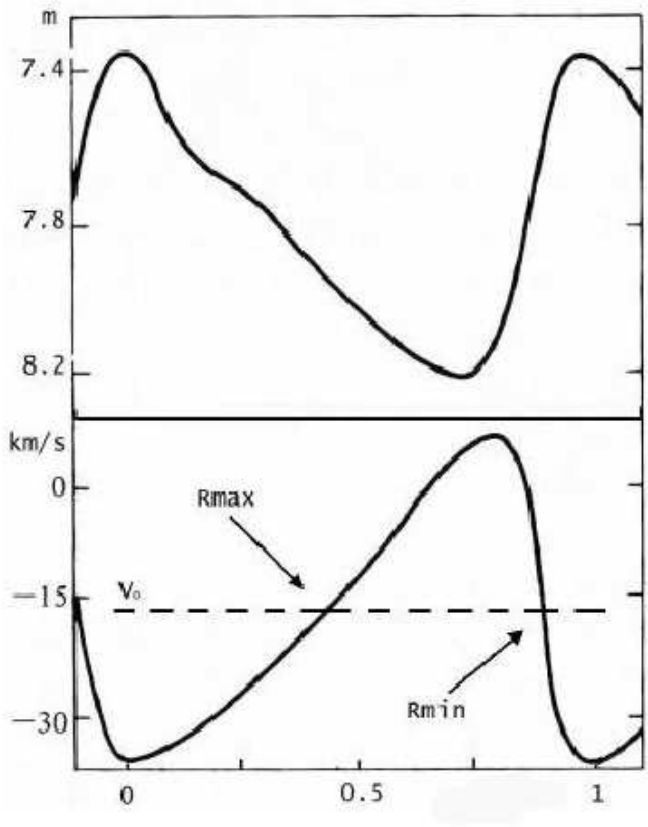


***Figure 2.2:*** *Behaviour of the light curve (upper panel) and of radial velocity curve for a typical radial pulsator. The dashed line in the lower panel shows the atmospheric zero velocity: the non vanishing value is due to the radial component of the motion of the star (Figure from Rose (1973).*

in the radial velocity of the starg. The radial velocity curve roughly reflect the light curve, with the minimum radial velocity coming at visible light maximum.

## 2.2 Pulsation mechanisms

Excellent reviews of the theory of stellar pulsation (Cox, 1974, King & Cox, 1968, Cox, 1980) available in literature make superflous any detailed treatment of the subject in this work. I wish only to remark the physical mechanisms driving pulsation in classical variable stars. In 1926 Eddington suggested that the stellar pulsation was driven by the so called “valve mechanism”. The idea is to see if a layer in the atmosphere release heat during a compression phase, or retains it. In the latter case, the layer contributes to the instability of the structure. The successful identification of actual mechanisms responsible

for the pulsations of most kinds of variable stars has been affected only in the past 40 year but now the causes of pulsation, in common types of variable stars, are reasonably well known. These mechanisms are associated to the envelope ionization phenomenon, which basically involves the ionization of an abundant element such as hydrogen (H) or helium (He) at critical depth below the stellar surface *. Pulsational instability arises from the modulation of the flux variations, with the partial ionization zones absorbing heat when they are most compressed and losing heat when most expanded causing light variations. The reason for this behaviour is that opacity increases in the regions where partial ionization occurs. The overall opacity of a stellar layer can be, in fact, expressed by the Rosseland mean opacity *k*:

$$k = k_o \rho^n T^{-s} \tag{2.1}$$

where $k_o$ is a constant, $\rho$ is the density and $T$ the temperature. For the gas in the stellar envelope, where no important element is undergoing ionization, $n$ is $\sim 1$ and $s \sim 3.5$. As $T$ increases, the opacity decreases and the leakage of energy would therefore increase during compression and the gas cannot serve as Eddington's valve. However, in a region where an abundant element is being ionized, $s$ can be smaller or even negative with the result that the gas can become more opaque driving compression and this is just what is needed to create Eddington's valve. This valve mechanism has become known as the $k$ mechanism. There is a second way in which the ionization zones in a RR Lyrae star can act to produce Eddington's valve. In the partial ionization regime energy, which would ordinarly go into raising the temperature of the gas, largely goes into ionization. The layer will therefore tend to absorb heat during compression, leading to a pressure maximum which comes after minimum volume and hence providing a driving force for pulsation. This effect has been called the $\gamma$ mechanism (King & Cox, 1968). In addiction to the $k$ and $\gamma$ mechanisms, others mechanisms have been proposed in the literature and can contribute to driving stellar pulsation. Cox (1985) lists six other possible excitation mechanism for pulsating stars but them are expected to be unimportant for RR Lyrae like

*The temperature of the second helium ionization zone is $3 \cdot 10^4$ K to $6 \cdot 10^4$ K, whereas the hydrogen ionization zone occurs at temperatures lower than $3 \cdot 10^4$ K. These temperatures are found very high in the envelope of an RR Lyrae star. Even the hight temperature edge to the helim second ionization zone occurs at radii more than 90 percent of the distance from the center of the star to the surface.

stars.

We have noted in previous chapter that all radially pulsating variables occupy a specific region of the HR diagram. For example, dealing with RR Lyrae in particular, HB stars which are too hot or too cool at the surface do not pulsate. Any theory of radial pulsation must not only explain why stars within the instability strip pulsate, but why stars outside the strip do not.Moreover, the precise high and low temperature boundaries of the RR Lyrae instability strip are difficult to predict theoretically, bacause such a prediction requires an understanding of the role of the complicated process of convection in RR Lyrae pulsation. That is particularly true for the low temperature (red) edge to the instability strip. It is believed that horizontal branch stars cooler than the red edge do not pulsate because the onset of convection inhibit the pulsational mechanism. The location of the hot (blue) edge of the instability strip is easier to calculate because the envelopes of stars at that temperature can be more easly described by models in which radiation is the dominant means of energy tranport. Pulsation halts at the blue edge because the relevant ionization zones are too high in the atmosfere of the star, where density is too low for the ionization zone to effectivly dam the flow of energy and serve as an adequate valve to drive pulsation.

## 2.3 Theoretical approches to stellar pulsation: brief history

As stated in the previous section, a detailed theory of pulsation able to explain and reproduce all the observations must be more complicated than the Eddington approch. In fact this author treated the problem of stellar pulsation in terms of linear and adiabatic oscillations deriving pulsational periods in good agreement with the observed ones. However, to study the modal stability, it is necessary to take into account non adiabatic effects.

Historically, the next important development was by Cox (1955) and by Ledoux, Simon & Bierlaire (1955). They found that the nuclear driving was many orders of magnitude smaller than the radiative damping. The overall conclusion was that no source of instability could be found interior to about 0.85 of the stellar radius, and that the driving mechanism, whatever is nature, would have to lie outside this level. Nearly simultane-

ously with these works, Zhevakin (1953, 1954a,b) suggested that the region of second helium ionization might be a suitable site for valve mechanism.

All these developments let to the study of the outer, non adiabatic regions of the star in an attempt to locate the source of the instability. The effectiveness of the $He^+$ ionization as a driving mechanism was first conclusivly demontrated by the linear non abiabatic calculations of Baker and Kippenhahn (1962), Cox (1963) and Castor (1971). Their studies provided important information on the physics of the pulsational behavior as well as on the position of the high temperature edge of the instability strip.

By definition, linear (small amplitude) calculations do not predict pulsational amplitudes, hence, in view to evaluate the pulsational limit cycle and the modal stability, a nonlinear approach is necessary. In the last thirty years there have been many efforts to develope non linear theoretical analysis. The first important nonlinear approach was developed by Christy (1966, 1967, 1968), who firstly showed that nonlinear radiative models can reproduce tha main observational properties of RR Lyrae variables. He found, for example, that the first overtone pulsators are located at mean effective temperatures larger that the fundamental ones in agreement with the observed behaviour. However, the majority of the stellar envelope models computed by Christy were followed in time only for a small number of periods and, therefore, Christy's approach could not provide firm information concerning the approach to limit cycle stability of radial motion.

This problem was solved by Stellingwerf (1974) who developed a "relaxation method " for evaluating the limiting amplitude modal behavior based on a linear perturbation analysis. Moreover, Stellingwerf (1975) settled the physics underlying the destabilization due to both the hydrogen and helium ionization regions, and also the method to handle, through the inclusion of an artificial viscosity pressure, the development and the propagation of the shocks both in the ionization zones and in the deeper layers of stellar envelopes. All along sixties and seventies, several results concerning the periods and the determination of the blu edge of the instability strip were obtained in close agreement with observational data. However both linear and non linear calculations could not account for the quenching of the pulsation instability close to the red edge of the instability strip. Baker & Kippenhahn (1965) first suggested that it is the onset of an efficient convective transfer that restore stability at low effective temperatures and, in turn, that determines the red

edge of the IS. Indeed, moving toward cooler effective temperature, convection becomes the main flux carrier in the regions of stellar envelope that drive the pulsational instability, and therefore it inhibits radiative destabilization of these crucial layers.

**Convection** occurs in cool thin, turbolent layers near the ionization zones in the outer stellar envelope. Although unstable, these zones are inefficient thermal flux carriers, so high convective velocities, extensive overshooting into stable regions, and the persistence of superadiabatic gradients are expected. Furthermore, these thin unstable regions sweep throught considerable distances as the star pulsates, so time-dependent growth of instability is also important. Bohm-Vitense (1958) developed a theory known as a mixing lenght theory of convection that is unables to handle all the mentioned complications. An attempt to apply this theory was performed by Baker & Kippenhahn, who neglected interaction between pulsation and convection. They assumed that the convective flux does not depend at all on radial pulsation, by they pointed out the leading effect of the convective mechanism. On the basis of linear, non abiabatic models including time-indipendent mixing lenght treatment of convective trasport in the static structures of the star, they suggested that as one moves from the blue to the red static structure of the IS, the apparence of convective regions implies at first an increase in the thickness of the hydrogen and first helium ionization zones, and then quenching of the pulsation. However, the linear models by Baker & Kippenhahn supply red edges cooler than the observed ones and, in turn, on instability strip too extended when compared with observational values.

Time-dependent versions of the mixing-lenght theory have been proposed by Unno (1967) and by Gough (1977), who stressed the need for the inclusion of turbolent pressure terms. The nonlinear calculation performed adopting this approch, presented strong spatial oscillation in the thermal eigenfunctions (in the total integral work) at the base of the envelope due to a resonace between the local convective field and the low pulsation efficiency of these (nearly adiabatic) regions. To overcame these difficulties, *ad hoc* assumptionson for the extension and efficiency of convective trasport have been adopted (Baker & Gough 1979, Gonczi & Osaki 1980). The difficulties inherent with these models were concerned that spacial variations took place on scale lenghts shorter than the mixing-lenght, and therefore small perturbations produce large excursions in the convective flux. This mechanism represents a real physical effect that can not be treated with a *local* mixing-lenght

theory.

The physical correct approach to handle the coupling between radial and convective motion is more complicated. In the ionization regions the convective or dissipative time scale is much shorter than the pulsation period and thus a time-dependent theory of convection is required. Moreover the convectively unstable regions of radial variables are inefficient thermal flux careers due to their low density. This implies that an extensive region of the stellar envelope is characterized by a superadiabatic gradient and by high convective velocities. At the same time, over a full pulsational cycle, the ionization zones sweep back and forth, moving into a region which presents a change in pressure scale height. All these peculiar features can be properly handled only by developing a *nonlocal* treatment of convective trasport which allows us to take into account the whole physical structure of the stellar envelope.

This torny and longstanding problem was solved by Deupree (1977, 1979) and by Stellingwerf (1982, 1984) who developed two different formulations to account for the coupling between radial pulsational and convective motions. In his two-dimensional formulation, Deupree treated nonlocal, nonlinear and time dependent effects in a homogeneous context, but difficulties emerged in the identification and resolution of different physical processes due to poor spatial resolution. However, Deupree accounted for the first theoretical contraint on the width of the fundamental mode instability strip, even if uncertainties in the evaluation of the mode stability close a limit cycle.

In his successful approach to the treatment of the pulsation/convection interaction, Stellingwerf (1984), following the prescriptions by Castor (1968), developed a unidimentional, nonlinear, non local and time dependent treatment of convection, and succeeded in evaluating, at fixed astrophysical parameters, the pulsational quenching caused by convection and, in turn, the location of the cool RR Lyrae instability boundaries. Improvements to this approach have been settled by Bono & Stellinwerf (1994) who analyzed the role played by limiting amplitudes calculations on modal behavior and pulsational amplitudes. A series of paper ( Bono & Stellingwerf, 1994, Bono et al.1997ab, Caputo et al. 2000) has been devoted to the full amplitude pulsational behaviour of radial variables in the IS and its dependence on astrophysical parameters, widely confirming the plausability of the physical assumptions adopted by Stellingwerf for deriving the hydrodinamical equations

for turbolent energy. Also this work is in part devoted to this scope.
Before proceeding with the description of the hydrodinamical code developed by Stellingwerf I remind that an approach similar to Stellingwerf's theory was developed by other authors (Gehmeyer & Winkler 1992a,b, Feuchtinger & Dorfi, 1998, Feughtinger, 1999). In particular the formulation more recently developed by Feughtinger (1999) is based on a convective scheme proposed by Kuhfub (1986) who, in turn, followed the prescriptions by Castor-Stellingwerf approach. They performed the inclusion of an extra equation which accounts for turbolent-convective energy transport.

## 2.4 Computational methods

In this section I will shortly describe the implicit lagrangian hydrodynamic code developed by Stellingwerf (1982, 1984) and later modified by Bono & Stellinwerf (1994). The extreme interior of the star does not partecipate in the pulsation and is, therefore, excluded. Neutrino losses are absent too. The luminosity is constant at the base of the envelope and the chemical composition is homogeneous. The physical structure of the stellar envelope is computed from layers immediately above the deeper regions, where the nuclear reactions take place, to the surface. The pulsational phenomenon is assumed to be a spherical symmetry radial motion. As a consequence, magnetic fields as well as non-radial effects are neglected. Mass-loss phenomena are not treated in the code too.
Once the physical characteristics of a star, namely mass $M$, luminosity $L$, effective temperature $T_e$ and chemical composition have been fixed, as first step the computing procedure provides the calculation of the static stellar envelope structure ($L(m)$, $R(m)$, $T(m)$, $P(m)$) by means of a linear, radiative, nonadiabatic code. This code also provides periods, growth rates and eigenfunctions for the selected pulsational modes, as well as the total kinetic energy, the hydrogen-zone work, the helium zone work and the interior work. The information carried out by the linear analysis is used to select the best models and modes to be investigated in the nonlinear case. The non linear modal stability is evaluated at limiting amplitude for each studied mode. The equations governing both dynamical and convective interactions[†] are integrated in time, until the initial perturbation and the

[†]The equations of stellar pulsation mechanism are the fundamental equations of hydrodynamic and heat transport; these relations are reported in Appendix A

nonlinear fluctuations due to superposition of hight order modes settled down. The set of equations of pulsation are indeed complemented by equation for the radial velocity that, at the first step, is initiated using for each mode, the $\delta$r/r eigenfunction obtained by the linear radiative analysis. The radial eigenfunction is forced out of equilibrium with typical profiles of a few tens of km/s. Than the dynamical behavior is followed in time by means of the nonlinar hydrocode till it attains a stable limit cycle, if any.

# 3

# Updated pulsation models of RR Lyrae and BL Herculis stars

*In this chapter, the computed pulsation models of RR Lyrae (Section 3.1) and BL Herculis stars (Section 3.2) are presented. For each models the bolometric light curve is trasformed in the Johnson-Cousins filters and, in the case of RR Lyrae stars, also into the SDSS (Subsection 3.1.4) photometric bands. Relevant relations connecting pulsation observables, such as the period and the amplitude of the oscillation, to the intrinsic stellar parameters are derived. The dependence of theoretical predictions on the adopted efficiency of convection is also investigated in detail for both the types of pulsators. In the next chapter I will compare these models with the observed variables in Galactic globular clusters and I will demonstrate the self consistence of the adopted theoretical scenario.*

## 3.1 RR Lyrae (Di Criscienzo et al. 2004, ApJ, 612; Marconi et al., 2006, MNRAS, 371)

The existing grid of nonlinear and convective pulsation models (see Bono et al. 2001, 2003) has been extended with new fundamental (F) and first-overtone (FO) models sets for $Z$=0.0001, $M$=0.80$M_{\odot}$, log$L/L_{\odot}$=1.72, 1.81, 1.91 (Di Criscienzo et al. 2004) and

***Table 3.1:*** *Stellar parameters for the full set of pulsation models. All the computations, except those with Z=0.0004, have been performed assuming two values of the mixing lenght parameter, namely $l/H_p$=1.5 and 2.0.*

| $Y$ | $Z$ | $M/M_\odot$ | $\log L/L_\odot$ |
|---|---|---|---|
| 0.24 | 0.0001 | 0.80 | 1.72, 1.81, 1.91 |
| | | 0.75 | 1.61, 1.72, 1.81 |
| | | 0.70 | 1.72 |
| | | 0.65 | 1.61 |
| 0.24 | 0.0004 | 0.70 | 1.61, 1.72, 1.81 |
| 0.24 | 0.001 | 0.75 | 1.71 |
| | | 0.65 | 1.51, 1.61, 1.72 |
| 0.255 | 0.006 | 0.58 | 1.55, 1.65, 1.75 |

$M$=0.65$M_\odot$ and $\log L/L_\odot$=1.61 (Marconi et al 2003). The whole set of available pulsation models is listed in Table 3.1.

A mixing length parameter $l/H_p$=1.5 (see previous chapter) is adopted in order to close the system of convective and dynamical equations. However, to gain some insight into how the boundaries for instability are dependent on convection (see Caputo et al. 2000), for the first time I have computed additional models with $l/H_p$=2.0, also in view of the values for the mixing length parameter recently used in HB model computations. The adopted metal abundances are those typical of Galactic globular cluster and for each $Z$ we assume different masses and luminosity levels in order to explore the dependence on these parameters. For each given set of input parameters, the computations are performed by decreasing the effective temperature $T_e$ by steps of 100-200 K. In the following, I will consider the results from the bluest pulsating model to the reddest one bearing in mind that increasing (decreasing) by 100 K the effective temperature of the bluest (reddest) pulsators yields non-pulsating structures.

Since the adopted nonlinear approach supplies not only the pulsation period, but also the luminosity variation along the whole pulsation cycle, I have trasformed the bolometric light curves into the observational plane by adopting bolometric corrections and temperature-color transformations provided by Castelli, Gratton & Kurucz (1997a,b, hereafter CGKa,b). In this way, amplitudes and $mean$ absolute magnitudes, either intensity-weighted and magnitude-weighted, are derived in the various photometric bands. As an example, Table 3.2 lists selected results for fundamental (F) pulsators with $Z$=0.001,

***Table 3.2:*** *Selected results for fundamental pulsating models at Z=0.001, Y=0.24, $M$=0.65$M_\odot$, $logL/L_\odot$=1.61 and $l/H_p$=1.5 (see text).*

| $T_e$ | | $M_U$ | $M_B$ | $M_V$ | $M_I$ | $M_K$ |
|---|---|---|---|---|---|---|
| 6000(FRE) | | 1.242 | 1.265 | 0.814 | 0.179 | -0.586 |
| 6100 | | 1.207 | 1.229 | 0.802 | 0.194 | -0.534 |
| 6300 | | 1.149 | 1.164 | 0.781 | 0.225 | -0.431 |
| 6500 | | 1.104 | 1.104 | 0.761 | 0.258 | -0.332 |
| 6700 | | 1.067 | 1.050 | 0.744 | 0.292 | -0.233 |
| 6900(FBE) | | 1.037 | 1.001 | 0.729 | 0.327 | -0.139 |
| $T_e$ | P | $\langle M_U \rangle$ | $\langle M_B \rangle$ | $\langle M_V \rangle$ | $\langle M_I \rangle$ | $\langle M_K \rangle$ |
| 6000 | 0.6598 | 1.246 | 1.265 | 0.819 | 0.188 | -0.575 |
| 6100 | 0.6254 | 1.225 | 1.241 | 0.812 | 0.200 | -0.540 |
| 6300 | 0.5626 | 1.163 | 1.168 | 0.787 | 0.239 | -0.436 |
| 6500 | 0.5061 | 1.119 | 1.104 | 0.768 | 0.268 | -0.342 |
| 6700 | 0.4567 | 1.077 | 1.043 | 0.759 | 0.317 | -0.239 |
| 6900 | 0.4137 | 1.037 | 1.010 | 0.770 | 0.376 | -0.137 |
| $T_e$ | P | $(M_U)$ | $(M_B)$ | $(M_V)$ | $(M_I)$ | $(M_K)$ |
| 6000 | 0.6598 | 1.253 | 1.273 | 0.823 | 0.190 | -0.573 |
| 6100 | 0.6254 | 1.238 | 1.257 | 0.820 | 0.204 | -0.537 |
| 6300 | 0.5626 | 1.187 | 1.198 | 0.804 | 0.239 | -0.433 |
| 6500 | 0.5061 | 1.168 | 1.167 | 0.805 | 0.283 | -0.338 |
| 6700 | 0.4567 | 1.164 | 1.156 | 0.824 | 0.341 | -0.234 |
| 6900 | 0.4137 | 1.184 | 1.180 | 0.869 | 0.412 | -0.131 |

$M$=0.65$M_\odot$, $logL/L_\odot$=1.61 and $l/H_p$=1.5. For each given effective temperature, are reported the static magnitude, i.e. the value the star would have were it not pulsating, the period $P$ (in days),the mean intensity-weighted $\langle M_i \rangle$ and magnitude-weighted $(M_i)$ magnitudes. Table 3.3 has the same meaning, but holds for FO pulsators.

As well known since the original Ritter's formulation $P\rho^{1/2}$=$Q$ ($\rho$ is the mean star density and $Q$ the pulsation constant), the basic physics underlying radial variability suggests that the pulsation period depends on the mass, the luminosity and the effective temperature of pulsators. As a fact, a linear interpolation among all the models listed in Table 3.1 supplies a refined version of earlier pulsation equations (see, e.g., van Albada & Baker 1971, Bono et al. 1997a), as given by:

$$\log P_F = 11.038(\pm 0.003) + 0.833 \log L - 0.651 \log M - 3.350 \log T_e + 0.008 \log Z \quad (3.1)$$

***Table 3.3:*** *As in Table 3.2, but for first-overtone pulsating models*

| $T_e$ | | $M_U$ | $M_B$ | $M_V$ | $M_I$ | $M_K$ |
|---|---|---|---|---|---|---|
| 6600(FORE) | | 1.085 | 1.076 | 0.752 | 0.275 | -0.282 |
| 6700 | | 1.068 | 1.050 | 0.744 | 0.293 | -0.233 |
| 6900 | | 1.037 | 1.000 | 0.728 | 0.327 | -0.139 |
| 7000 | | 1.024 | 0.977 | 0.722 | 0.346 | -0.092 |
| 7100 | | 1.012 | 0.955 | 0.716 | 0.364 | -0.046 |
| 7200(FOBE) | | 1.001 | 0.934 | 0.711 | 0.383 | 0.000 |
| $T_e$ | P | $\langle M_U \rangle$ | $\langle M_B \rangle$ | $\langle M_V \rangle$ | $\langle M_I \rangle$ | $\langle M_K \rangle$ |
| 6600 | 0.3558 | 1.100 | 1.091 | 0.762 | 0.277 | -0.296 |
| 6700 | 0.3362 | 1.083 | 1.063 | 0.754 | 0.295 | -0.251 |
| 6900 | 0.3055 | 1.052 | 1.011 | 0.742 | 0.336 | -0.155 |
| 7000 | 0.2921 | 1.036 | 0.986 | 0.738 | 0.357 | -0.109 |
| 7100 | 0.2779 | 1.020 | 0.962 | 0.734 | 0.378 | -0.059 |
| 7200 | 0.2663 | 1.008 | 0.941 | 0.727 | 0.396 | -0.007 |
| $T_e$ | P | $(M_U)$ | $(M_B)$ | $(M_V)$ | $(M_I)$ | $(M_K)$ |
| 6600 | 0.3558 | 1.115 | 1.111 | 0.775 | 0.282 | -0.295 |
| 6700 | 0.3362 | 1.109 | 1.097 | 0.775 | 0.304 | -0.249 |
| 6900 | 0.3055 | 1.092 | 1.066 | 0.776 | 0.349 | -0.153 |
| 7000 | 0.2921 | 1.085 | 1.052 | 0.778 | 0.372 | -0.106 |
| 7100 | 0.2779 | 1.073 | 1.033 | 0.776 | 0.394 | -0.057 |
| 7200 | 0.2663 | 1.045 | 0.992 | 0.757 | 0.407 | -0.005 |

where the luminosity $L$ and the mass $M$ are in solar units. To derive this relation I have fundamentalised the period of FO pulsators by adopting log$P_F$=log$P_{FO}$+0.130$\pm$0.004 (Marconi et al. 2003).

Before proceeding, let me first recall the data in Tables 3.2 and 3.3 . As discussed in previous studies (Marconi et al. 2003) the synthetic mean magnitudes ($M_i$) of fundamental pulsators, as derived by averaging the magnitude over one period, are fainter than the corresponding static values with the discrepancy increasing as the pulsation amplitude increases. A smaller discrepancy is present between intensity-averaged magnitudes and static values. The key element governing such a behavior is the overall morphology of the light curve in the sense that the difference between static and mean magnitudes increases from symmetric (low amplitude) to asymmetric (high amplitude) light curves, moving namely from the red to the blue fundamental edge (see also Bono, Caputo, Stellingwerf

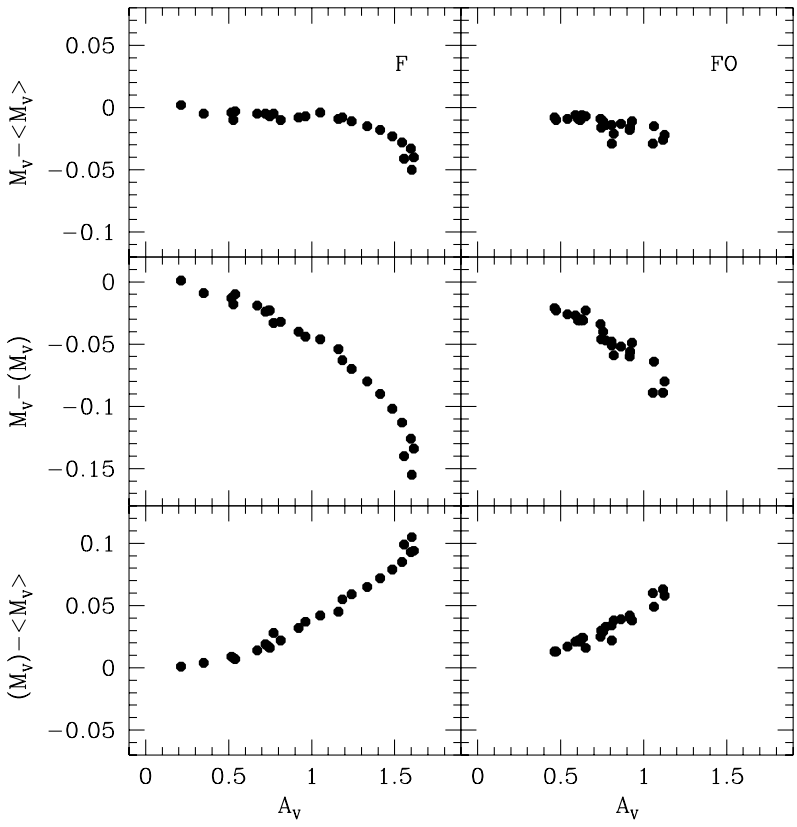


***Figure 3.1:*** *Comparison between static and mean magnitudes of fundamental (F) and first-overtone (FO) pulsators for models with M=0.65 and Z=0.001*

1995b). Since at fixed effective temperature the amplitude decreases from blue to visual to infrared, the difference between static and mean values for $K$ magnitudes is almost negligible, whereas $(M_B)$, $(M_V)$ and $(M_I)$ differ from the corresponding static values by up to $\sim$ 0.18 mag, $\sim$ 0.14 mag, and $\sim$ 0.08 mag, respectively, at $A_V$=1.6 mag. As for FO pulsators, the discrepancy is less pronounced, given their low-amplitude and quite symmetric light curves. In Fig. 3.1 I show the synthetic visual magnitudes for F and FO pulsators, by plotting the discrepancy between static and mean values, as well as the difference between the two means, as a function of the visual amplitude $A_V$. It is quite relevant to notice that the predicted differences $(M_V) - \langle M_V \rangle$, as well as the corresponding rather small amounts inferred from Table 3.2 and Table 3.3 for the $K$-band, are in close agreement with observed differences $(V) - \langle V \rangle$ and $(K) - \langle K \rangle$, as reported in previous studies on RR Lyrae stars (e.g. Fernley 1993).

However, since the aim of this work is to provide a handly tool for the analysis of observed data, all the following relations will be given for intensity-averaged magnitudes which are, as one can see in Fig. 3.1, better representative of the static ones andare also the commonly used observed magnitudes.

### 3.1.1 The instability strip

It is well known that radial pulsation occurs in a quite well-defined region of the HR diagram, the so-named "instability strip", that depends on the type of pulsation and the intrinsic parameters of pulsators. In simple words, pulsation does not occur for any combination of $M$, $L$ and $T_e$. For each given mass and luminosity, there is a maximum and minimum effective temperature for the onset of either fundamental or first-overtone pulsation. As already known, the data in Table 3.2 and 3.3, as those presented in previous papers (see, e.g., Bono, Caputo & Marconi 1995a, Bono et al. 1997a,b, Caputo et al. 2000, Bono et al. 2002 and references therein) show that, for fixed mass and luminosity, FO pulsators are generally bluer than F pulsators, in full agreement with the observed behavior of $c$-type and $ab$-type RR Lyrae stars. This yields that the first-overtone blue edge (FOBE) and the fundamental red edge (FRE) can be generally taken as the limits of the whole instability strip. Moreover, the models show that the fundamental pulsation blue edge (FBE) is generally bluer than the first-overtone red edge (FORE), suggesting that both the pulsation modes can be stable in a middle region of the instability region. The FOBE is almost insensitive to metallicity variations whereas the FRE tends to be slightly redder, for fixed mass and luminosity, when increasing the metal content.

Finally one should also consider that varying the value of the mixing length parameter $l/H_p$ will modify the edges of the pulsation region, shrinking the width of the whole instability strip if increasing the efficiency of convection in the star external layers. As the depth of convection increases from high to low effective temperature, and the effect of convection is to quench pulsation, we expect that varying the value of the mixing length parameter will modify the red edge of the instability strip by a larger amount with respect to the blue edge. In order to study this effect, all the models listed in Table 3.1, but the case $Z$=0.0004, have been recomputed by adopting $l/H_p$=2.0. The results confirm the previous hypothesis. In particular the FOBE effective temperature decreases by $\sim$ 100 K,

while the FRE one increases by $\sim$ 300 K. Moreaover, we notice taht for the same $l/H_p$ variation the fundamental blue edge changes by 100 K at most, while the first overtone red edge gets hotter ny about 200 K. However, it is of interest to note that with $Z$=0.006 and $\log L/L_{\odot} \geq 1.65$ the FO instability strip disappears when $l/H_p$=2.0 is adopted. Such a result, and with the observational evidence of $c$-type RR Lyrae stars with such a metal content, seem to suggest that $l/H_p$=2.0 is a upper limit value for metal-rich pulsational models. Concerning the location of the instability strip theoretical edges in the $M_V$-log$P$ diagram, taking also into account the above mentioned effects of the mixing-length parameter, a linear regression to all the computed models yields:

$$M_V^{FOBE} = -1.19 - 2.23 \log M - 2.54 \log P_{FO} + 0.10(l/H_p - 1.5) \tag{3.2}$$

and

$$M_V^{FRE} = 0.12 - 1.88 \log M - 1.96 \log P_F - 0.28(l/H_p - 1.5) \tag{3.3}$$

with a standard deviation of 0.05 and 0.06 mag, respectively.

### 3.1.2 Pulsational amplitudes

Fig. 3.2 shows bolometric light curves with $l/H_p$=1.5 (solid line) and $l/H_p$=2.0 (dashed line) for a number of F and FO models. I have calculated these models with $M$=0.80 $M_{\odot}$ and varying luminosity and effective temperature. In agreement with the results presented in previous papers (Bono & Stellingwerf 1994, Bono et al. 1997a), the morphological features of the predicted light curves appear a function of luminosity and effective temperature, thus providing a useful tool to constrain such fundamental intrinsic parameters. In particular, Bono & Stellingwerf (1994) have already discussed that moving toward lower luminosity levels, for a fixed mass, the morphology of the light curve of FO models becomes very similar to that of fundamental pulsators, changing from almost sinusoidal to sawtooth and with a significant increase of the bolometric amplitude. In this context, the use of the Fourier parameters of observed light curves (see, e.g., Kovacs & Walker 2001 and references therein) appears as a promising way to approach the determination of the intrinsic parameters, even though the obvious ultimate goal to take into account all the observed features (e.g., bump, double-peak) is the best fit of the whole light curve, as recently presented by Bono, Castellani & Marconi (2000, 2002), Castellani, Degl'Innocenti

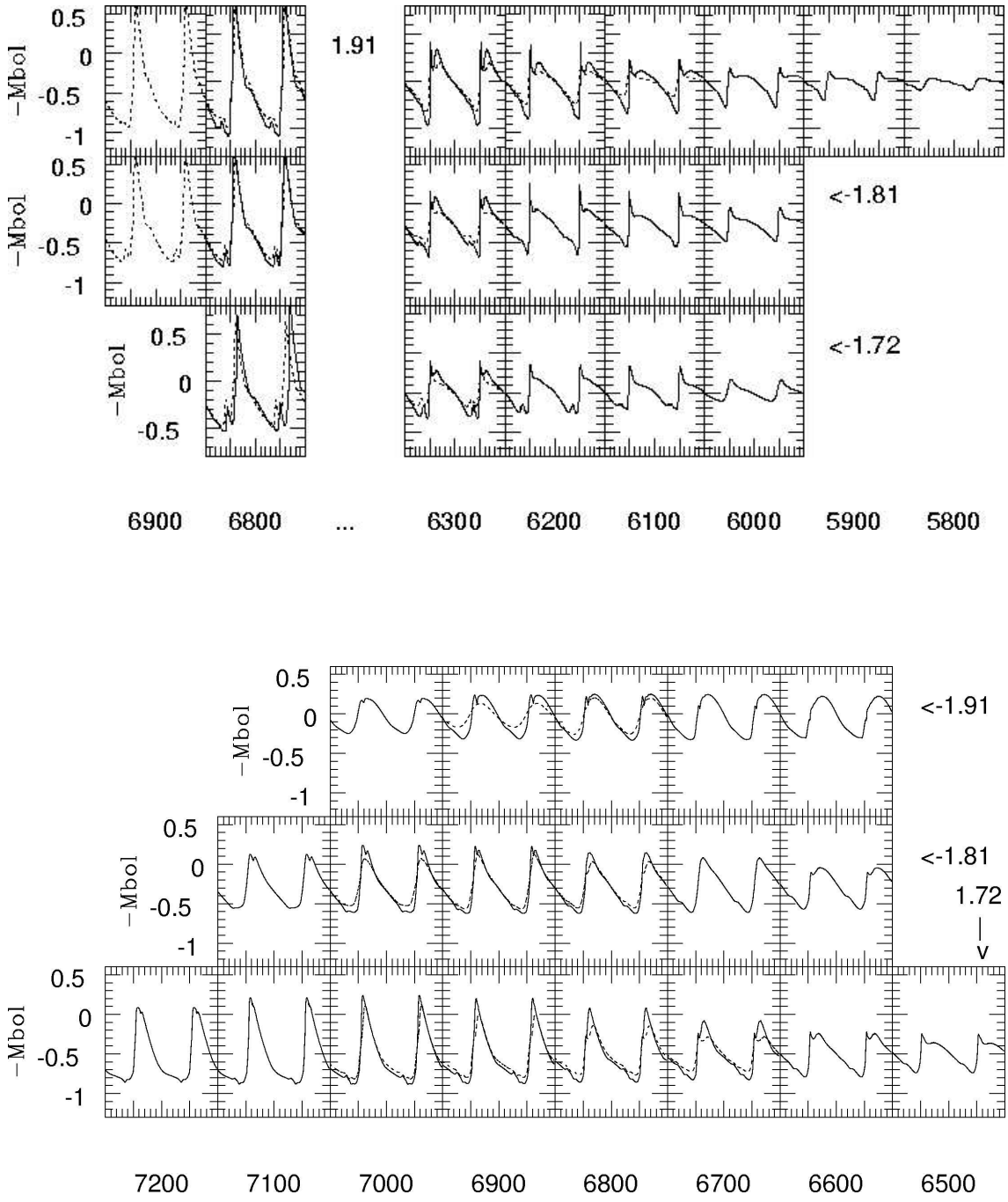


***Figure 3.2:*** *Upper panel: bolometric light curves with $l/H_p$=1.5 (solid line) and $l/H_p$=2.0 (dashed line) for a number of F models with $M = 0.80 M_\odot$ at varying luminosity and effective temperature. Bottom panel: the same but for FO models*

***Table 3.4:*** *Effects of the mixing-length parameter $l/H_p$ on the period, color and visual amplitude of fundamental models with Z=0.001, 0.75 $M_\odot$ and log$L/L_\odot$=1.61.*

| $T_e$(K) | $P$(days) | $\langle M_B\rangle - \langle M_V\rangle$ | $A_V$ | $P$(days) | $\langle M_B\rangle - \langle M_V\rangle$ | $A_V$ |
|---|---|---|---|---|---|---|
| | ($l/H_p$=1.5) | | | ($l/H_p$=2.0) | | |
| 6100 | 0.5697 | 0.423 | 0.517 | stable | – | – |
| 6200 | 0.5400 | 0.405 | 0.748 | stable | – | – |
| 6300 | 0.5120 | 0.385 | 0.813 | 0.5109 | 0.379 | 0.154 |
| 6400 | 0.4859 | 0.362 | 0.922 | 0.4854 | 0.362 | 0.548 |
| 6500 | 0.4622 | 0.337 | 1.162 | 0.4604 | 0.342 | 0.649 |
| 6600 | 0.4385 | 0.310 | 1.240 | 0.4384 | 0.320 | 0.851 |
| 6700 | 0.4170 | 0.285 | 1.413 | 0.4164 | 0.295 | 1.074 |
| 6800 | 0.3969 | 0.263 | 1.544 | 0.3966 | 0.271 | 1.260 |
| 6900 | 0.3779 | 0.244 | 1.615 | 0.3780 | 0.250 | 1.385 |
| 7000 | FO | – | – | 0.3608 | 0.231 | 1.416 |

& Marconi (2002), Marconi & Clementini (2005). Here, as a broad outline of the pulsational behavior, let me consider the quite linear correlation between fundamental bolometric amplitudes and periods (logarithmic scale), for fixed mass and luminosity. As a first point it is important to mention that the pulsation amplitudes, while sharing with the periods the property of being sound measurements independent of reddening and distance uncertainties, do significantly depend on the adopted efficiency of the convective transfer. As an example, I list in Table 3.4 the computed periods, colors and visual amplitudes for fundamental pulsators with $Z$=0.001, 0.75$M_\odot$, log$L/L_\odot$=1.61 and $l/H_p$=1.5 and 2.0. One has that both the period and the color are almost independent of the adopted value for the mixing-length parameter, whereas the amplitude decreases with increasing the efficiency of convection, for fixed effective temperature (see the dashed light curve in Fig. 3.2). Moreover, given the already mentioned effects of the same $l/H_p$ variation on the fundamental red edge (where the amplitude reaches its minimum value) and blue edge (where the amplitude reaches its maximum value), the $A_V - \log T_e$ slope becomes steeper with increasing the $l/H_p$ value.

As a whole, after transforming all the bolometric light curves into the observational plane, Fig. 3.3 shows that all over the explored metallicity range the Period-Magnitude-

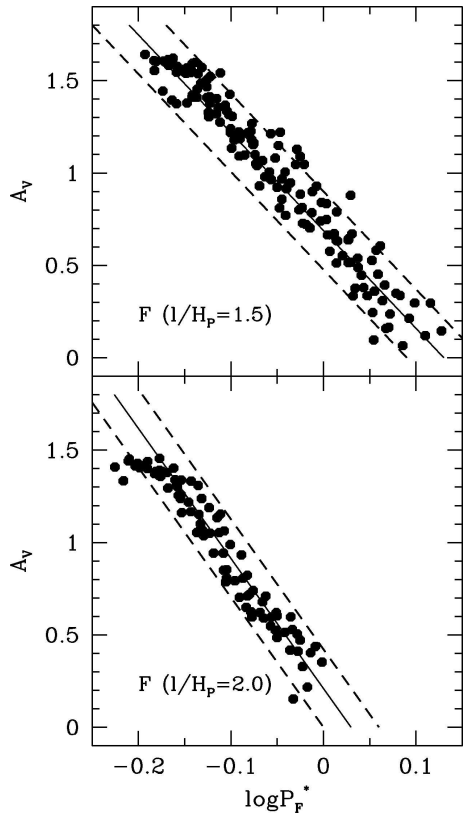


***Figure 3.3:*** *Period-Magnitude-Amplitude ($PMA_V$) relations for fundamental models under the two values of the mixing lenght parameter. The solid lines are the linear regression through the data (see equations 3.4 and 3.5 in the text), while the dashed lines depict the standard deviation.*

Amplitude ($PMA_V$) relation for fundamental pulsators can be approximated as

$$\log P_F^* = \log P_F + 0.385\langle M_V\rangle + 0.30\log M = 0.13 - 0.189A_V \tag{3.4}$$

at $l/H_p$=1.5, and

$$\log P_F^* = \log P_F + 0.385\langle M_V\rangle + 0.35\log M = 0.03 - 0.142A_V \tag{3.5}$$

at $l/H_p$=2.0, with a standard deviation (dashed lines) of 0.04 and 0.03 mag, respectively. Closing this section devoted to pulsation amplitudes, I notice that increasing the $l/H_p$ value yields smaller amplitudes for fixed $BV$ color. This is shown in Fig. 3.4, where the visual amplitude $A_V$ is plotted as a function of the intensity-weighted $\langle M_B\rangle - \langle M_V\rangle$ color for F pulsators with $l/H_p$=1.5 (upper panel) and $l/H_p$=2.0 (lower panel). At variance with the results derived with static colors, here one derives that the amplitude-color correlation is not strictly linear as a consequence of the fact that at larger amplitudes the intensity-averaged color becomes bluer than the static one. As a whole, in the explored range of

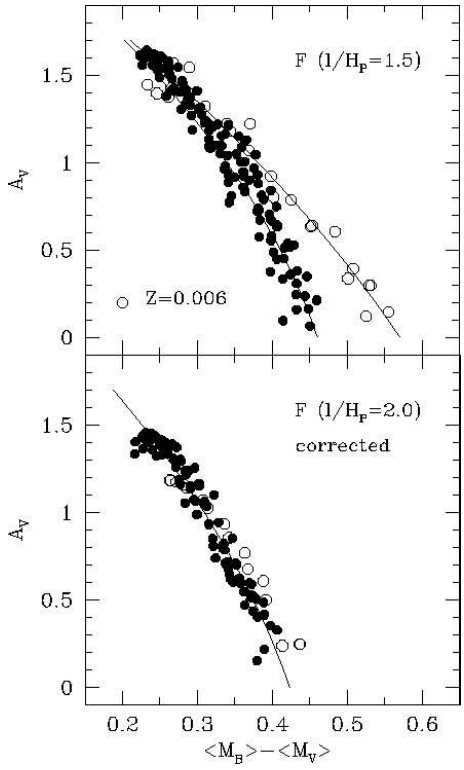


***Figure 3.4:*** *Upper panel: visual amplitude $A_V$ as a function of the intensity-weighted $\langle M_B\rangle - \langle M_V\rangle$ color for F pulsators with $l/H_p$=1.5. The solid lines depict the linear regression through the data (see equations 3.6 and 3.7 in the text). Lower panel: as above, but with $l/H_p$=2.0. The color index is corrected for the metal content and the solid line is the linear regression through the data (see equation 3.8 in the text).*

mass and luminosity, all the results with $l/H_p$=1.5 and $Z \leq 0.001$ suggest the following Color-Amplitude ($CA$) relation

$$\langle M_B\rangle - \langle M_V\rangle = 0.469 - 0.077A_V - 0.044A_V^2 \tag{3.6}$$

with a standard deviation of 0.04 mag, while at $Z$=0.006:

$$\langle M_B\rangle - \langle M_V\rangle = 0.568 - 0.156A_V - 0.033A_V^2 \tag{3.7}$$

with a standard deviation of 0.02 mag. As for the case $l/H_p$=2.0, the regression through all the models yields:

$$\langle M_B\rangle - \langle M_V\rangle = 0.465 - 0.079A_V - 0.035A_V^2 + 0.014\log Z \tag{3.8}$$

with a standard deviation of 0.03 mag.

### 3.1.3 Some important relations for RR Lyrae studies

The obvious outcome of the period relation (see equation 3.1) into the observational plane is the Period-Magnitude-Color ($PMC$) relation, where the pulsation period for each given mass is correlated with the pulsator absolute magnitude and color. When using linear pulsating models, this could be made by simply transforming luminosity and effective temperature into absolute magnitude and color, but the result is a *static* $PMC$ relation which cannot be directly compared to observed variables. On the contrary, the non linear approach we used supplies *mean* magnitudes and colors.

Based on intensity-averaged magnitudes, the linear interpolation through the results (adopting fundamentalised periods for FO models and B-V color for example) gives for each adopted metal content $Z$:

$$\log P'_F = \log P_F + 0.34\langle M_V\rangle + 0.54 \log M = a(Z) + b(Z)[\langle M_B\rangle - \langle M_V\rangle] \quad (3.9)$$

where the coefficients $a(Z)$ and $b(Z)$ are listed in the following Table 3.5.

According to the predicted $PMC$ relations, for a sample of RR Lyrae stars at the same

***Table 3.5:*** *Predicted Period-Magnitude-Color relation log$P'_F$=a+b[$\langle M_B\rangle - \langle M_V\rangle$] with intensity-averaged $BV$ magnitudes.*

| $Z$ | a | b |
|---|---|---|
| 0.0001 | $-0.552 \pm 0.014$ | $1.290 \pm 0.029$ |
| 0.0004 | $-0.543 \pm 0.014$ | $1.256 \pm 0.029$ |
| 0.001 | $-0.545 \pm 0.014$ | $1.208 \pm 0.028$ |
| 0.006 | $-0.522 \pm 0.018$ | $1.019 \pm 0.029$ |

distance and with the same reddening, e.g. for variables in a given globular cluster with no differential reddening, one could estimate the mass range spanned by the variables with an uncertainty lower than 2%, once periods and static colors are firmly known. If the cluster distance modulus and reddening are independently determined, then the mass absolute values can be inferred too. Alternatively, once period and color are measured, the relations can be used to get the distance to individual RR Lyrae stars with known mass and reddening.

However, it is of interest to mention that the magnitude dispersion due to the finite width of the instability strip is rather close to the effect of interstellar extinction. Based on

such an evidence, the Wesenheit functions (see Dickens & Saunders 1965) $W(BV)$=$V - 3.1(B-V)$, $W(VI)$=$V - 2.54(V-I)$, etc., which have been widely used in Cepheid studies (see Madore 1982 and Madore & Freedman 1991), can be adopted also for RR Lyrae stars (see Kovacs & Jurcsik 1997, Kovacs & Walker 2001) to provide a reddening-free $PW$ relation, where also the dispersion of magnitude at a given period is significantly reduced. Before proceeding, let me remark the deep difference between the $PMC$ and $PW$ relations: the former one is defined by the intrinsic properties of the variables and cancels the effects of the finite width of the instability strip, while the latter depends on the properties of the interstellar medium and removes differential or total reddening effect. Therefore, in the case of variables at the same distance and with the same mass and metal content, the scatter in observed $PMC$ relations, excluding photometric errors, should mainly depend on reddening, whereas the scatter in observed $PW$ relations is a residual effect of the finite width of the strip.

Using $\langle W(BV)\rangle$ quantities based on intensity-averaged magnitudes, a linear interpolation through F and fundamentalised FO models yields the Period-Wesenheit $PW(BV)$ relation

$$\langle W(BV)\rangle = -1.655(\pm 0.054) - 2.737(\pm 0.027)\log P_F^W \tag{3.10}$$

where

$$\log P_F^W = \log P_F + 0.54\log M + 0.03\log Z \tag{3.11}$$

As for the $\langle W(VI)\rangle$ function, the linear interpolation through F and fundamentalised FO models yields

$$\langle W(VI)\rangle = -1.670(\pm 0.030) - 2.750(\pm 0.013)\log P_F^W \tag{3.12}$$

where

$$\log P_F^W = \log P_F + 0.65\log M \tag{3.13}$$

It is of interest to note that RR Lyrae stars observed in the Large Magellanic Cloud yield $\delta\langle W(VI)\rangle/\delta\ \log P_F \sim -2.75$ (Soszynski et al. 2003) which is the predicted slope at constant mass. Moreover, variables observed in Galactic globular clusters suggest $\delta(W(BV))/\delta\log P_F \sim -2.47$ and $\delta(W(VI))/\delta\log P_F \sim -2.51$ (see Kovacs &

Walker 2001), where $(W(BV))$ and $(W(VI))$ are magnitude-averaged quantities. Also these results appear in reasonable agreement with the predicted slopes we get at roughly constant mass and metal content, namely $\delta(W(BV))/\delta \log P_F = -2.66(\pm 0.03)$ and $\delta(W(VI))/\delta \log P_F = -2.64(\pm 0.02)$.

Let me now consider the quite plain correlation between the absolute magnitude in a given $i$-band and luminosity, $M_i = -2.5 \log L + BC_i$, where the bolometric correction $BC_i$ depends on the star effective temperature, mass and luminosity. Since also the pulsation period is governed (see equation 3.1) by the effective temperature, mass and luminosity, the absolute magnitude $M_i$ of radial pulsating stars is expected to be a function of mass, luminosity and period. It is obvious that the dependence of $M_i$ on mass, luminosity and period is governed by the dependence of $BC_i$ on the effective temperature. Fig. 3.5 shows the quite different dependence of visual and near-infrared static absolute magnitudes on the pulsation period. For any given mass and luminosity, an increase of $T_e$ yields shorter periods, while, following the BC variation, $M_V$ becomes slowly brighter and $M_K$ significantly fainter. On the other hand, if increasing the luminosity at constant mass and effective temperature, the period increases and both $M_V$ and $M_K$ become brighter. In summary, one has a sort of $degeneracy$ (see the arrows in the lower panel in Fig.3.5) between the luminosity and effective temperature effects on $M_K$. As a result, for fixed period, $M_V$ depends mainly on luminosity, with a negligible dependence on the mass, whereas $M_K$ shows small but non negligible variations both with luminosity and mass (see also Bono et al. 2001, 2003). According to all the models, the predicted period-magnitude relations in the near-infrared bandpass ($PM_K$) is:

$$\langle M_K \rangle = -0.094 - 2.158 \log P_F - 1.436 \log M - 0.712 \log L \tag{3.14}$$

with a standard deviation of $\pm$ 0.04 mag. The importance of the RR Lyrae near-infrared $PM_K$ relation to get accurate distances to globular clusters has already been discussed by several authors (see Bono et al. 2001 and references therein) and it will not be discussed further. It is enough to mention that near-infrared magnitudes are very little affected by reddening and that adopting for the RR Lyrae stars in a given globular cluster, that is for variables at constant age and metal content, a luminosity dispersion of $\delta \log L \sim \pm$ 0.06

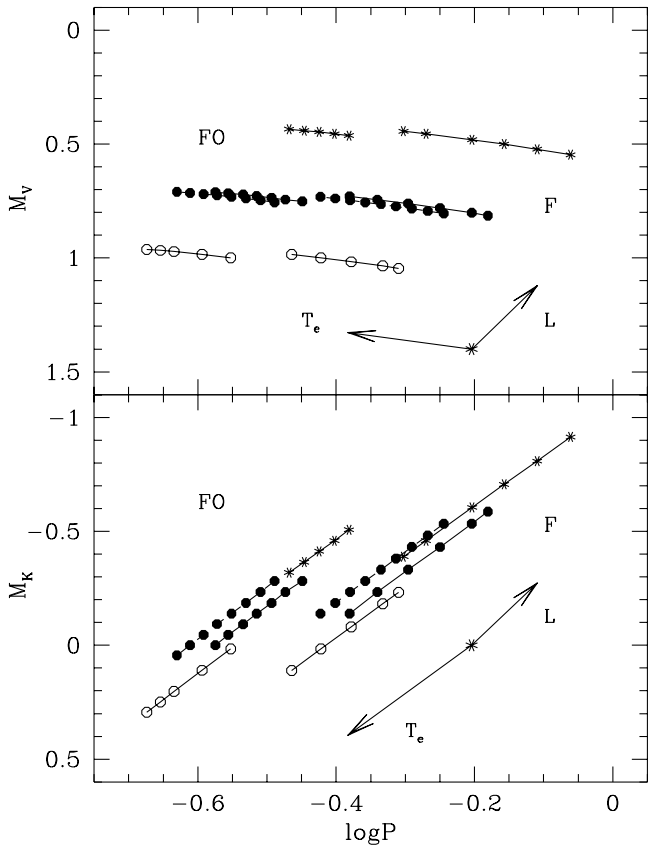


***Figure 3.5:*** *Upper panel: predicted V-band absolute magnitudes for fundamental and first overtone pulsators for a fixed chemical composition (Y=0.24, Z=0.001) and mass (M=0.65 $M_{\odot}$ ), but with different lumisosity levels (log $L/L_{\odot}$=1.51, 1.61, 1.72) . Lower panel: same as in the upper panel, but for K-band absolute magnitudes.*

and a mass spread* of $\pm$3%, yields a dispersion $\delta M_V \sim \pm$ 0.17 mag and $\delta M_K \sim \pm$ 0.05 mag, at fixed period.

### 3.1.4 New results in the SDSS filters

As already mentioned in the first chapter of this work, the characteristic variability of RR Lyrae stars make them very important traces to probe the properties of the old stellar populations and studies of their pulsation behaviour have provided much of our present knowledge of the structure, kinematics, and metal abundance distribution of the halo.

*Based on current computations, the mass spread of HB models near the RR Lyrae instability strip depends on $Z$, decreasing with increasing the metal content.

Moreover, they have been adopted in the recent literature as fundamental targets of surveys devoted to the identification of specific populations and galactic substructures (see e.g. Wu et al. 2005, Brown et al. 2004, Vivas et al. 2004 and references therein). In particular, the Sloan Digital Survey (SDSS) for RR Lyrae (Ivezic et al. 2000) and the QUEST RR Lyrae survey (Vivas et al. 2001, 2004, 2006) detected the tidal stream from the Sagittarius dSph galaxy and other density enhancements in the halo that may be other tidal streams, supporting the idea that RR Lyrae surveys are crucial to trace the merger history of the Milky Way. In the context of the VLT Survey Telescope (VST) GTO (see Alcalá et al. 2006) my "research group" has planned a survey (STREGA@VST, see Marconi et al. 2006) devoted to the exploration of the southern part of the Fornax stream (Lynden-Bell 1982, Dinescu et al. 2004) and the tidal interaction of the involved satellite galaxies and globular clusters with the Milky Way halo. To this purpose RR Lyrae will be used as tracers of the oldest stellar populations through multi-epoch observations in the SDSS *u*,*g*, *r* and *i* and *z* filters. As you will see in the next chapter the comparison of data with theoretical period-luminosity-color, period-luminosity-amplitude and Wesenheit relations can provide information on the individual RR Lyrae distances and in turn on the spatial distribution of the investigated stellar system. However, in order to correctly compare model predictions with observations we have transformed all the predicted pulsation observables (given in the previous sections for Johnson-Cousins photometric band) into the SDSS photometric filters (which are the filters that will be mounted on VST). In particular, as the adoption of linear transformations from one photometric system to another introduces uncertainties (limited precision and strong dependence on the color range), we directly build magnitudes and colors for our RR-Lyrae models by convolving model atmosphere fluxes with SDSS transmission functions [†]

The results of the application of this procedure to the computed models discussed in Marconi et al. 2006. Here I only remind the most important results.

- As already found for the Johnson-Cousins bands, the pulsation amplitudes vary with the wavelenght, increasing from $u$ to $g$ and decreasing from $g$ to $z$. Moreover, for a fixed filter, the amplitudes of fundamental pulsators decrease from the blue to the red edge, whereas the first overtone ones increase moving from the blue edge to

[†]The SDSS transmission curves are available at url http://www.sdss.org/dr3/instruments/imager/index.html.

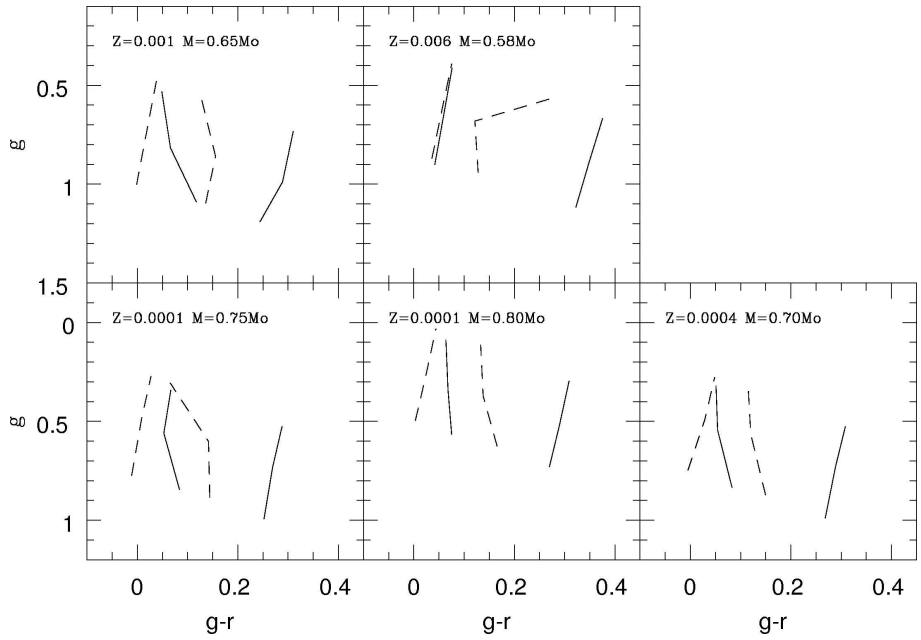


***Figure 3.6:*** *Predicted instability strip boundaries for both F (solid lines) and FO (dashed lines) models in the intensity-averaged* g *versus* g-r *plane. The adopted metal abundances and stellar masses are labelld.*

the middle of the instability strip and decrease as the red edge is approached.

- It also is important to note that, similarly to what happens for the Johnson-Cousins filters, the difference between magnitude-averaged and intensity-averaged magnitudes increases as the corresponding pulsation amplitude increases, reaching the highest values in the *u* and *g* bands. Moreover we confirm that intensity-averaged magnitudes better reproduce the behaviour of static values than the magnitude-averaged ones. Indeed the difference between the latter mean values and the static ones can reach 0.2 mag in the *g* band.

- Fig. 3.6 shows the predicted instability strip boundaries for both fundamental (solid lines) and first overtone (dashed lines) models in the intensity-averaged *g* versus *g-r* plane, for the metal abundances labelled in the different panels. Concerning the behaviour of the boundaries in the magnitude-period diagram, a linear regression throught all models yields, by taking into account the first (for the FOBE) and the last (for the FRE) pulsating models, the mass-dependent analytical relations reported in Table 3.6. Only for the $u$ filter we also find a non negligible dependence on the metal content and in all cases the standard deviations are of the order of few

***Table 3.6:*** *Analytical relations for the FOBE and FRE in the form* $M_i = a + b\log P + c\log M + d\log Z$. *The dispersion* $\sigma$ *(mag) is also reported.*

| $M_i$ | $boundary$ | $a$ | $b$ | $c$ | $d$ | $\sigma$ |
|---|---|---|---|---|---|---|
| u | FOBE | 0.40 | -2.32 | -1.95 | 0.086 | 0.03 |
| | FRE | 1.64 | -1.79 | -2.43 | 0.12 | 0.03 |
| g | FOBE | -1.04 | -2.43 | -2.14 | | 0.04 |
| | FRE | 0.18 | -1.99 | -2.34 | | 0.02 |
| r | FOBE | -1.12 | 2.63 | -1.85 | | 0.03 |
| | FRE | -0.07 | -2.23 | -1.92 | | 0.02 |
| i | FOBE | -1.11 | -2.72 | -1.86 | | 0.03 |
| | FRE | -0.18 | -2.34 | -1.96 | | 0.01 |
| z | FOBE | -1.09 | -2.78 | -1.91 | | 0.02 |
| | FRE | -0.22 | -2.40 | -2.05 | | 0.01 |

hundredths of magnitude.

- The transformed multifilter light curves can be reported in different color-color planes. Fig. 3.7 shows the theoretical loops in the *g-r* vs *u-g*, *r-i* vs *g-r* and *i-z* vs *r-i* diagrams for selected models at each adopted metallicity. We notice that the metallicity effect is more evident in *g-r* vs *u-g* plane due to the significant sensitivity of the *u* band on metal abundance. On the other hand, in the $r-i$ vs $g-r$ plane the loops are very narrow and the effect of metallicity is smaller, so that, once the metallicity is known, the comparison between theory and observations in this plane could be used to evaluate color excesses. As for the $i-z$ vs $r-i$ diagram, the predicted loops are very close to each other and the metallicity dependence is much less evident than for the other color combinations.

- Figs. 3.8 and 3.9 show the amplitude ratios between the Johnson V and the SDSS *g* bands (left top panel of each figure) and between the *u, r, i, z* and the *g* bands, for fundamental and first overtone models respectively.

  We notice that the *g* band amplitude is systematically higher than the V amplitude, independently of the period and the adopted metal abundance (see labels). At the same time the amplitudes in the *r, i, z* filters scale with a constant mean ratio (ranging from about 0.7 to 0.5 from *r* to *z*) with the *g* band amplitude, thus suggesting that only few points along the lightcurves in these filters will be required, if the

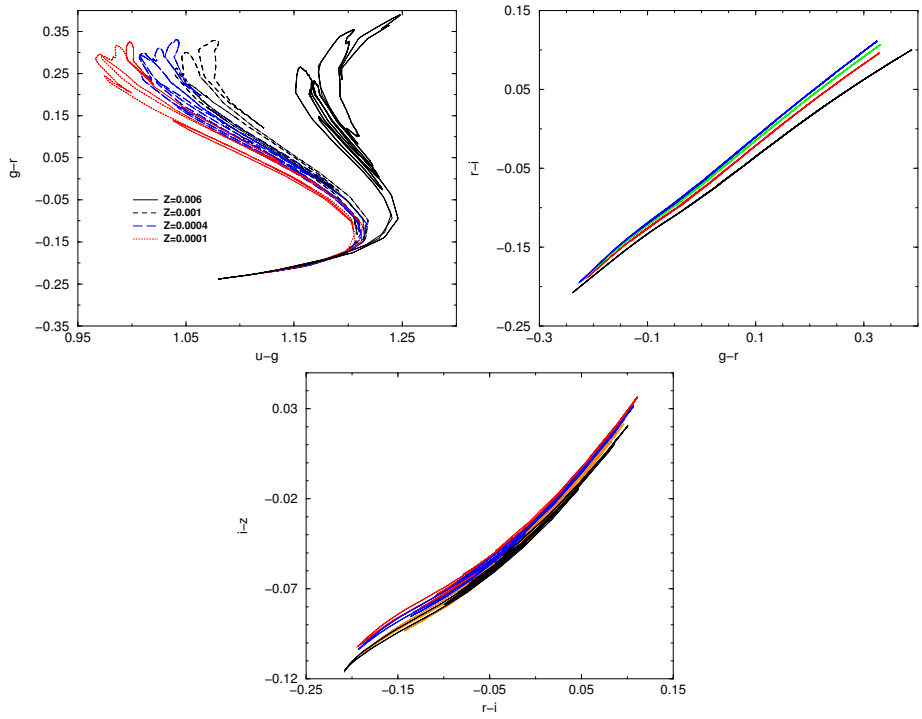


***Figure 3.7:*** *Theoretical loops in the* g-r *vs* u-g *(left),* r-i *vs* g-r *(middle) and* i-z *vs* r-i *(right) diagram for selected models at each adopted metallicity.*

g curve is accurately sampled. As for the *u* band, the scatter is larger due to the significant dependence on the adopted metallicity. This occurrence is more evident for fundamental models, which are characterized by more asymmetric light curves and higher pulsation amplitudes.

## 3.2 BL Herculis stars **(Marconi & Di Criscienzo, 2006, A&A, in press)**

To study BL Herculis stars, we have adopted the same pulsation code and the same physical and numerical assumptions used to compute RR Lyrae models. The various assumptions of mass, luminosity and metallicity, as reported in Table 3.7, are consistent with the evolutionary prescriptions (see Pietrinferni et al. 2004, 2006). This is the first time that a similar analysis is performed.

Linear regression through the model parameters allows us, also in this case, to derive analytical relations connecting the period of models to the intrinsic stellar parameters, namely mass, luminosity and effective temperature, i.e:

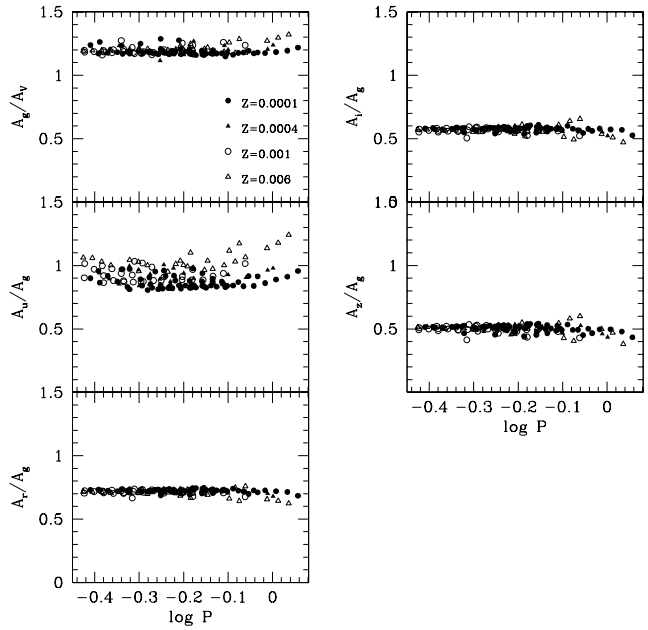


***Figure 3.8:*** *Amplitude ratios between the Johnson V and the SDSS* g *bands (left top panel) and between the* u, r, i, z *and the* g *bands for fundamental models.*

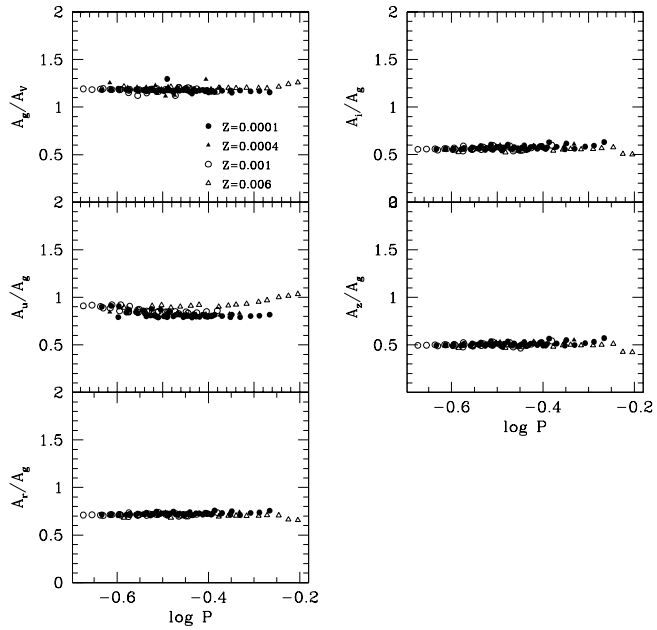


***Figure 3.9:*** *The same as the previous figure but for first overtone models.*

***Table 3.7:*** *Input parameters of the computed BL Her models. An helium abundance Y=0.24 has been adopted*

| Z | M/M$_\odot$ | LogL/L$_\odot$ | FOBE | FBE | FORE | FRE |
|---|---|---|---|---|---|---|
| 0.0001 | 0.60 | 1.95 | - | 6850 | - | 5750 |
| | | 2.05 | - | 6750 | - | 5650 |
| | | 2.15 | - | 6750 | - | 5550 |
| | 0.65 | 1.91 | 6950 | 6850 | 6100 | 5750 |
| | | 2.01 | 6750 | 6850 | 6300 | 5750 |
| | | 2.11 | - | 6750 | - | 5550 |
| 0.001 | 0.50 | 2.11 | - | 6650 | - | 5450 |
| | | 2.41 | - | 6350 | - | 5150 |
| | 0.55 | 1.81 | 6875 | 6850 | 6400 | 5650 |
| | | 1.91 | - | 6850 | - | 5550 |
| | | 2.01 | - | 6750 | - | 5450 |
| | 0.65 | 1.81 | 7050 | 6750 | 6650 | 5750 |
| | | 1.91 | 6850 | 6750 | 6150 | 5650 |
| | | 2.01 | 6650 | 6850 | 6350 | 5650 |
| 0.004 | 0.55 | 1.81 | - | 6950 | - | 5750 |
| | | 1.91 | - | 6850 | - | 5650 |
| | | 2.01 | - | 6750 | - | 5450 |

$$\log P = 11.579(\pm 0.015) + 0.893 \log L - 0.89 \log M - 3.54 \log T_e \tag{3.15}$$

for fundamental pulsators and:

$$logP = 10.784(\pm 0.003) + 0.806 \log L - 0.66 \log M - 3.31 \log T_e \tag{3.16}$$

for first overtone ones.

As for RR Lyrae stars, also in this case, for each given metallicity, mass and luminosity, we have calculated the maximum and minimum effective temperature. It is important to note that these calculations confirm the earlier suggestion by Bono et al. 1997 (a, b, c) that, for a given helium content and mass, there exist an "intersection" luminosity $L_{IP}$ where $T_e(FOBE)$=$T_e(FBE)$ above which only the fundamental mode has a stable non-linear limit cycle. As shown by Di Criscienzo et al. 2006, current evolutionary models show that the BL Her variables occur at luminosity higher than this intersection point: therefore in the following I will consider only fundamental models. The location of the

red boundary of the instability strip is expected to depend on the efficiency of convection and, in particular, on the value of the mixing length parameter $l/H_p$ we assume to close the nonlinear system of dynamical and convective equations. To test this occurrence we have computed additional models to derive the position of the FRE when $l/H_p$ is increased from 1.5 to 2.0 and we confirm the general trend shown by RR Lyrae and Classical Cepheid models (Fiorentino et al. 2006, in preparation) that the FRE moves toward higher effective temparatures as $l/H_p$ increases. In addiction, one finds that this effect is less important with increasing the luminosity. In particular for $M = 0.50M_{\odot}$ and Z=0.001 the FRE blueshift is of about 200 K at $\log L/L_{\odot} = 2.01$ but reduces to less than 100 K for $\log L/L_{\odot} = 2.41$. This occurrence is due to the reduced density values, and in turn to the increase of the required superadiabaticity, in the outer layers of stellar structures with low mass and very high luminosity.

### 3.2.1 Light curves and pulsation amplitudes

A subsample of bolometric light curves obtained for the calculated models ($Z$=0.001, $M$=0.65$M_{\odot}$ and the labelled luminosity levels) is shown in Fig. 3.10.

All these curves show a large variety of shapes, which is perhaps the most striking feature of BL Her models as already suggested by Moskalik and Buchler (1994). In all the sequences the presence and the progression of the main bump is evident in analogy of what observed to Classical Cepheids with periods around 10 days (the well known Hertzsprung progression). In order to compare theoretical results with observations, the bolometric lights curves have been transformed into the photometric bands UBVRIJK, using bolometric corrections and temperature-color relations provided by Castelli, Gratton & Kurucz (1997a,b). In this way, light-curve amplitudes and mean absolute magnitudes, either intensity-weighted $\langle M \rangle$ or magnitude-weighted (M), are derived in various photometric bands. After having tested that also in this case, intensity-weighted magnitudes approximate better the static values than magnitude-weighted ones, similarly to what found for RR Lyrae and Classical and Anomalous Cepheids (Caputo, Marconi, Ripepi 1999, Marconi et al. 2003, 2004), in the following I give all the relations with $\langle M \rangle$ because empirical investigations usually provide this type of mean values.

Fig. 3.11 shows the behaviour of visual amplitudes as a function of the period for different values of metallicity, mass and luminosity. As for RR Lyrae models we find that,

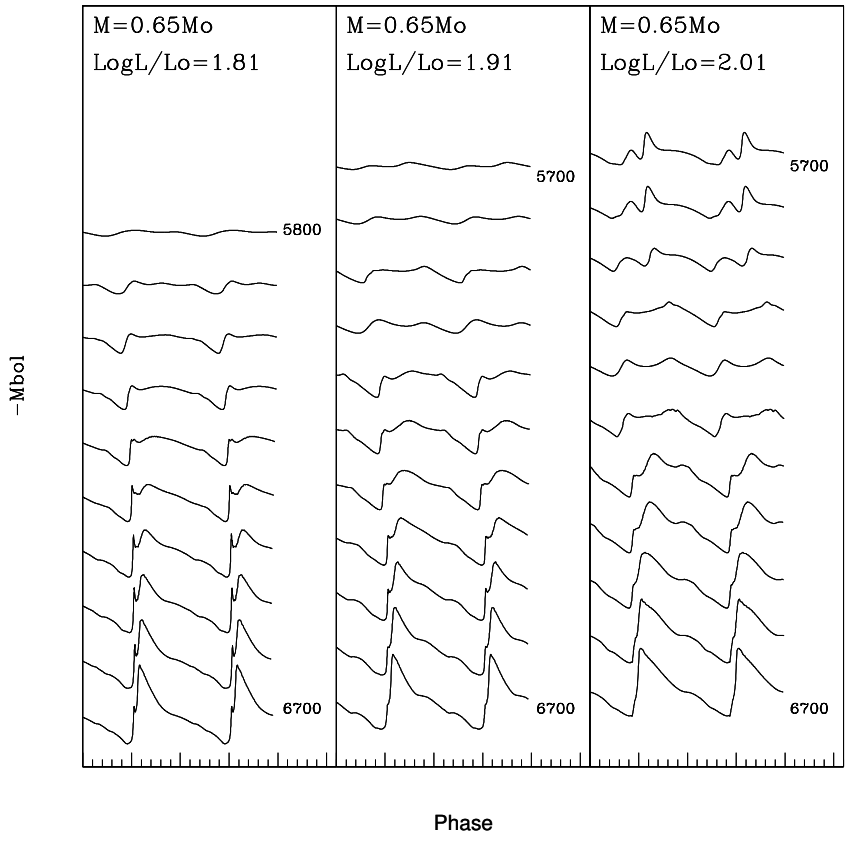


***Figure 3.10:*** *Theoretical bolometric light curves for a subsample (Z=0.001 and M=0.65 $M_{\odot}$) of fundamental models. The luminosity levels are labelled.*

for each period, the amplitude increases as the luminosity increases and as the mass decreases (middle and bottom left panels respectively), while it remains quite constant in the considered metallicity range, at fixed mass and luminosity (top left panel).

It is important to stress that part of the observed behaviour in the period-amplitude diagram is due to the dependence of period on mass and luminosity, as simply derived even from a simple linear adiabatic approach. The change in the pulsation in amplitude is mainly related to the distance from the FBE, as shown in the two right panels of the same figure. The deviation from linearity of the hightest luminosity level models (top panel of Fig. 3.11) is related to complex coupling between pulsation and convection for these low density and cool structures (see also the discussion in Bono et al. 1997c for a similar behaviour in high luminosity RR Lyrae stars). However in the range of linearity we obtain:

$$\log P = -0.033(\pm 0.034) - 1.15 \log M - 0.475 \log\langle M_V \rangle - 0.195 A_V \tag{3.17}$$

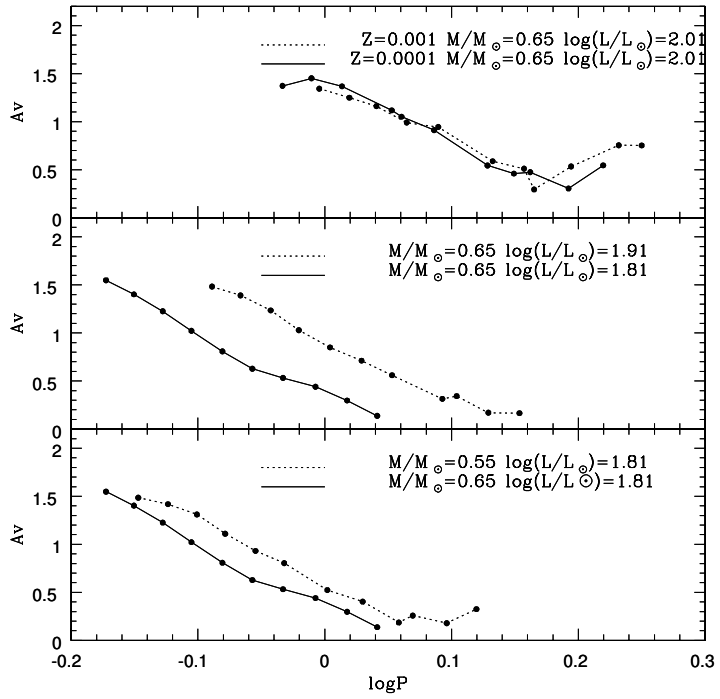


***Figure 3.11:*** *Right panels: visual amplitudes versus periods for selected models varying the metallicity at fixed mass and luminosity (upper panel), varying the luminosity at fixed mass and metallicity (Z=0.001, intermediate panel) and varying the mass at fixed luminosity and metallicity (Z=0.001, lower panel.). Left panels: the same but visual amplitudes are now plotted versus* $\Delta$ *log(P)=logP*$-$*log*$P_{FOBE}$

It is important to stress that this dependence of the period on amplitude is, within the errors, in agreement with those found for RR Lyrae in previous section.

### 3.2.2 The instability strip

A linear regression through the data reported in Table 3.7 provides the following analytical relations:

$$\log T_e(FBE) = 3.912(\pm 0.005) - 0.035 \log L + 0.048 \log M \tag{3.18}$$

$$\log T_e(FRE) = 3.925(\pm 0.005) - 0.075 \log L + 0.118 \log M \tag{3.19}$$

with a rms of 0.005 , valid on the adopted range of metallicity and stellar mass. The location of these edges in the $M_V$-log$P$ plane is presented in Fig. 3.12 and the corresponding

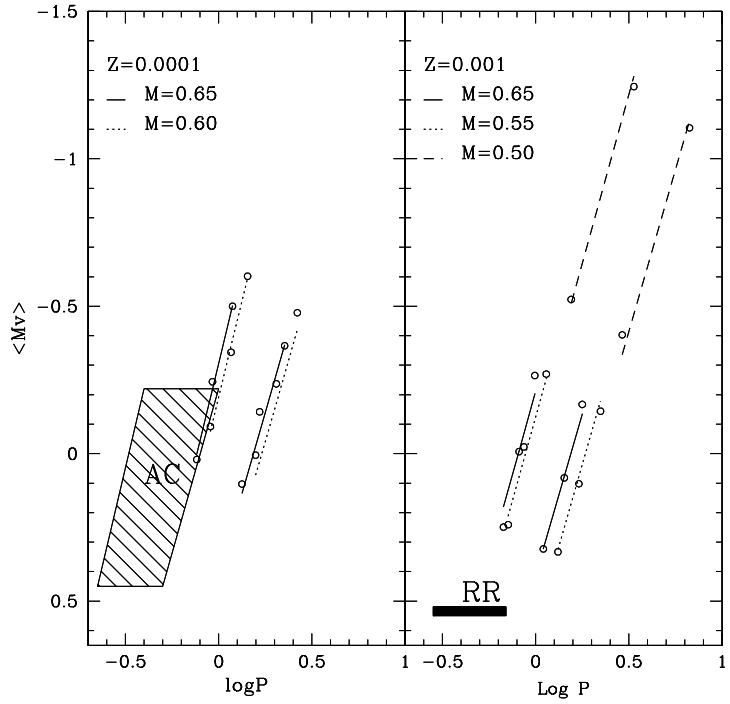


***Figure 3.12:*** *Dependence of the boundaries of the pulsation region on luminosity in the $M_V$-log$P$ plane for the labeled values of mass and metallicity. In the left panel is also reported the AC instability strip for a mass of 1.3$M_\odot$ (Marconi et al. 2004) while in the right one the predicted RR Lyrae instability strip for $Z$=0.001, as obtained by synthetic simulations, is shown.*

analytical relations are:

$$\langle M_V(FBE)\rangle = -0.36(\pm 0.04) - 1.55\log M - 2.37\log P + 0.05(\pm 0.03)\log Z \quad (3.20)$$

$$\langle M_V(FRE)\rangle = 0.14(\pm 0.03) - 2.25\log M - 2.17\log P + 0.05(\pm 0.02)\log Z \quad (3.21)$$

From the same figure, we note that the BL Her instability strip is the extension at higher luminosities of the fundamental instability region for RR Lyrae stars, whereas it does overlap the one for Anomalous Cepheids (ACs), since the AC FRE is hotter than the BL Her FBE (see also Caputo et al. 2004). This results, also related to the significant mass difference between the two classes of pulsators, is fully consistent with the empirical evidence that ACs are brighter than BL Her stars, for a given period.

# 4

# Comparison with observed RR Lyrae stars and Population II Cepheids

*In this chapter I compare the pulsational models of RR Lyrae and BL Herculis stars with the variables observed in metal poor fields, especially Galactic globular clusters. In particular I use the pulsational relations obtained for RR lyrae in the previous chapter, leaving the mass as a free parameter and using the average mass of the RR Lyrae stars, as derived from synthetic HB simulations based on HB models at different metallicity. This approach allow us to obtain individual distance moduli for the observed stars. As for Population II Cepheids, I directly combine the calculated pulsational models with the updated evolutionary scenario to obtain syntetic models and mass independent relations. These are used to estimates the distance moduli of those Galactic globular clusters which have a blue Horizontal Branch and a very small number of RR Lyrae. A comparison between the distances obtained for RR Lyrae and for Population II Cepheids is performed in order to demostrate the self consistency of the adopted theoretical scenario.*

## 4.1 RR Lyrae

### 4.1.1 Comparison of models in Johnson-Cousin filters with current observations (Di Criscienzo et al. 2004, ApJ, 612)

The selected clusters are listed in Table 4.1, together with their [Fe/H] value (Kraft & Ivans 2003), HB type, apparent distance modulus $\mu_V$ and $E(B-V)$ reddening (from Harris 1996), and the source of RR Lyrae data*. The last two columns in Table 4.1 give the overall metal content $Z$ for a solar-scaled chemical composition (i.e., $\log Z$=[Fe/H]$-1.70$) and the average mass of the RR Lyrae stars, as derived from synthetic simulations based on HB models with $Z$=0.0001, 0.0003, 0.0006, 0.001, 0.003 and 0.006 (see Cassisi et al. 2004 and Fig. 4.1). A general overview of data is shown in Fig. 4.2, where the variables are plotted in the color-magnitude diagram according to intensity-averaged magnitudes, scaled to an arbitrary value $V_r$, and intrinsic colors, as derived using $E(B-V)$ values in Table 4.1. Filled and open dots are $RR_{ab}$ and $RR_c$ stars, as given by the authors, and some outliers with respect to the average distribution are marked.

Starting with the $PW$ relation, which is independent of the adopted mixing-length parameter, I show in Fig. 4.3 the comparison between observed $\langle W(BV)\rangle$ quantities and the predicted relation (see equation 3.10). For each cluster, $\log P_F^W$ is evaluated according to the mass and metal content listed in Table 4.1, while the solid lines drawn in the panels depict the predicted behavior at constant mass and metallicity, as reasonably adopted for RR Lyrae stars in a given globular cluster. In this reddening-free diagram, only the NGC 6934 variables exhibit a considerable scatter, suggesting that observational errors are possibly occurring in the data. For the remaining clusters, with the exception of very few outliers, the observed data fit quite well the predicted slope, allowing us to derive the intrinsic distance moduli labelled in the various panels of the figure and listed in column (2) of Table 4.2. It is quite interesting to note that these theoretical distance moduli appear in agreement with previous empirical determinations. This is shown in Fig. 4.4, where the

*[Fe/H] value by Harris (1996). Ref. (RR Lyrae) - Wa94: Walker 1994;SS95: Silbermann & Smith 1995; Co99: Corwin et al. 1999; Ol99:Olech et al. 1999; Wa96: Walker 1996; Ka01: Kaluzny et al. 2001;LC99: Lee & Carney 1999; Pi02: Piersimoni et al. 2002; CC01:Corwin & Carney 2001; Ka00: Kaluzny et al. 2000; Ca99: Caputo etal. 1999; Wa98: Walker 1998; Wa99: Walker, private communication.

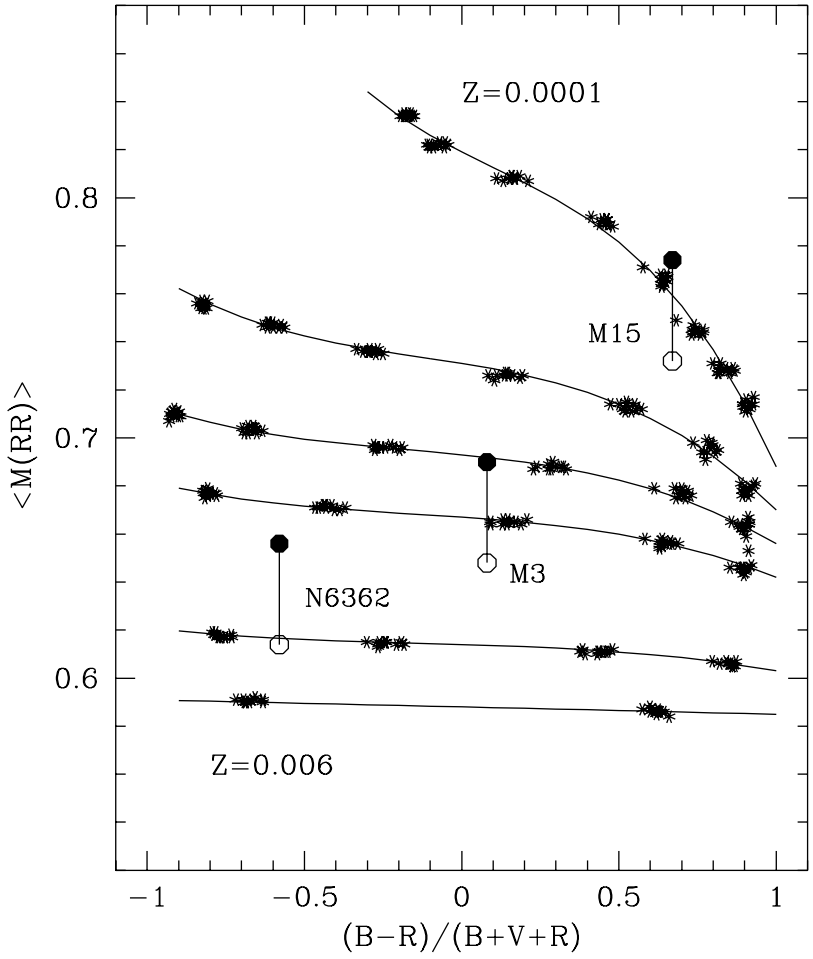


***Figure 4.1:*** *The average mass $\langle M(RR)\rangle$ (solar units) of synthetic RR Lyrae pulsators versus the HB morphology, as inferred from synthetic simulations with metal content Z=0.0001, 0.0003, 0.0006, 0.001, 0.003 and 0.006 (top to bottom). The large dots depict three selected clusters (M15, M3 and NGC 6362) which are plotted according to their observed HB type and measured [Fe/H] value (see Table 4.1), under the assumption of solar-scaled ([$\alpha$/Fe]=0, filled dots) or $\alpha$-enriched ([$\alpha$/Fe]$\sim$0.5, open dots) chemical compositions.*

***Table 4.1:*** *Selected RR Lyrae rich Galactic globular clusters listed with their [Fe/H] value (Kraft & Ivans 2003), HB type, apparent distance modulus $\mu_V$ and $E(B-V)$ reddening (Harris 1996). The reference of RR Lyrae data is also given (see the footnote in this page). The last two columns give the overall metal content $Z$, adopting a solar-scaled chemical composition, and the average mass $\langle M(RR)\rangle$ of RR Lyrae stars, as estimated by synthetic horizontal branch simulations*

| NGC/IC | [Fe/H] | HB | $\mu_V$ (mag) | $E(B-V)$ (mag) | Ref. | log$Z$ [$\alpha$/Fe=0] | $\langle M(RR)\rangle$ $M/M_\odot$ |
|---|---|---|---|---|---|---|---|
| 4590-M68 | $-2.43$ | 0.44 | 15.19 | 0.05 | Wa94 | $-4.13$ | 0.80 |
| 7078-M15 | $-2.42$ | 0.67 | 15.37 | 0.10 | SS95 | $-4.12$ | 0.77 |
| 5466 | $-2.22$ | 0.58 | 16.00 | 0.00 | Co99 | $-3.92$ | 0.74 |
| 6809-M55 | $-1.85$ | 0.87 | 13.87 | 0.08 | Ol99 | $-3.55$ | 0.69 |
| 4499* | $-1.60$ | 0.11 | 17.09 | 0.23 | Wa96 | $-3.30$ | 0.70 |
| 6934 | $-1.59$ | 0.25 | 16.29 | 0.10 | Ka01 | $-3.20$ | 0.70 |
| 7089-M2 | $-1.56$ | 0.96 | 15.49 | 0.06 | LC99 | $-3.26$ | 0.66 |
| 3201 | $-1.56$ | 0.08 | 14.21 | 0.23 | Pi02 | $-3.26$ | 0.69 |
| 5272-M3 | $-1.50$ | 0.08 | 15.12 | 0.01 | CC01 | $-3.20$ | 0.69 |
| 5904-M5 | $-1.26$ | 0.31 | 14.46 | 0.03 | Ka00+Ca99 | $-2.96$ | 0.66 |
| 1851 | $-1.19$ | $-0.36$ | 15.47 | 0.02 | Wa98 | $-2.89$ | 0.66 |
| 6362 | $-1.15$ | $-0.58$ | 14.67 | 0.09 | Wa99 | $-2.85$ | 0.66 |

***Table 4.2:*** *$E(B-V)$ values and distance moduli (both in magnitudes) for the selected clusters, as obtained from the various predicted relations.*

| NGC/IC | $\mu_0$ $PWBV$ | $E(B-V)$ $CA_{1.5}$ | $E(B-V)$ $CA_{2.0}$ | $\mu_V$ $PMA_{1.5}$ | $\mu_V$ $PMA_{2.0}$ |
|---|---|---|---|---|---|
| 4590-M68 | 15.08±0.07 | $-$0.01±0.02 | +0.04±0.02 | 15.05±0.10 | 15.24±0.10 |
| 7078-M15 | 15.13±0.08 | +0.02±0.02 | +0.07±0.02 | 15.23±0.08 | 15.41±0.08 |
| 5466 | 16.07±0.07 | $-$0.01±0.04 | +0.04±0.03 | 16.07±0.09 | 16.21±0.08 |
| 6809-M55 | 13.60±0.09 | +0.07±0.04 | +0.12±0.04 | 13.85±0.05 | 14.01±0.05 |
| 4499 | 16.45±0.08 | +0.16±0.04 | +0.21±0.04 | 17.01±0.08 | 17.17±0.08 |
| 6934 | 15.86±0.12 | +0.10±0.09 | +0.15±0.09 | 16.20±0.14 | 16.35±0.13 |
| 7089-M2 | 15.45±0.11 | $-$0.03±0.03 | +0.02±0.03 | 15.45±0.09 | 15.63±0.09 |
| 3201 | 13.28±0.08 | +0.24±0.04 | +0.29±0.04 | 14.10±0.13 | 14.28±0.12 |
| 5272-M3 | 15.06±0.07 | $-$0.03±0.02 | +0.01±0.02 | 15.00±0.08 | 15.18±0.07 |
| 5904-M5 | 14.27±0.16 | +0.00±0.03 | +0.05±0.03 | 14.36±0.09 | 14.54±0.09 |
| 1851 | 15.42±0.13 | $-$0.03±0.04 | +0.02±0.04 | 15.38±0.17 | 15.56±0.17 |
| 6362 | 14.45±0.09 | +0.01±0.03 | +0.06±0.03 | 14.55±0.06 | 14.71±0.05 |

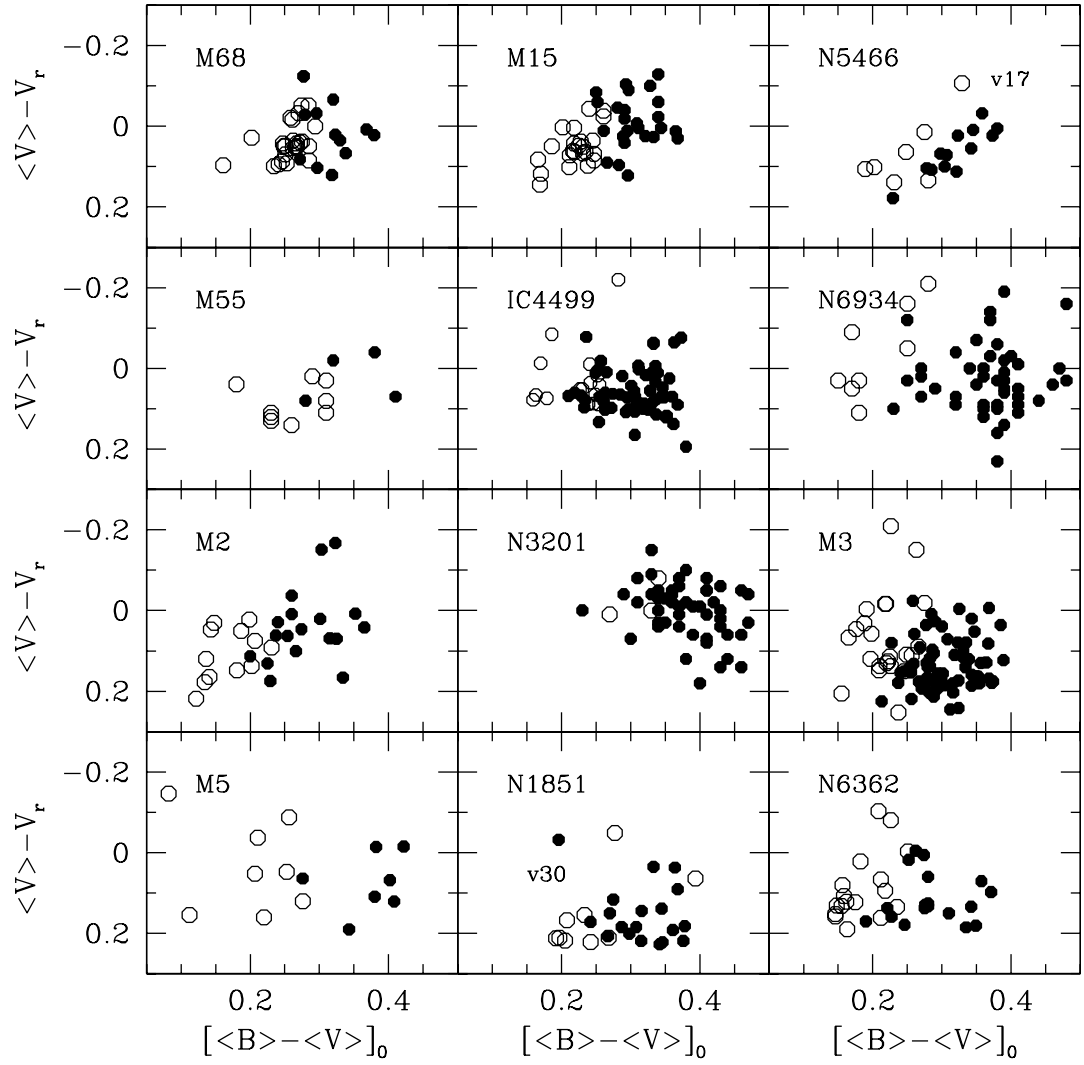


***Figure 4.2:*** *Color-magnitude diagram of globular cluster $RR_{ab}$ (filled symbols) and $RR_c$ (open symbols) variables, according to intensity-averaged magnitudes scaled to an arbitrary value $V_r$ and $\langle B\rangle - \langle V\rangle$ colors corrected with the $E(B-V)$ values in Table 4.1.*

relative values with respect to IC 4499, taken as reference cluster, are plotted versus the evaluations given by Kovacs & Walker (2001). Before proceeding with further comparison between theory and observation, one has to notice that all other predictions depend on the adopted mixing-length parameter. One may attempt to have a look on such an issue making use of the predicted Color-Amplitude fundamental relation, which is independent of the pulsator mass, and of the reddening values given in Table 4.1. Fig.4.5 shows the visual amplitude of $RR_{ab}$ stars in our sample versus the intrinsic color $[\langle B\rangle - \langle V\rangle]_0$, in

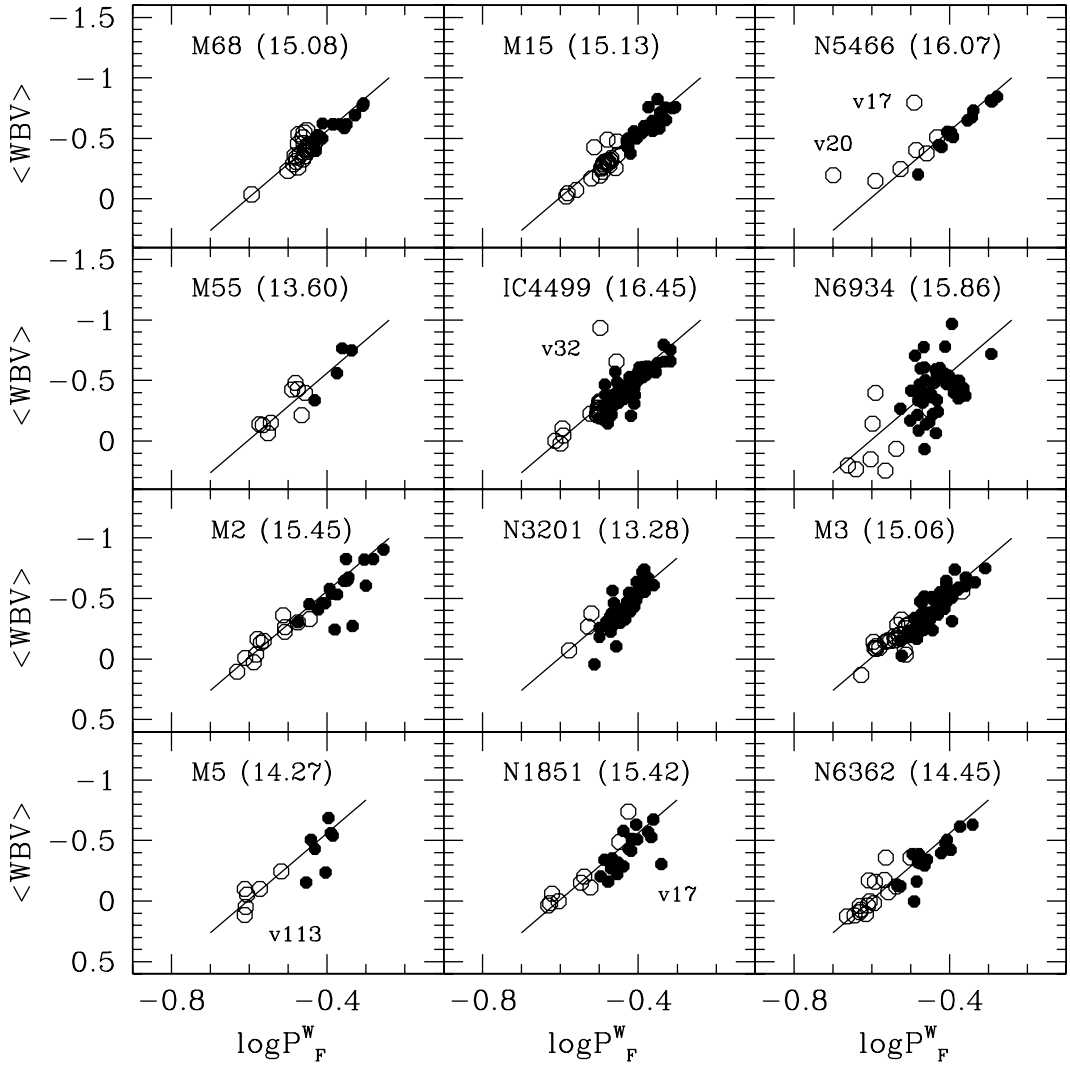


***Figure 4.3:*** *Comparison between predicted and observed $PW(BV)$ relations (symbols as in Fig. 4.1). The period of c-type variables is fundamentalised and the solid lines depict the predicted behavior at constant mass. The derived intrinsic distance moduli are given in each panel.*

comparison with the theoretical relations at $l/H_p$=1.5 (equation 3.6: solid line) and 2.0 (equation 3.8: dashed line). Disregarding M5 and M55, for the scarcity of data, and NGC 6934, for the well known significantly inhomogeneous reddening, one finds that all the remaining clusters seem to exclude $l/H_p$=1.5, except NGC 3201 and NGC 5466. On this basis, even if tempted to take $l/H_p$=2.0 as the preferred choice, I keep both the alternative values and use equations 3.6 and 3.8 to derive the $E(B-V)$ values listed in columns (3) and (4) of Table 4.2.

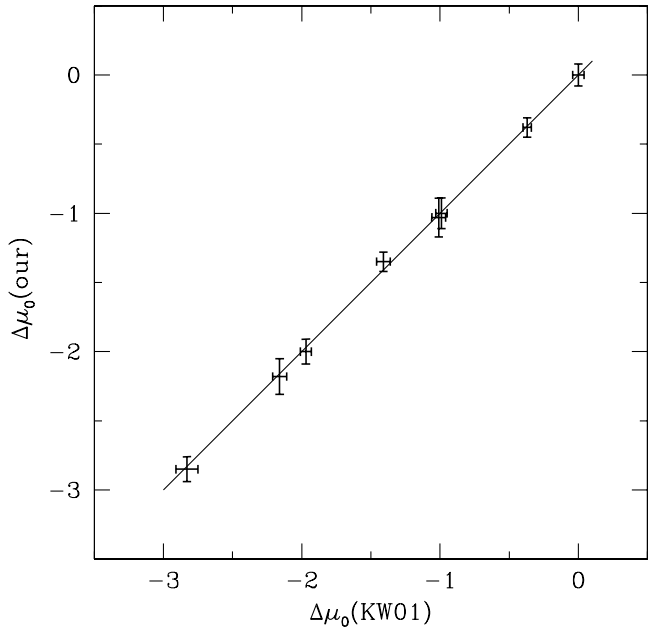


***Figure 4.4:*** *Comparison between our predicted intrinsic distance moduli and those derived by Kovacs & Walker (2001). The values are scaled to the intrinsic distance modulus of IC 4499.*

Adopting again the mass values in Table 4.1, I use now the predicted $PMA$ relation (see equations 3.4 and 3.5) for fundamental pulsators to estimate the apparent distance modulus. Fig. 4.6 shows the $RR_{ab}$ variables plotted in the $A_V$-log$P_F^*$ plane, in comparison with the predicted behavior at constant mass and $l/H_p$=1.5 (solid line). The derived apparent distance moduli are labelled in the various panels and listed in column (5) in Table 4.2, while the following column in the same table gives the results of a similar comparison, but with $l/H_p$=2.0.

Finally, I show in Fig. 4.7 the comparison between the observed distribution of RR Lyrae stars in the $\langle V\rangle$-log$P$ plane and the predicted edges of the instability strip, as estimated inserting the mass values in Table 4.1 into equations 3.2 and 3.3. I start fitting the predicted FOBE at $l/H_p$=1.5 (solid line at the left) to the observed distribution of $c$-type variables under the condition that no $c$-type variables are left in the hot stable region. As

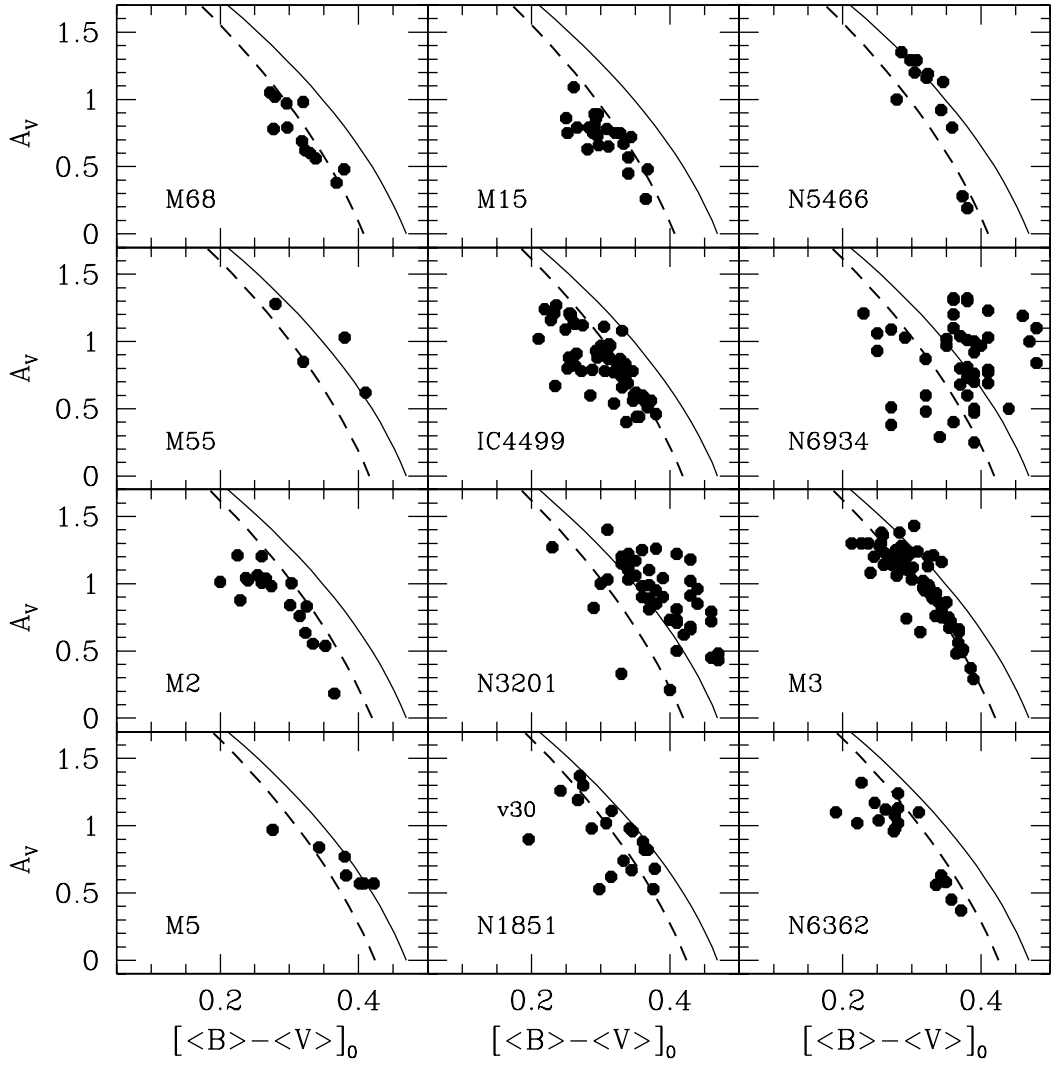


***Figure 4.5:*** *Visual amplitude of cluster $ab$-type variables versus the intrinsic $[\langle B\rangle - \langle V\rangle]_0$ color, compared with the predicted relation at $l/H_p$=1.5 (solid line) and $l/H_p$=2.0 (dashed line).*

shown in Fig.4.7, the apparent distance modulus derived in such a way (the values are labelled in the panels and listed in column (2) of Table 4.3) yields a quite good agreement between the $ab$-type distribution and the predicted FRE (solid line at the right), except for M68, M15, NGC 5466, M55 and NGC3201. For these clusters, the observed period distribution of $ab$-type variables would suggest a red edge as depicted by the dashed line. In other words, under the assumption that the whole instability strip is populated, for these clusters the right value of the distance modulus to fit the observed distribution of $ab$-type variables is smaller by $\sim 0.15$ mag than the value derived from the FOBE-procedure (see

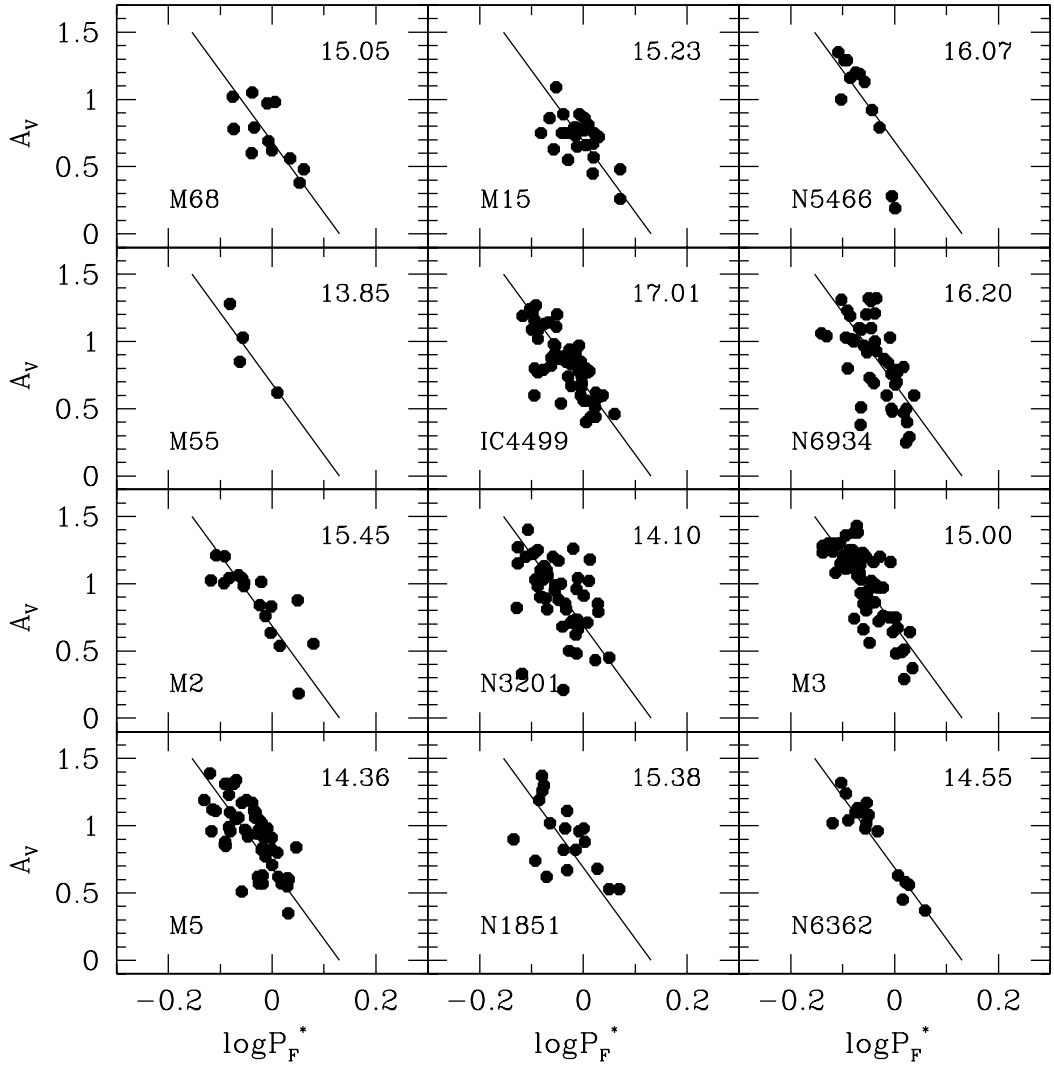


***Figure 4.6:*** *As in Fig. 4.5, but for the $PMA$ relation of fundamental pulsators at $l/H_p$=1.5. The solid lines are the predicted slope at constant mass. The derived apparent distance moduli are given in each panel.*

column (3) in Table 4.3).

Let me now repeat the comparison, but with $l/H_p$=2.0. Since the predicted FOBE becomes fainter by $\sim$ 0.05 mag, the right distance modulus to fit the observed distribution of $c$-type variables decreases by the same quantity. However, the predicted FRE becomes brighter by $\sim$ 0.14 mag and, as shown in Fig.4.8 , for some clusters several $ab$-type variables would have longer periods than the predicted FRE. Specifically, for IC 4499, NGC 6934, M2, M3, M5, NGC1851 and NGC6362 the comparison of the predicted FRE to the

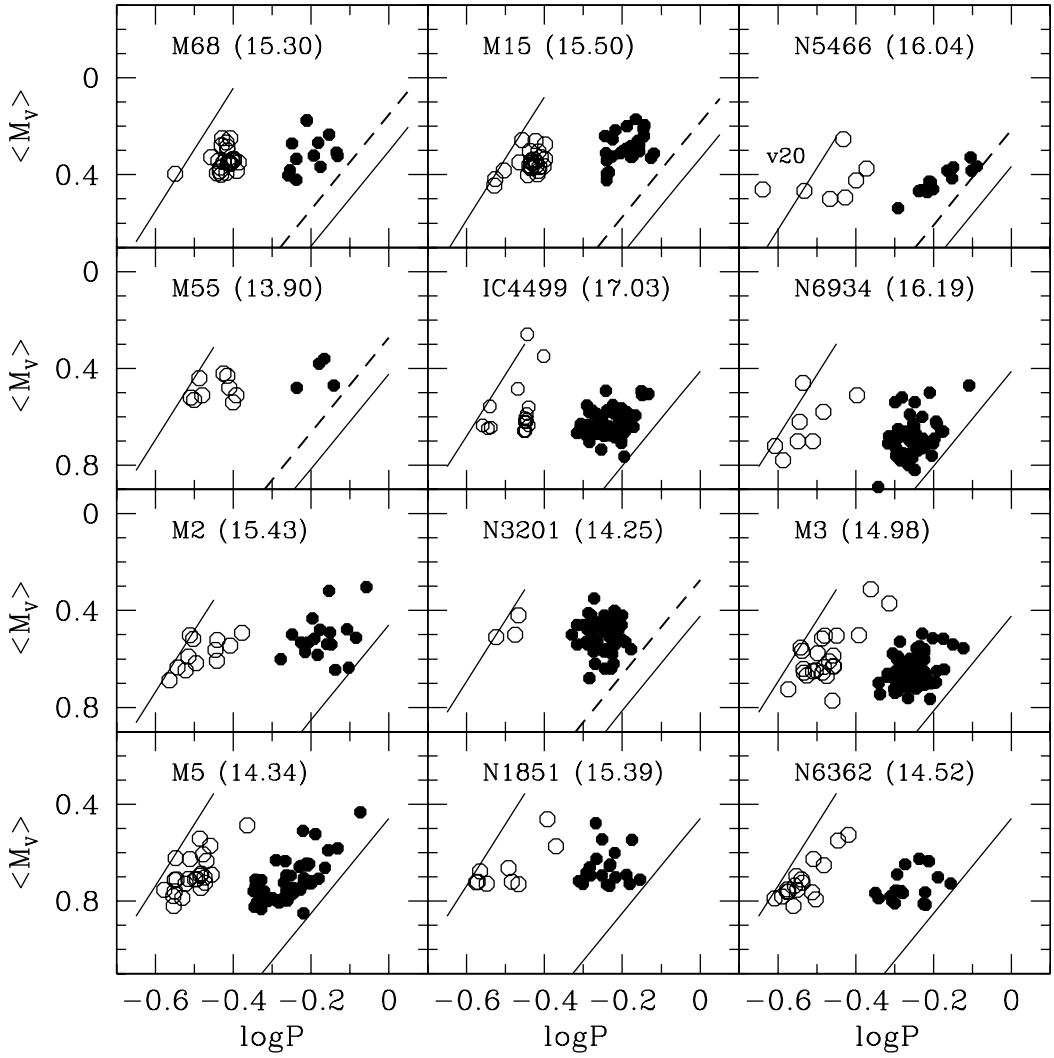


***Figure 4.7:*** *Observed distribution of RR Lyrae stars in the $M_V$-log$P$ plane in comparison with the predicted edges of the instability strip at $l/H_p$=1.5 (solid lines). The distance modulus labelled in each panel is obtained by fitting the observed distribution of c-type variables (open symbols) to the predicted FOBE. The dashed lines depict the observed red limit of ab-type variables under the hypothesis of a well populated instability strip.*

observed red edge (dashed line) would yield now a distance modulus which is larger by $\sim 0.10$ mag than the one derived from the FOBE-procedure.

I summarize in Table 4.3 the distance moduli inferred from the $M_V$-log$P$ distribution. One can conclude that the assumption $l/H_p$=1.5 yields rather discordant results for M68, M15, NGC 5466, M55, and NGC3201, whereas a quite close agreement is obtained with $l/H_p$=2.0. On the other hand, the assumption $l/H_p$=2.0 yields rather discordant results for

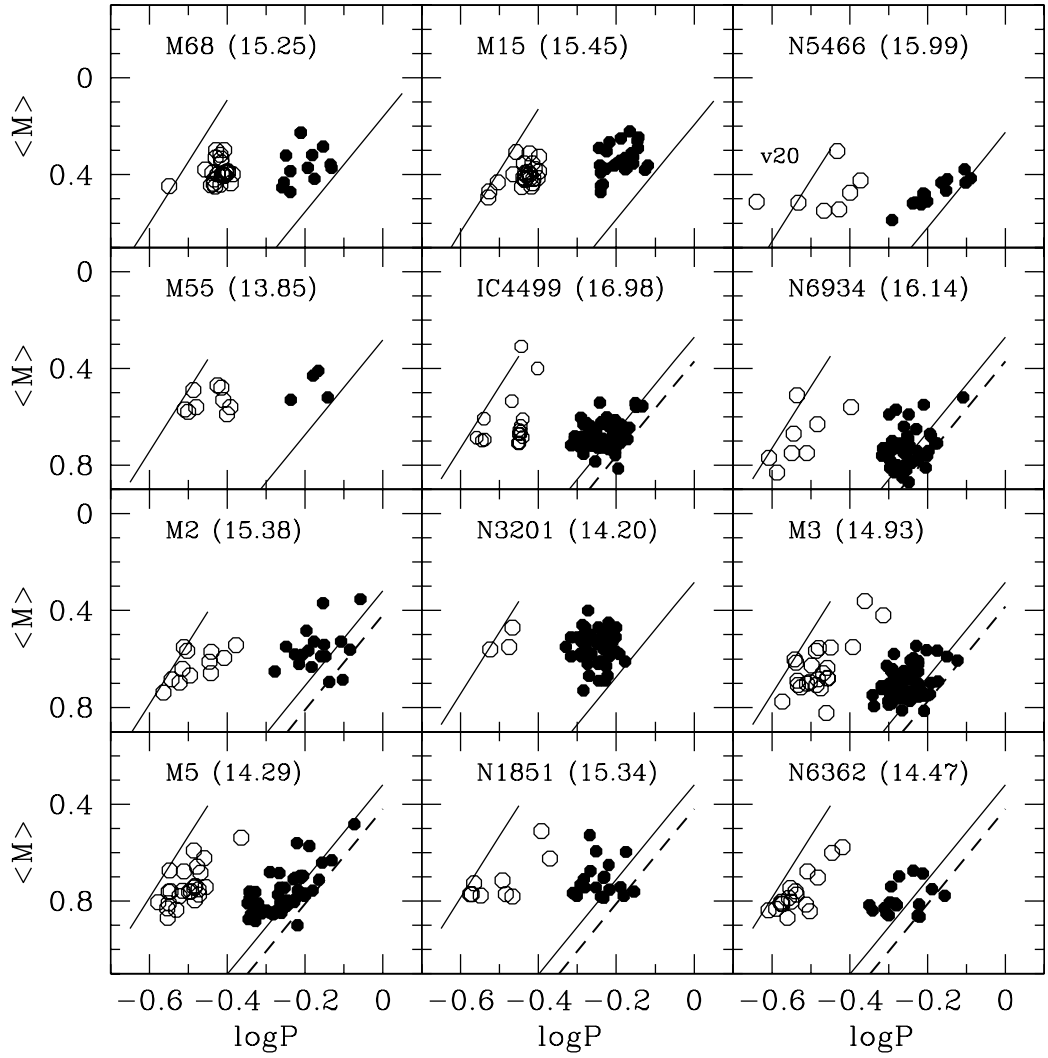


***Figure 4.8:*** *As in Fig. 4.7, but adopting $l/H_p$=2.0.*

the remaining clusters (IC 4499, NGC 6934, M2, M3, M5, NGC1851 and NGC6362), for which a better agreement is reached with $l/H_p$=1.5. In summary, present results would suggest that the assumption of a constant mixing-length parameter should be revisited. However, recent evolutionary studies seem to exclude any trend of the $l/H_p$ ratio with the metal content (see Palmieri et al. 2002, Lastennet et al. 2003). Conversely, specific tests aiming at fitting the light curves of observed pulsators (both RR Lyrae stars and Classic Cepheids) with modeled curves have shown that first overtone (hotter pulsators) light curves are well reproduced with $l/H_p$=1.5, whereas in the case of fundamental variables (cooler pulsators) a value $l/H_p \geq 1.8$ is needed in order to properly reproduce both

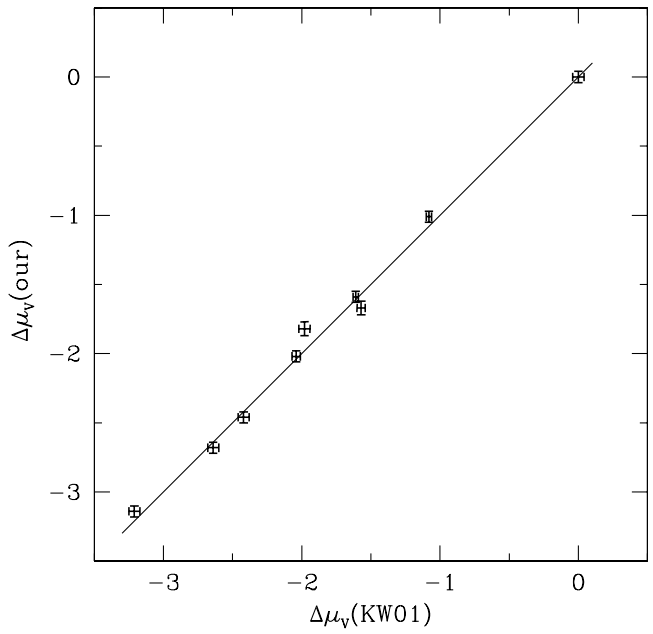


***Figure 4.9:*** *As in Fig. 4.4, but with the apparent distance moduli reported in column (6) of Table 4.3.*

the amplitude and the morphology of observed curves (see Bono, Castellani & Marconi 2000, 2002; Castellani, Degl'Innocenti & Marconi 2002; Di Criscienzo, Marconi, Caputo 2003, Marconi & Clementini 2005). According to such a suggestion of a mixing-length parameter increasing from the FOBE to the FRE, we eventually list in column (6) of Table 4.3 the apparent distance modulus of each cluster, as given by the weighted mean over the values listed in column (6) of Table 4.2 and in column (2) and column (5) of Table 4.3. As shown in Fig. 4.9, the comparison between our relative distance moduli and those obtained by Kovacs & Walker (2001) on the basis of empirical relations based on Fourier parameters of the light curves discloses again a quite good agreement. As for the absolute values, let us remark that the distance moduli reported in Table 4.3 hold adopting the SHB simulations depicted in Fig.4.1, CGKa and CGKb bolometric corrections, as well as solar-scaled chemical compositions. Concerning this last point, the

***Table 4.3:*** *FOBE and FRE distance moduli (both in magnitudes) for the selected clusters, as obtained with different assumptions on the mixing-length parameter. The last column gives the adopted average distance modulus.*

| NGC | $\mu_V$(FOBE$_{1.5}$) | $\mu_V$(FRE$_{1.5}$) | $\mu_V$(FOBE$_{2.0}$) | $\mu_V$(FRE$_{2.0}$) | $\langle\mu_V\rangle$ |
|---|---|---|---|---|---|
| 4590-M68 | 15.30±0.07 | 15.15±0.08 | 15.25±0.07 | 15.25±0.08 | 15.27±0.05 |
| 7078-M15 | 15.50±0.07 | 15.35±0.08 | 15.45±0.07 | 15.45±0.08 | 15.46±0.04 |
| 5466 | 16.04±0.07 | 14.99±0.08 | 15.99±0.07 | 15.99±0.08 | 16.08±0.04 |
| 6809-M55 | 13.90±0.07 | 13.75±0.08 | 13.85±0.07 | 13.85±0.08 | 13.95±0.04 |
| 4499 | 17.03±0.07 | 17.03±0.08 | 16.98±0.07 | 17.08±0.08 | 17.09±0.04 |
| 6934 | 16.19±0.07 | 16.19±0.08 | 16.14±0.07 | 16.24±0.08 | 16.23±0.05 |
| 7089-M2 | 15.43±0.07 | 15.43±0.08 | 15.38±0.07 | 15.48±0.08 | 15.50±0.04 |
| 3201 | 14.25±0.07 | 14.10±0.08 | 14.20±0.07 | 14.20±0.08 | 14.24±0.05 |
| 5272-M3 | 14.98±0.07 | 14.98±0.08 | 14.93±0.07 | 15.03±0.08 | 15.07±0.04 |
| 5904-M5 | 14.34±0.07 | 14.34±0.08 | 14.29±0.07 | 14.39±0.08 | 14.41±0.04 |
| 1851 | 15.39±0.07 | 15.39±0.08 | 15.34±0.07 | 15.44±0.08 | 15.42±0.05 |
| 6362 | 14.52±0.07 | 14.52±0.08 | 14.47±0.07 | 14.57±0.08 | 14.63±0.04 |

same Fig. 4.1 shows the decrease of the RR Lyrae average mass ($\Delta\log M \sim -0.03$) if adopting $\alpha$-enriched ([$\alpha$/Fe]$\sim$0.5) chemical mixtures, namely $\Delta\log Z \sim$0.38 for any fixed [Fe/H] value. As a consequence, the values listed in Table 4.2 and Table 4.3 should be decreased by $\Delta\mu_V$(FOBE/FRE)$\sim -0.06$ mag, $\Delta\mu_V(PMA) \sim -0.03$ mag and $\Delta\mu_0(PW) \sim -0.01$ mag.

### 4.1.2 The Period-Amplitude relation (Bono et al. 2006, MNRAS, submitted)

Besides this role as distance indicators, in the last few years it has also been suggested that the RR Lyrae stars can be used for metal abundance determination using the distribution of the fundamental mode variables (RR$_{ab}$) in the Period-Amplitude ($PA$) plane, *i.e.*, in the Bailey diagram. In particular Alcock et al. (2000) used the visual amplitude $A_V$ of RR$_{ab}$ stars in the globular clusters M15 ([Fe/H]=$-$2.1), M3 ([Fe/H]=$-$1.6), and M5 ([Fe/H]=$-$1.4) to determine the following calibration:

$$[Fe/H] = -2.60 - 8.85(\log P_{ab} + 0.15A_V) \tag{4.1}$$

with an intrinsic accuracy of $\sim$ 0.3 dex. By adopting this relation, Alcock et al. (2000) estimated a median metallicity of [Fe/H]$\sim -1.6$ for a huge sample of RR$_{ab}$ stars in the

bar of the Large Magellanic Cloud (LMC), while Brown et al. (2004) derived a mean metallicity [Fe/H]=$-1.8\pm0.3$ for the 29 RR$_{ab}$ variables they identified in a halo field of M31. The suggested dependence of the Bailey diagram on the metal abundance is based on the observational evidence that, for a given amplitude, RR$_{ab}$ stars in Oosterhoff type II globular clusters tend to have longer periods than those in Oosterhoff type I clusters. On this ground, as already been argued by Clement & Shelton (1999), the $PA_V$diagram might not be a function of metal abundance: rather, it should depend on the evolutionary status of the RR Lyrae stars. The purpose of the present investigation is to use the extensive sets of nonlinear, convective pulsation models computed and described in the previous chapter to examine the $PA_V$ relation for RR$_{ab}$ stars in globular clusters. As just stressed in previous chapter, all the models pulsating in the fundamental mode show a linear correlation between the bolometric amplitude and the period (logarithmic scale) in the sense that, at fixed mass and luminosity, the amplitude increases when moving toward shorter periods. Varying the mass or the luminosity, one has that the amplitude increases as the luminosity increases or, by a less amount, as the mass decreases, for fixed period. In section 3.1 I have shown that all over the explored metallicity range the correlation between pulsation period, magnitude, amplitude, and mass can be approximated as by equation 3.4 at $l/H_p$=1.5, and equation 3.5 at $l/H_p$=2.0. According to these relations, the RR$_{ab}$ distribution in the $PA_V$ diagram, as described by the *pulsational* parameters

$$k(1.5)_{puls} = 0.13 - \log P_F - 0.189 A_V \tag{4.2}$$

and

$$k(2.0)_{puls} = 0.03 - \log P_F - 0.142 A_V, \tag{4.3}$$

is a function of the pulsator *evolutionary* properties, as given by

$$k(1.5)_{ev} = 0.385\langle M_V\rangle + 0.30 \log M \tag{4.4}$$

and

$$k(2.0)_{ev} = 0.385\langle M_V\rangle + 0.35 \log M \tag{4.5}$$

At variance with $k(1.5)_{puls}$ and $k(2.0)_{puls}$, the values of $k(1.5)_{ev}$ and $k(2.0)_{ev}$ cannot be directly estimated from observations, although one can expect that they depend on the

***Table 4.4:*** *Selected results of SHB simulations. For each metal content and mean mass of HB stars, the predicted mean values of the HB type and of the RR Lyrae mass, absolute magnitude and $k_{ev}$ parameters are listed, together with the rms dispersion about the mean.*

| $M(HB)$ | $\langle$HB$\rangle$ | $\langle M(RR)\rangle$ | $\langle M_V(RR)\rangle$ | $\langle k(1.5)_{ev}\rangle$ er | $\langle k(2.0)_{ev}\rangle$ er |
|---|---|---|---|---|---|
| | | | Z=0.0001 | | |
| 0.68 | +0.960±0.007 | 0.703±0.004 | 0.347±0.015 | 0.088±0.006 | 0.080±0.006 |
| 0.70 | +0.904±0.019 | 0.714±0.003 | 0.377±0.007 | 0.101±0.003 | 0.094±0.003 |
| 0.72 | +0.832±0.016 | 0.729±0.003 | 0.405±0.005 | 0.115±0.002 | 0.108±0.003 |
| 0.74 | +0.735±0.018 | 0.746±0.002 | 0.424±0.002 | 0.125±0.001 | 0.119±0.001 |
| 0.76 | +0.622±0.030 | 0.767±0.001 | 0.437±0.001 | 0.134±0.001 | 0.128±0.001 |
| 0.78 | +0.427±0.030 | 0.792±0.001 | 0.451±0.002 | 0.143±0.001 | 0.138±0.001 |
| 0.80 | +0.145±0.013 | 0.808±0.001 | 0.459±0.001 | 0.149±0.001 | 0.144±0.001 |
| 0.82 | −0.086±0.013 | 0.822±0.001 | 0.460±0.001 | 0.152±0.001 | 0.148±0.001 |
| 0.84 | −0.185±0.017 | 0.835±0.001 | 0.457±0.002 | 0.152±0.001 | 0.148±0.001 |
| | | | Z=0.0003 | | |
| 0.64 | +0.969 ±0.008 | 0.662±0.007 | 0.356±0.042 | 0.084±0.018 | 0.075±0.018 |
| 0.66 | +0.905 ±0.010 | 0.678±0.003 | 0.436±0.008 | 0.117±0.004 | 0.109±0.004 |
| 0.68 | +0.779 ±0.008 | 0.696±0.002 | 0.490±0.004 | 0.142±0.002 | 0.134±0.002 |
| 0.70 | +0.522 ±0.026 | 0.714±0.001 | 0.532±0.003 | 0.161±0.001 | 0.154±0.001 |
| 0.72 | +0.112 ±0.027 | 0.726±0.001 | 0.550±0.002 | 0.170±0.001 | 0.163±0.001 |
| 0.74 | −0.291±0.029 | 0.737±0.001 | 0.556±0.001 | 0.174±0.001 | 0.168±0.001 |
| 0.76 | −0.601±0.023 | 0.747±0.001 | 0.555±0.001 | 0.176±0.001 | 0.170±0.001 |
| 0.78 | −0.818±0.013 | 0.756±0.001 | 0.552±0.002 | 0.176±0.001 | 0.170±0.001 |
| | | | Z=0.0006 | | |
| 0.62 | +0.969 ±0.010 | 0.648±0.006 | 0.373±0.031 | 0.087±0.013 | 0.078±0.013 |
| 0.64 | +0.893 ±0.011 | 0.664±0.002 | 0.478±0.014 | 0.131±0.006 | 0.122±0.006 |
| 0.66 | +0.696 ±0.017 | 0.677±0.001 | 0.535±0.006 | 0.155±0.003 | 0.147±0.003 |
| 0.68 | +0.275 ±0.034 | 0.688±0.001 | 0.568±0.002 | 0.170±0.001 | 0.162±0.001 |
| 0.70 | −0.242±0.016 | 0.696±0.001 | 0.580±0.002 | 0.176±0.001 | 0.168±0.001 |
| 0.72 | −0.686±0.022 | 0.704±0.001 | 0.585±0.001 | 0.180±0.001 | 0.172±0.001 |
| 0.74 | −0.908±0.010 | 0.710±0.001 | 0.588±0.002 | 0.182±0.001 | 0.174±0.001 |
| 0.76 | −0.986±0.005 | 0.715±0.002 | 0.590±0.003 | 0.183±0.001 | 0.176±0.001 |
| | | | Z=0.001 | | |
| 0.60 | +0.977±0.006 | 0.636±0.005 | 0.409±0.063 | 0.099 ±0.025 | 0.089±0.025 |
| 0.62 | +0.889±0.014 | 0.646±0.003 | 0.514±0.022 | 0.141 ±0.009 | 0.132±0.009 |
| 0.64 | +0.639±0.032 | 0.657±0.002 | 0.583±0.010 | 0.170 ±0.004 | 0.161±0.004 |
| 0.66 | +0.108±0.024 | 0.665±0.001 | 0.609±0.003 | 0.181 ±0.001 | 0.172±0.001 |
| 0.68 | −0.436±0.027 | 0.672±0.001 | 0.624±0.003 | 0.188 ±0.001 | 0.180±0.001 |
| 0.70 | −0.803±0.010 | 0.678±0.001 | 0.631±0.002 | 0.192 ±0.001 | 0.184±0.001 |
| 0.72 | −0.961±0.007 | 0.682±0.002 | 0.634±0.003 | 0.194 ±0.001 | 0.186±0.001 |
| | | | Z=0.003 | | |
| 0.56 | +0.969±0.008 | 0.598±0.004 | 0.562±0.073 | 0.149 ±0.029 | 0.138±0.029 |
| 0.58 | +0.839±0.019 | 0.605±0.002 | 0.683±0.025 | 0.198 ±0.010 | 0.187±0.010 |
| 0.60 | +0.402±0.032 | 0.611±0.001 | 0.733±0.006 | 0.218 ±0.002 | 0.208±0.002 |
| 0.62 | −0.247±0.036 | 0.615±0.001 | 0.755±0.006 | 0.227 ±0.002 | 0.217±0.002 |
| 0.64 | −0.771±0.016 | 0.618±0.001 | 0.769±0.006 | 0.234 ±0.003 | 0.223±0.003 |
| 0.66 | −0.965±0.006 | 0.620±0.001 | 0.775±0.009 | 0.236 ±0.004 | 0.226±0.004 |
| | | | Z=0.006 | | |
| 0.54 | +0.968±0.006 | 0.577±0.006 | 0.632±0.103 | 0.172 ±0.041 | 0.160 ±0.041 |
| 0.56 | +0.793±0.021 | 0.584±0.001 | 0.798±0.015 | 0.237 ±0.006 | 0.226 ±0.006 |
| 0.58 | +0.290±0.025 | 0.588±0.001 | 0.840±0.009 | 0.254 ±0.004 | 0.243 ±0.004 |
| 0.60 | −0.420±0.023 | 0.590±0.001 | 0.857±0.006 | 0.261 ±0.002 | 0.250 ±0.002 |
| 0.62 | −0.862±0.005 | 0.592±0.001 | 0.877±0.008 | 0.270 ±0.003 | 0.258 ±0.003 |
| 0.64 | −0.985±0.004 | 0.593±0.004 | 0.878±0.041 | 0.270 ±0.016 | 0.259 ±0.017 |

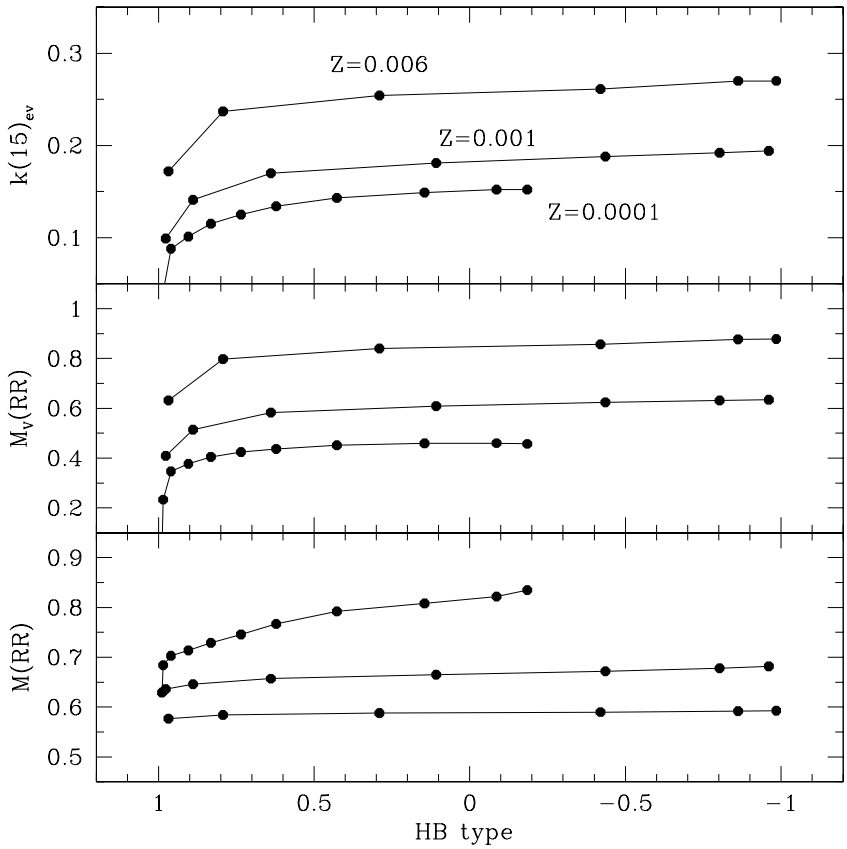


***Figure 4.10:*** *Average mass $M$(RR) in solar units, absolute visual magnitude $M_V$(RR) and evolutionary parameter $k(1.5)_{ev}$ inferred by SHB simulations with Z=0.0001, 0.001, and 0.006, assuming an original helium content Y=0.23.*

metal content and on the evolutionary status of the pulsators. As a fact, all the synthetic horizontal branches (SHB) simulations (see, e.g., Demarque et al. 2000, Catelan et al. 2004; Cassisi et al. 2004) show that, for a fixed metallicity, the average mass of HB stars in the RR Lyrae region decreases when moving from a red to a blue HB star distribution, whereas the average luminosity shown an opposite behaviour. On the other hand, for a fixed HB morphology, an increase in the metal content causes a decrease in the same intrinsic parameters. Using the SHBs computed in Cassisi et al. 2004 for various metal abundances and assuming an original He content $Y$=0.23, we list in Table 4.4 some selected predictions concerning SHB simulations where the number of predicted RR Lyrae stars is at least the 5% of the global HB star population. For each metal content $Z$ and

mean[†] mass $M(HB)$ of HB stars, they give the average HB type (Lee 1990), the predicted mean values of the RR Lyrae mass and the absolute magnitude. In columns (5) and (6) we have reported the calculated $k_{ev}$ parameters, together with the rms dispersion about the mean. Note that these synthetic simulations adopt the edges of the pulsation region determined in previous chapter and that the mean values are derived by averaging the results of 10 different simulations.

As shown also in Fig. 4.10 for some selected metal abundances, three points are worth mentioning:

1. the $k_{ev}$ parameter attains, at fixed metallicity, rather constant values from red to moderately blue HB morphology (i.e. HB type ranging from $\sim -0.9$ to $\sim$ +0.5), whereas it significantly decreases for the bluer populations;

2. for HB types redder that $\sim$ +0.5, the $k_{ev}$ parameter increases when moving from low to high metal abundances;

3. the size of this effect varies with the metallicity range. As a matter of example, we get $\Delta k(1.5)_{ev} \sim 0.03$ for $0.0001 \leq Z \leq 0.001$ and $\Delta k(1.5)_{ev} \sim 0.08$ for $0.001 \leq Z \leq 0.006$.

In summary, the constraints provided by pulsation and evolution theory indicate that the $PA_V$ distribution of RR$_{ab}$ stars in globular clusters depends on the cluster HB morphology *and* metal abundance.

Let me discuss now about the $PA_V$ diagram in Galactic globular clusters.

For the Galactic globular clusters with visual amplitude $A_V$ available in the literature, we give in Table 4.1.2 the observed HB type (Harris 1990), the average period of $RR_{ab}$ variables and the iron-to-hydrogen content on the Kraft & Ivans (2003) scale. For $\omega$ Cen, which is characterized by a wide spread in metal abundance, we give the average value ([Fe/H]=$-1.62\pm0.27$) based on Rey et al. (2000) data and the HB type according to Piersimoni et al. (2006, in preparation). As for NGC 6441, it should be mentioned that this cluster shows a very unusual HB extending from a stubby red to a very blue component (Rich et al. 1997). Moreover, the periods of the observed RR$_{ab}$ are too long

[†]The SHBs are produced assuming a gaussian random distribution of HB masses centered on $M(HB)$ with a standard deviation $\sigma \sim 0.02 M_{\odot}$.

***Table 4.5:*** *Selected parameters for Galactic globular clusters: HB type, average period of $ab$-type RR Lyrae stars and iron-to-hydrogen content [Fe/H]$_K$ according to the Kraft & Ivans (2003) metallicity scale. For $\omega$ Cen, we list the average [Fe/H]$_R$ value from Rey et al. (2000) data.*

| Name | HB | $\langle \log P_{ab} \rangle$ | [Fe/H]$_K$ |
|---|---|---|---|
| Oosterhoff type II | | | |
| N4590 (M68) | +0.44 | −0.201 | −2.43 |
| N6426 | +0.58 | −0.153 | −2.43 |
| N7078 (M15) | +0.67 | −0.189 | −2.42 |
| N5053 | +0.52 | −0.174 | −2.41 |
| N6341 (M92) | +0.91 | −0.195 | −2.38 |
| N5466 | +0.58 | −0.172 | −2.22 |
| N5024 (M53) | +0.81 | −0.189 | −2.02 |
| N6809 (M55) | +0.87 | −0.181 | −1.85 |
| N6333 (M9) | +0.87 | −0.203 | −1.79 |
| N7089 (M2) | +0.96 | −0.168 | −1.56 |
| Oosterhoff type I | | | |
| N4147 | +0.55 | −0.282 | −1.79 |
| I4499 | +0.11 | −0.238 | −1.60 |
| N6934 | +0.25 | −0.252 | −1.59 |
| N3201 | +0.08 | −0.252 | −1.56 |
| N5272 (M3) | +0.08 | −0.257 | −1.50 |
| N7006 | −0.28 | −0.246 | −1.48 |
| N6715 (M54) | +0.75 | −0.237 | −1.47 |
| N6981 (M72) | +0.14 | −0.256 | −1.42 |
| N6229 | +0.24 | −0.270 | −1.41 |
| N6864 (M75) | −0.07 | −0.231 | −1.29 |
| N5904 (M5) | +0.31 | −0.263 | −1.26 |
| N1851 | −0.36 | −0.241 | −1.19 |
| N6362 | −0.58 | −0.265 | −1.15 |
| N6723 | −0.08 | −0.262 | −1.11 |
| N6171 (M107) | −0.73 | −0.272 | −1.10 |
| Peculiar clusters | | | |
| N5139 ($\omega$ Cen) | +0.92 | −0.189 | −1.62 |
| N6441 | ... | −0.132 | −0.85 |

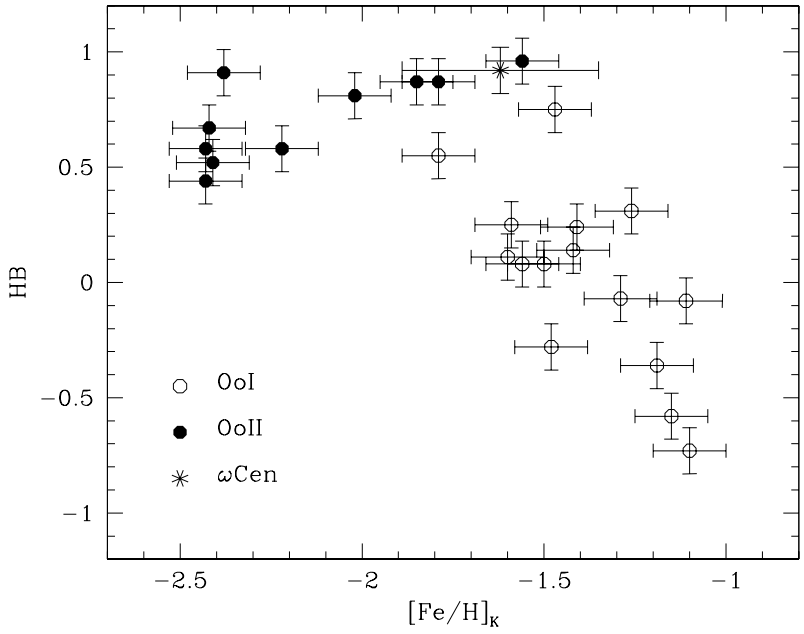


***Figure 4.11:*** *HB type versus [Fe/H]$_K$ for Oosterhoff type II (OoII, filled circles) and Oosterhoff type I (OoI, open circles) Galactic globular clusters. The error bars have been estimated by assuming $\epsilon$(HB)=$\pm$0.1 and $\epsilon$[Fe/H]$_K$=$\pm$0.1 For $\omega$ Cen (asterisk), we plot the average value [Fe/H]$_R = -1.62\pm0.27$ from Rey et al. (2000) data.*

for the cluster metallicity and no Oosterhoff classification has been made (see Pritzl et al. 2001).

Fig. 4.11 shows the cluster HB type as a function of the metal content [Fe/H]$_K$. It is worth noting that even our selected sample of RR Lyrae-rich globular clusters presents the so-called *second parameter* problem in the sense that a further intrinsic parameter besides the metal abundance is required to account for the observed HB morphology (see section 1.1.4). In particular, we note that OoI and OoII clusters seem to follow quite different behaviours: whereas the HB morphology of the OoI group becomes bluer as the cluster becomes more metal-poor, the HB morphology of the OoII group becomes bluer as the cluster becomes more metal-rich. This yields that OoII clusters with very blue

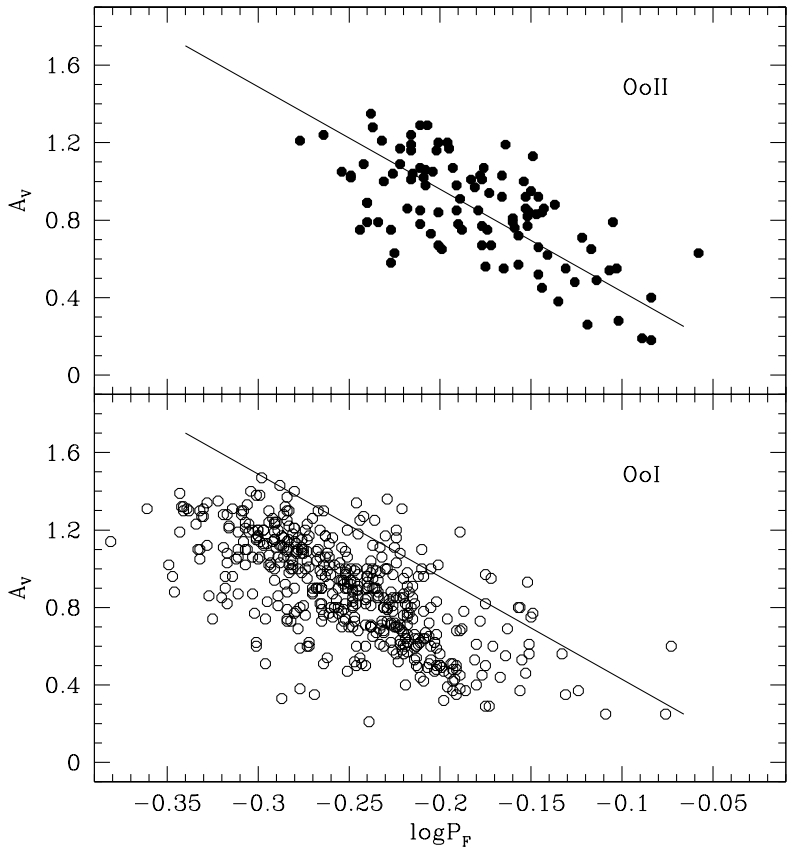


***Figure 4.12:*** *Visual amplitude versus period for RR$_{ab}$ stars in Oosterhoff type II (OoII, top panel) and Oosterhoff type I (OoI, bottom panel) globular clusters. The solid line shows the ridge line of variables in OoII clusters and is based on the predicted slope $\delta log P_F/\delta A_V = -0.189$.*

HB morphology, including $\omega$ Cen, appear to be the "natural" extension of OoI clusters to lower metal abundances.

Fig. 4.12 shows the $PA_V$ diagram for the observed RR$_{ab}$ stars in OoII (top panel) and OoI (bottom panel) clusters. The variables in $\omega$ Cen and in NGC 6441 have not been included in this figure and will be discussed separately. The solid line in the top panel is the ridge line of variables in OoII clusters and it was drawn by adopting the predicted slope (see equation 3.4] $\delta \log P_F/\delta A_V = -0.189$. The same line was also plotted in the bottom panel to make more evident that RR Lyrae stars in OoI clusters present, at fixed pulsation amplitude, systematically shorter periods. Based on the data plotted in Fig. 4.12, we derive the average $\langle k(1.5)_{puls} \rangle$ and $\langle k(2.0)_{puls} \rangle$ values listed in Table 4.6 (together with the rms deviation) and plotted in Figs. 4.13 and 4.14 versus the cluster [Fe/H]$_K$ and HB

***Table 4.6:*** *Mean $\langle k(1.5)_{puls} \rangle$ and $\langle k(2.0)_{puls} \rangle$ values for RR$_{ab}$ stars in Galactic globular clusters.*

| Name | HB | [Fe/H]$_K$ | $\langle k_{1.5} \rangle$ | $\langle k_{2.0} \rangle$ |
|---|---|---|---|---|
| Oosterhoff type II | | | | |
| N4590 | +0.44 | −2.43 | 0.183±0.026 | 0.112±0.024 |
| N6426 | +0.58 | −2.43 | 0.133±0.018 | 0.062±0.018 |
| N7078 | +0.67 | −2.42 | 0.186±0.030 | 0.112±0.030 |
| N5053 | +0.52 | −2.41 | 0.165±0.045 | 0.089±0.036 |
| N6341 | +0.91 | −2.38 | 0.146±0.026 | 0.083±0.026 |
| N5466 | +0.58 | −2.22 | 0.118±0.041 | 0.057±0.031 |
| N5024 | +0.81 | −2.02 | 0.139±0.029 | 0.074±0.028 |
| N6809 | +0.87 | −1.85 | 0.134±0.024 | 0.071±0.022 |
| N6333 | +0.87 | −1.79 | 0.132±0.017 | 0.084±0.017 |
| N7089 | +0.96 | −1.56 | 0.134±0.031 | 0.067±0.033 |
| Oosterhoff type I | | | | |
| N4147 | +0.55 | −1.79 | 0.217±0.021 | 0.158±0.025 |
| I4499 | +0.11 | −1.60 | 0.211±0.036 | 0.143±0.033 |
| N6934 | +0.25 | −1.59 | 0.221±0.037 | 0.154±0.031 |
| N3201 | +0.08 | −1.56 | 0.213±0.042 | 0.148±0.034 |
| N5272 | +0.08 | −1.50 | 0.196±0.032 | 0.136±0.027 |
| N7006 | −0.28 | −1.48 | 0.222±0.029 | 0.152±0.025 |
| N6715 | +0.75 | −1.47 | 0.222±0.037 | 0.151±0.032 |
| N6981 | +0.14 | −1.42 | 0.246±0.035 | 0.174±0.033 |
| N6229 | +0.24 | −1.41 | 0.221±0.024 | 0.158±0.019 |
| N6864 | −0.07 | −1.29 | 0.203±0.059 | 0.135±0.055 |
| N5904 | +0.31 | −1.26 | 0.213±0.049 | 0.150±0.048 |
| N1851 | −0.36 | −1.19 | 0.200±0.040 | 0.135±0.035 |
| N6362 | −0.58 | −1.15 | 0.220±0.030 | 0.156±0.029 |
| N6723 | −0.08 | −1.11 | 0.212±0.049 | 0.149±0.042 |
| N6171 | −0.73 | −1.10 | 0.241±0.043 | 0.173±0.041 |
| Peculiar clusters | | | | |
| N5139 | +0.92 | −1.62 | 0.150±0.043 | 0.092±0.052 |
| N6441 | ... | −0.85 | 0.106±0.025 | 0.048±0.025 |

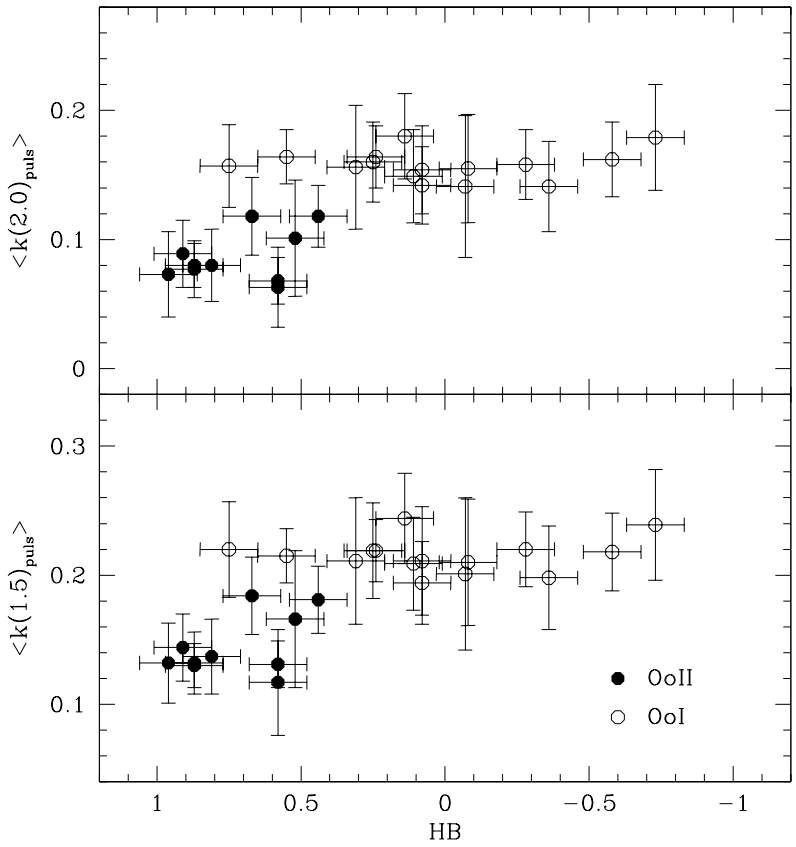


***Figure 4.13:*** *The average $\langle k(1.5)_{puls}\rangle$ and $\langle k(2.0)_{puls}\rangle$ values for RR$_{ab}$ stars in Oosterhoff type I (OoI, open circles) and Oosterhoff type II (OoII, filled circles) globular clusters plotted as a function of the cluster HB type.*

type. Bearing in mind the discussion on the $k_{ev}$ parameters listed in Table 4.4, the data in Table 4.6 show that:

1. among the OoI clusters with metal abundances ranging from [Fe/H]=$-1.8$ to $-1.1$ and HB types redder than +0.75, neither the $\langle k(1.5)_{puls}\rangle$ nor the $\langle k(2.0)_{puls}\rangle$ show significant variations with [Fe/H] or HB type;

2. among the OoII clusters with metal abundances ranging from [Fe/H]=$-2.4$ to $-1.6$ and HB types bluer than +0.44, both the $\langle k(1.5)_{puls}\rangle$ and the $\langle k(2.0)_{puls}\rangle$ present a mild decrease for clusters with bluer HB morphologies, though they are also the less metal-poor of the group;

3. for [Fe/H]=$-1.7\pm0.1$, we have both OoI and OoII clusters and the latter group has

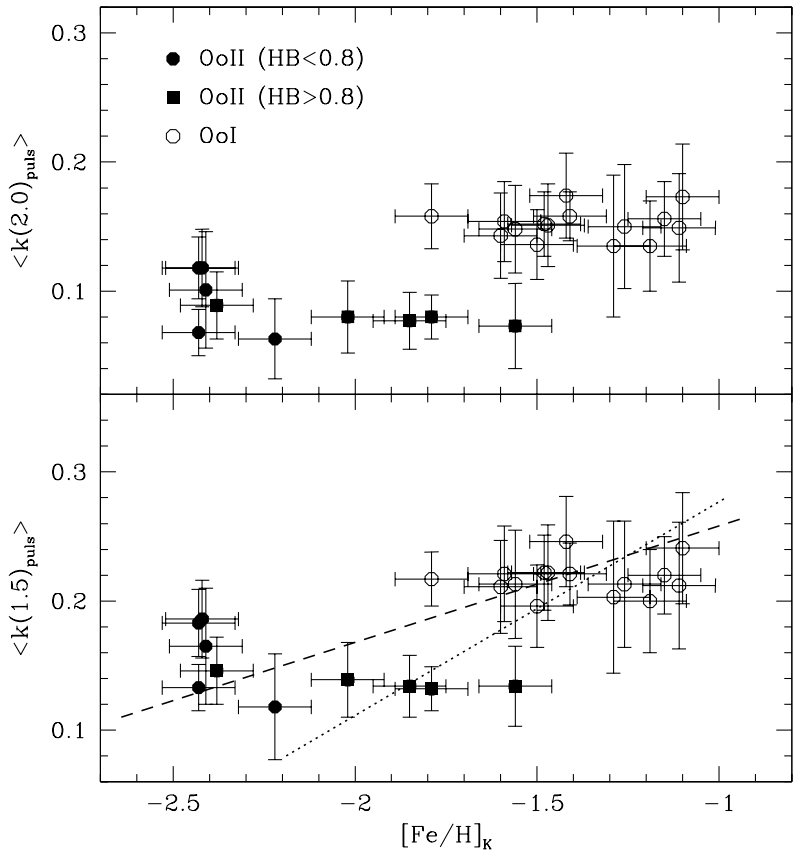


***Figure 4.14:*** *The average $\langle k(1.5)_{puls}\rangle$ and $\langle k(2.0)_{puls}\rangle$ values for RR$_{ab}$ stars in Oosterhoff type I (OoI, open circles) and Oosterhoff type II (OoII) globular clusters as a function of metal abundance. The filled circles mark OoII clusters with HB type ranging from red to moderately blue, while the filled squares refer to those with very blue HB type. The dashed and the dotted lines in the bottom panel display two different choices in the selection of the calibrating clusters. See text for more details.*

bluer HB types and smaller values of the $k$-parameters than the former one.

In summary, the Bailey diagram of the RR$_{ab}$ stars in Galactic globular clusters agrees with the evolutionary prescriptions and does not support the use of the $PA_V$ relation for robust metal abundance determinations. As an example, the linear fit to all the data in Fig. 4.14 yields [Fe/H]$\sim -3.1 + 7.7\ k(1.5)_{puls}$ which would predict the RR$_{ab}$ metallicity with the unpleasant average uncertainty of $\sim 0.4$ dex. The intrinsic error becomes even worse if the adopted empirical calibration relies on individual clusters. In particular, the use of OoI clusters together with OoII clusters with moderately blue HB morphology yields (dashed

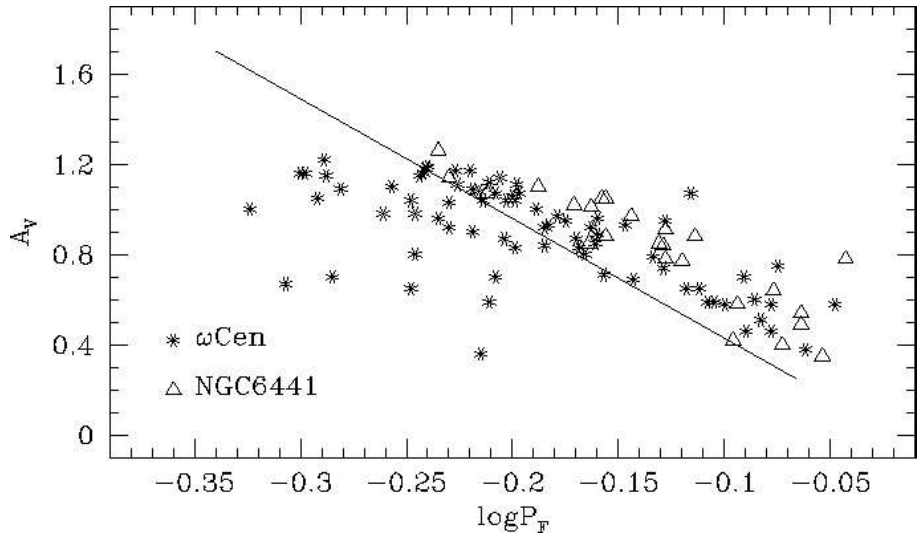


***Figure 4.15:*** *Same as in Fig. 4.11, but for RR$_{ab}$ stars in the two peculiar clusters NGC 6441 (triangles) and $\omega$ Cen (asterisks).*

line) [Fe/H]$\sim -3.9 + 11.1\ k(1.5)_{puls}$, while OoI clusters together with OoII clusters with very blue HB morphology yield (dotted line) [Fe/H]$\sim -2.7 + 5.8\ k(1.5)_{puls}$. It is worth noting that the adoption of the former relation to RR$_{ab}$ variables in OoII clusters with very blue HB stellar populations yields that the metallicity of these variables is underestimated by $\sim$ 0.7 dex, while the use of the latter relation to RR$_{ab}$ variables in OoII clusters with moderately blue HB stellar populations yields that the metallicity is overestimated by $\sim$ 0.5 dex.

Fig. 4.15 shows the $PA_V$ diagram of $ab$-type variables in NGC 6441 and $\omega$ Cen together with the ridge line of Oo II variables. Data plotted in this figure support the evidence that all the RR$_{ab}$ stars in NGC 6441 behave as OoII variables (see also the $\langle k(1.5)_{puls} \rangle$ and $\langle k(2.0)_{puls} \rangle$ values listed in Table 4.6), thus suggesting that the RR Lyrae metal abundance is significantly smaller than the current cluster value. This is at odds with the recent spectroscopic measurements by Clementini et al. (2005) which confirm that the RR Lyrae stars in NGC 6441 are metal-rich with [Fe/H]$\sim -0.7 \pm 0.3$, on the Zinn & West (1984) scale. On the other hand, if the variables are generated by the very blue HB component, we should expect small $k_{ev}$ values even with large metal abundances. However, the $Z$=0.003 and $Y \sim 0.25$ SHBs presented in Table 4.4 suggest $\langle k(1.5)_{ev} \rangle \sim$ 0.14 and $\langle k(2.0)_{puls} \rangle \sim 0.12$ at HB$\sim$ +0.95, which are still larger than the observed values. The new HB simulations with varying helium abundance (Caputo et al. 2006,

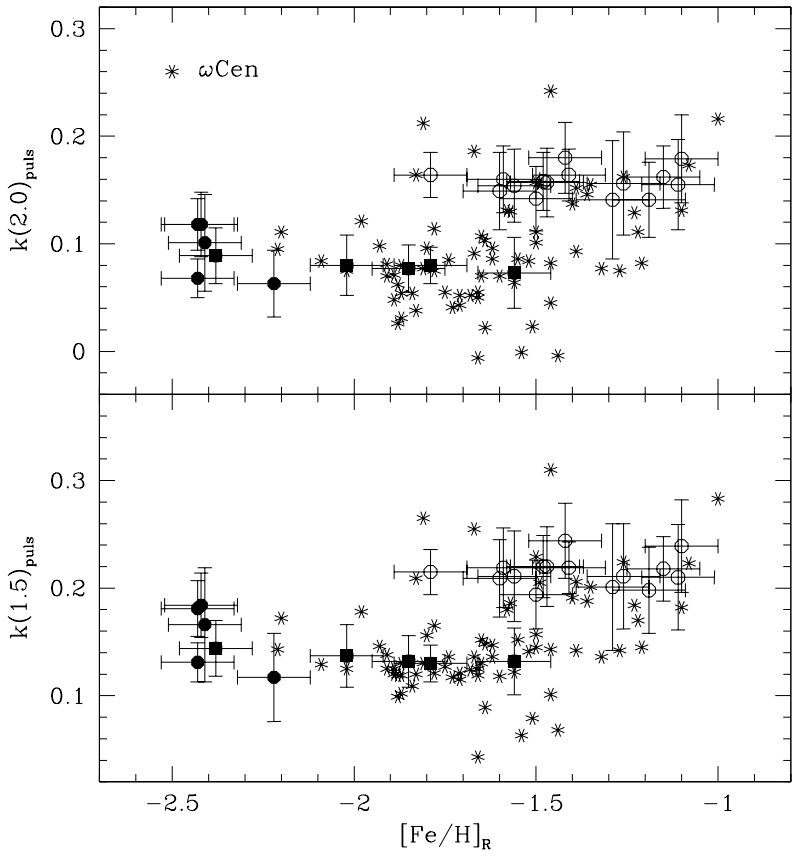


***Figure 4.16:*** *The $k(1.5)_{puls}$ and $k(2.0)_{puls}$ parameter for RR$_{ab}$ stars in $\omega$ Cen (asterisks) as a function of the metal abundance. Open circles, filled circles, and filled squares have the same meaning as in Fig. 4.14.*

in preparation) and the modeling of the observed light curves (Clementini & Marconi 2006, in preparation) will probably shed new lights on the unusual properties of variables in NGC 6441. As far as the variables in $\omega$ Cen are concerned, Fig. 4.16 shows the $k(1.5)_{puls}$ and $k(2.0)_{puls}$ values versus the [Fe/H]$_R$ metal abundance determined by Rey et al. (2000). As a first result, we note the quite large dispersion of the metallicity at constant $k_{puls}$, thus stressing the misleading use of the Bailey diagram for metal abundance determinations. Futhermore, the comparison with the data presented in Fig. 4.14, here repeated for the sake of clearness, indicates that the RR$_{ab}$ stars in $\omega$ Cen share the properties of both the Oosterhoff type I and type II clusters (see also Clement & Rowe 2000). However, it is worth mentioning that the agreement with the latter group only applies to OoII clusters with very blue HB morphology (HB type $\geq$ +0.8, filled squares) since the

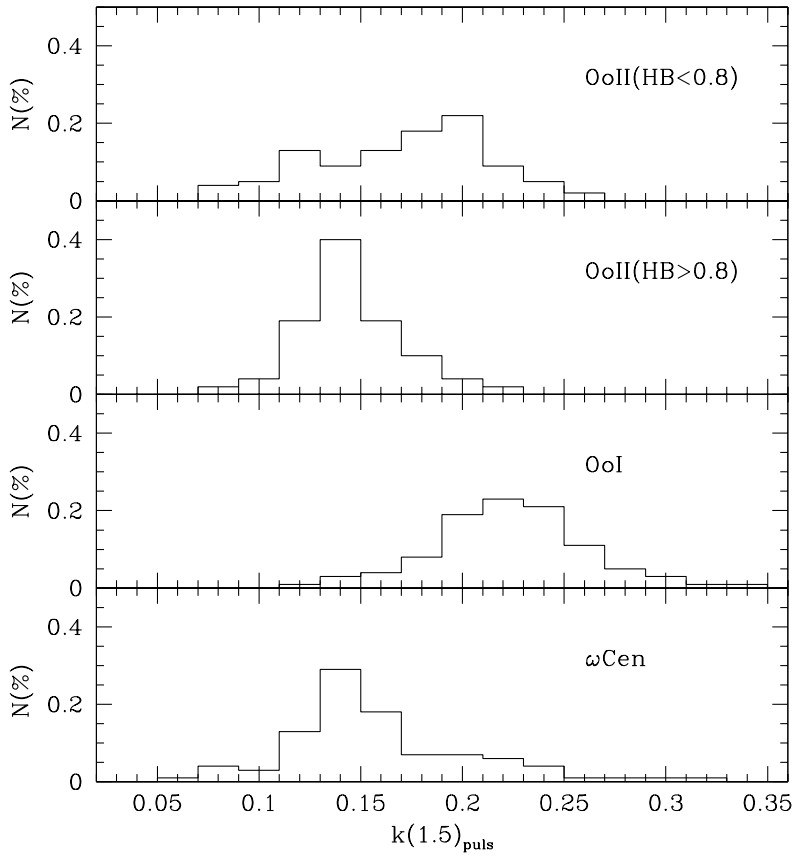


***Figure 4.17:*** *Frequency histograms distribution of the $k(1.5)_{puls}$ parameter for RR$_{ab}$ stars in $\omega$ Cen, OoI, and OoII globular clusters.*

$k(1.5)_{puls}$ values typical of variables associated to moderately blue HB morphology (e.g., M15-like) seem to be absent. The lack of this kind of variables shows up quite clearly from Fig. 4.17 which shows the frequency distribution of the $k(1.5)_{puls}$ values in $\omega$ Cen (bottom) in comparison with those fom OoI and OoII clusters. Note that this result, which holds also if the new metal abundances by Sollima et al. (2006) are adopted, cannot be explained as a significant difference between the Kraft & Ivans (2003) and the Rey et al. (2000) metallicity scales. As a matter of fact, by using the Gratton et al. (2004) metal abundance [Fe/H]$_G$ determinations for RR Lyrae stars in NGC 1851, NGC 3201, and in NGC 4590 we get [Fe/H]$_G$ $\sim$ $-$0.48+0.65[Fe/H]$_K$, while for $\omega$ Cen variables we derive [Fe/H]$_G$ $\sim$ $-$0.41+0.71[Fe/H]$_R$. Thus, we eventually estimate [Fe/H]$_K$ $\sim$ 0.1+1.1[Fe/H]$_R$.

The circumstantial empirical and theoretical evidence discussed in this section brought

into focus the deceptive use of the Bailey diagram of $RR_{ab}$ stars to estimate metal abundances. Therefore we are now facing the question: is there any possibility to exploit its dependence on the evolutionary status of the variables? It is well known that current updated HB models provide, for fixed metal content $Z$, slightly different luminosity values which are due to different assumptions on input physics (see, e.g., Castellani 2003). As a consequence, the theoretical $M_V$(RR)-[Fe/H] relations provided by the authors using different evolutionary codes show significant discrepancies both in the slope and in the zero-point. However, it has just been discussed that these discrepancies are mainly due to two factors of critical importance: (1) the conversion of bolometric luminosity and effective temperature into magnitudes and colors, i.e., the adopted bolometric correction and color-temperature transformations; (2) the scaling between the theoretical metal abundance $Z$ and the measured [Fe/H] values, i.e., the ratio $f$ between $\alpha$-elements and iron which is adopted in the relation $\log Z$=[Fe/H]$-1.73$+log$(0.638\,f+0.362)$.

Conversely, the mass of the RR Lyrae stars, as predicted by the evolutionary models, appears a more safe parameter, with an average variation of $\sim 2$ percent among the various computations available in the recent literature. On this ground the connection of the predicted relations inferred by the pulsation models with the average mass suggested by SHB simulations provides a reliable "pulsational" route to the determination of the absolute magnitude of RR Lyrae stars *in globular clusters with known metal content and HB morphology*. As for the current $PA_V$ relation, we have

$$M_V^{k(1.5)} = (k(1.5)_{puls} - 0.30 \log M)/0.385 \tag{4.6}$$

and

$$M_V^{k(2.0)} = (k(2.0)_{puls} - 0.35 \log M)/0.385 \tag{4.7}$$

For the clusters in our sample, the column (4) in Table 4.6 gives the average logarithmic mass of RR Lyrae stars suggested by the SHBs presented in Table 4.4, by adopting solar-scaled chemical compositions, i.e. $\log Z$=[Fe/H]$-1.73$. By inserting these masses into Eqs. 4.6 and 4.7, we estimate the absolute magnitudes plotted in Fig. 4.18 and Fig. 4.19. As shown by the solid lines drawn in these figures, the RR Lyrae stars in OoII clusters with HB type bluer than +0.8 (filled squares) and in OoI clusters (open circles) yield

$$M_V(RR_{ab}) = 0.12(\pm 0.05) + 2.62 k(1.5)_{puls}, \tag{4.8}$$

***Table 4.7:*** *Average mass (logarithm scale) of $RR_{ab}$ stars in Galactic globular clusters inferred by SHB computations based on HB evolutionary models with solar-scaled chemical compositions. These masses are combined with the observed $k(1.5)_{puls}$ and $k(2.0)_{puls}$ values to derive the average absolute magnitudes $\langle M_V \rangle$ listed in columns (5) and (6), respectively. The $\sigma_V$ value in the last column is the standard deviation of the mean.*

| Name | HB | $[Fe/H]_K$ | $\log M(RR)$ | $\langle M_V^{k(1.5)} \rangle$ | $\langle M_V^{k(2.0)} \rangle$ | $\sigma_V$ |
|---|---|---|---|---|---|---|
| Oosterhoff type II | | | | | | |
| N4590 | +0.44 | −2.43 | −0.089 | 0.54 | 0.37 | ±0.07 |
| N6426 | +0.58 | −2.43 | −0.097 | 0.42 | 0.25 | ±0.05 |
| N7078 | +0.67 | −2.42 | −0.109 | 0.57 | 0.39 | ±0.08 |
| N5053 | +0.52 | −2.41 | −0.094 | 0.50 | 0.32 | ±0.12 |
| N6341 | +0.91 | −2.38 | −0.141 | 0.49 | 0.34 | ±0.07 |
| N5466 | +0.58 | −2.22 | −0.114 | 0.40 | 0.25 | ±0.11 |
| N5024 | +0.81 | −2.02 | −0.149 | 0.48 | 0.33 | ±0.08 |
| N6809 | +0.87 | −1.85 | −0.162 | 0.47 | 0.33 | ±0.06 |
| N6333 | +0.87 | −1.79 | −0.165 | 0.47 | 0.34 | ±0.04 |
| N7089 | +0.96 | −1.56 | −0.178 | 0.49 | 0.34 | ±0.08 |
| Oosterhoff type I | | | | | | |
| N4147 | +0.55 | −1.79 | −0.147 | 0.68 | 0.54 | ±0.06 |
| IC4499 | +0.11 | −1.60 | −0.153 | 0.67 | 0.51 | ±0.09 |
| N6934 | +0.25 | −1.59 | −0.156 | 0.70 | 0.54 | ±0.10 |
| N3201 | +0.08 | −1.56 | −0.156 | 0.68 | 0.53 | ±0.11 |
| N5272 | +0.08 | −1.50 | −0.160 | 0.63 | 0.50 | ±0.08 |
| N7006 | −0.28 | −1.48 | −0.158 | 0.70 | 0.54 | ±0.08 |
| N6715 | +0.75 | −1.47 | −0.173 | 0.71 | 0.55 | ±0.10 |
| N6981 | +0.14 | −1.42 | −0.167 | 0.77 | 0.60 | ±0.09 |
| N6229 | +0.24 | −1.41 | −0.169 | 0.71 | 0.57 | ±0.06 |
| N6864 | −0.07 | −1.29 | −0.175 | 0.66 | 0.51 | ±0.15 |
| N5904 | +0.31 | −1.26 | −0.181 | 0.69 | 0.55 | ±0.13 |
| N1851 | −0.36 | −1.19 | −0.180 | 0.66 | 0.52 | ±0.10 |
| N6362 | −0.58 | −1.15 | −0.181 | 0.71 | 0.57 | ±0.08 |
| N6723 | −0.08 | −1.11 | −0.188 | 0.70 | 0.56 | ±0.13 |
| N6171 | −0.73 | −1.10 | −0.184 | 0.77 | 0.62 | ±0.11 |

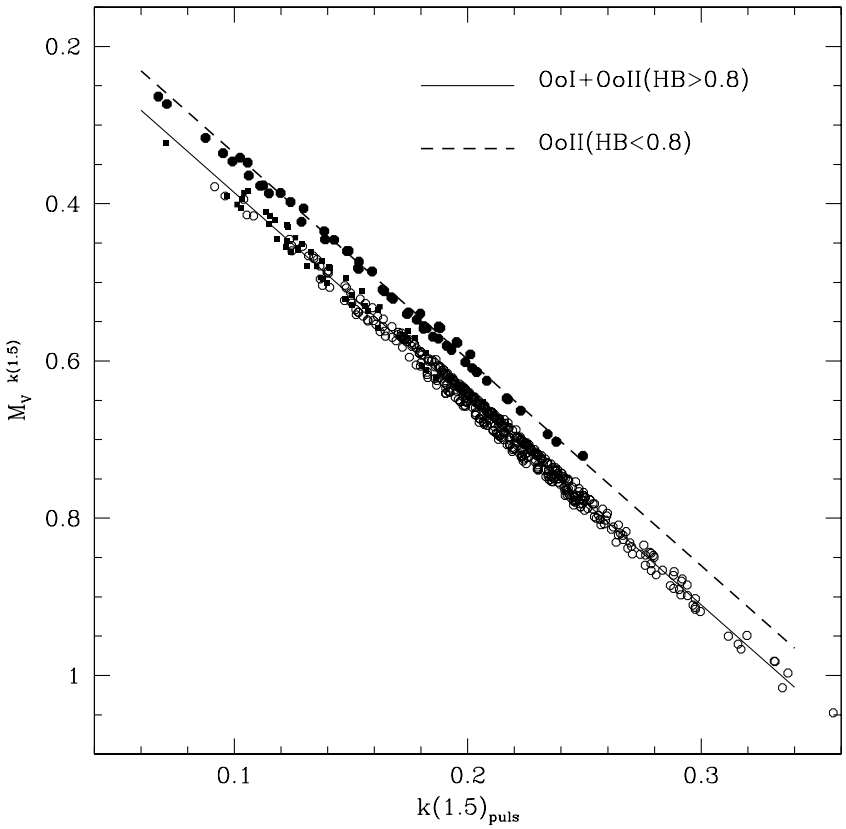


***Figure 4.18:*** *Predicted absolute magnitude of $RR_{ab}$ stars in Galactic globular clusters versus the $k(1.5)_{puls}$ value, adopting solar-scaled chemical compositions. The symbols have the same meaning as in Fig. 4.14. The solid line is Eq.4.8.*

and

$$M_V(RR_{ab}) = 0.15(\pm 0.05) + 2.62k(2.0)_{puls}, \tag{4.9}$$

whereas for the variables in OoII clusters (filled circles) with moderately blue HB morphology the zero-point of the relation (dashed line) is brighter by 0.05 mag.

Eventually, we give in columns (5) and (6) in Table 4.6 the RR Lyrae average absolute magnitude based on the predicted $PA_V$ relations with $l/H_p$=1.5 and $l/H_p$=2.0, respectively, adopting solar-scaled chemical compositions. The same data are plotted in Fig. 4.20 as a function of the cluster metal content [Fe/H]$_K$. A linear regression over the entire sample yields the average slope of $\sim$ 0.20 mag dex$^{-1}$ and a zero-point of $\sim$0.94 and $\sim$0.82 mag with $l/H_p$=1.5 and $l/H_p$=2.0, respectively. Note that adopting $\alpha$-enhanced chemical compositions, e.g. $f$=3 ([$\alpha$/Fe]$\sim$ 0.5), yields absolute magnitudes fainter by

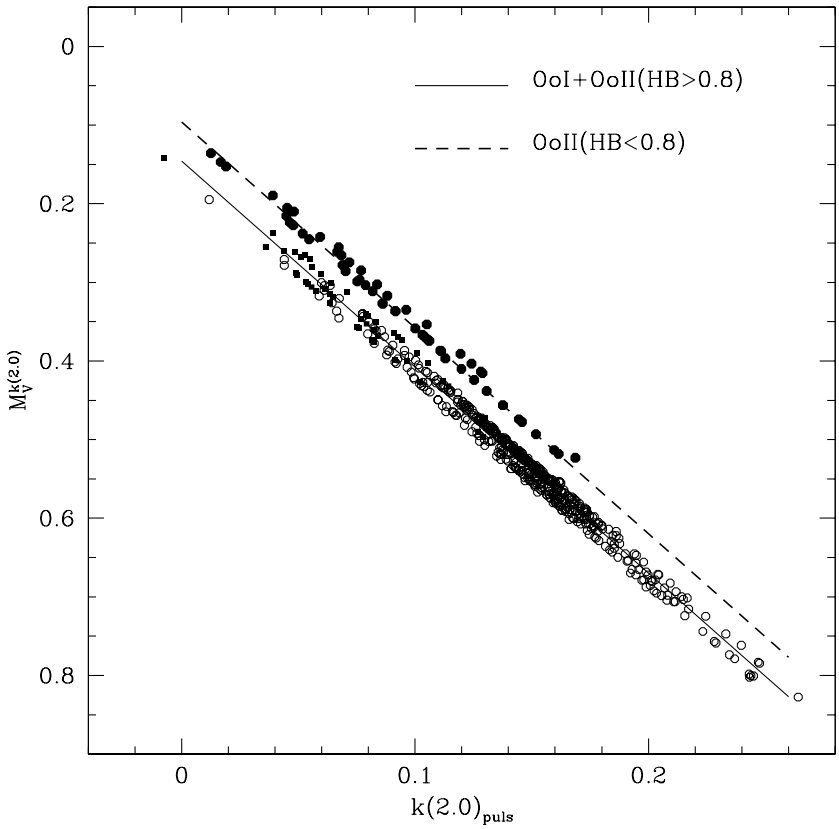


***Figure 4.19:*** *As in Fig. 4.18, but with $k(2.0)_{puls}$. The solid line is Eq. 4.9.*

only 0.02 mag, at fixed [Fe/H].

As already discussed, the choice between the two different values of the mixing-length parameter is quite difficult and, probably, the best solution might be given by a value which increases when the effective temperature decreases, i.e. from short to long period variables. However, we wish to mention that using Eqs. 4.8 and 4.9 with the sample of RR$_{ab}$ stars in $\omega$Cen, we find a cluster distance modulus of $\mu_0$=13.67$\pm$0.09 mag and 13.80$\pm$0.09 mag, respectively. Although these two distance estimates are slightly different, they agree quite well with the values obtained using different distance indicators, such as 13.75$\pm$0.04 mag based on the eclipsing binary OGLEGC-17 (Thompson et al. 2001; Kaluzny et al. 2002), 13.74$\pm$0.11 mag suggested by the First Overtone Blue Edge method (Caputo et al. 2002), and 13.70$\pm$0.06 mag inferred by the $K-$band Period-Luminosity relations of RR Lyrae stars (Del Principe et al. 2006).

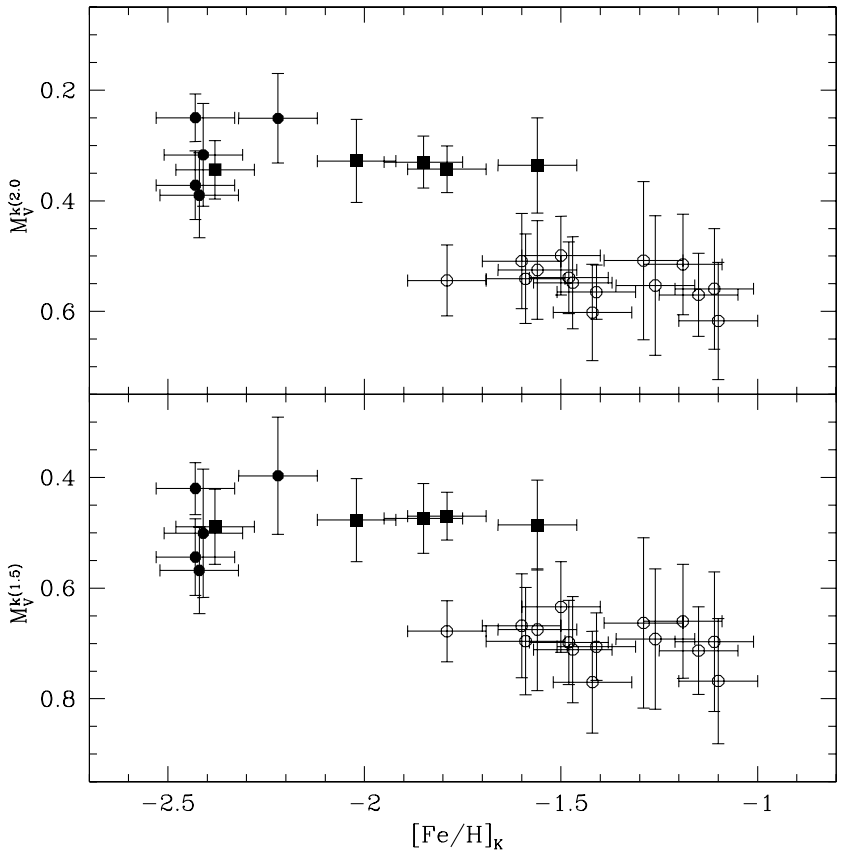


***Figure 4.20:*** *Average absolute magnitude of $RR_{ab}$ stars in Galactic globular clusters versus $[Fe/H]_K$, adopting solar-scaled chemical compositions. The symbols have the same meaning as in Fig. 4.14.*

### 4.1.3 Comparison of models in SDSS filter with current observations

**(Marconi et al. 2006, MNRAS, 371)**

In this section the predicted color-color loops in the various SDSS filter combinations (as presented in section 3.1.4) are compared with observed RR Lyrae samples. This work is described in detail Marconi et al 2006. In particular we have tested model predictions with data from the QUEST survey (see e.g. Vivas et al. 2001) and observations in the Draco galaxy (Bonanos et al. 2004). The first sample, a large census of field RR Lyrae, should map the history of the outer halo of our Galaxy, the second should represent an example of RR Lyrae in a different enviroment. Both the samples are positionally matched against the SDSS-DR4 ( Adelman-McCarthy et al. 2006) catalogue using a search radius of 0.1 arcsec and subsequently dereddened (using IR maps, see Schlegel, Finkbeiner & Davis,

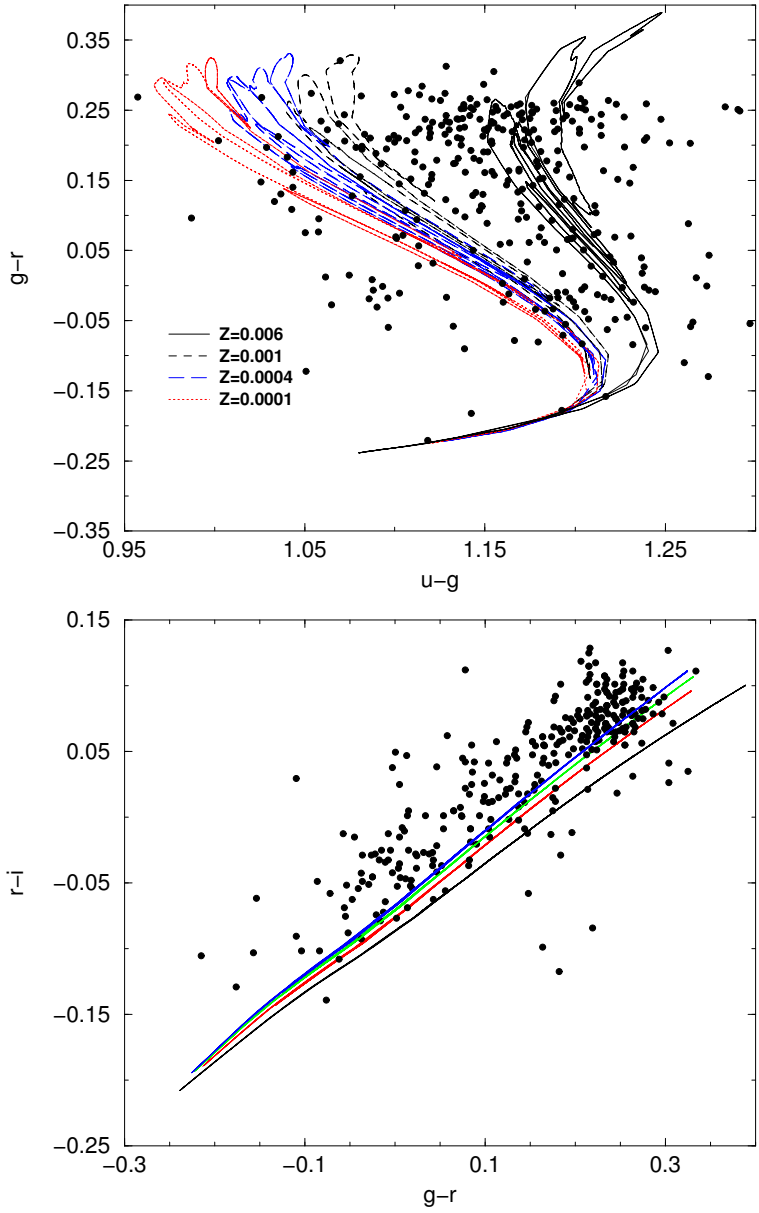


***Figure 4.21:*** *Comparison between the theoretical loops shown in Fig. 3.7 and the QUEST RR Lyrae data (see text for details).*

1998). Figs. 4.21 show the distributions for the QUEST data, as observed in the *g-r* vs *u-g* (upper panel) and *r-i* vs *g-r* plane (lower panel) respectively. Superimposed, we show the theoretical loops for the labeled metallicities. we do not report the mean magnitudes because SDSS observations consist of one or, at most, two phase points. The QUEST data which are expected to trace metal poor ($Z < 0.001$) and distant halo stars (see Vivas et al. 2001) are not matched by the corresponding model loops, with the discrepancy larger than the mean uncertainty resulting from photometric ($\sigma(u-g) < 0.03$ mag) and

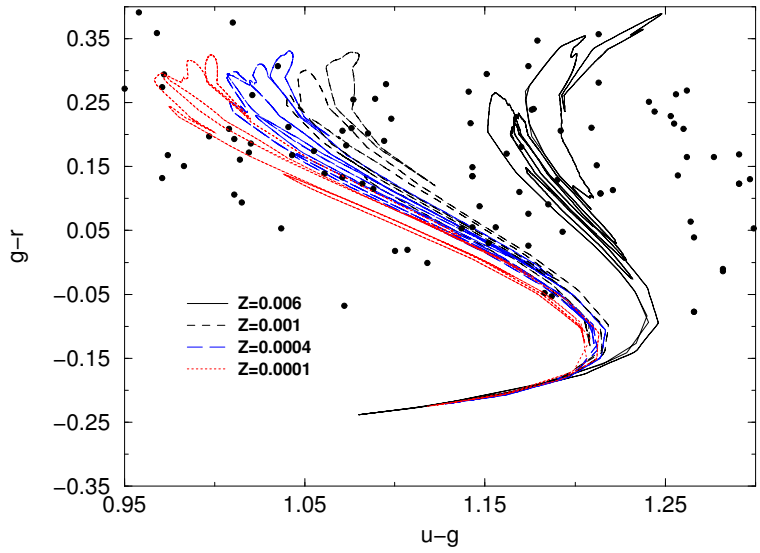


***Figure 4.22:*** *The same of Fig. 4.21 but for Draco RR Lyrae.*

reddening errors (less than 0.01 mag in colors, see also Ivezic et al.2005). Fig. 4.22 shows the comparison with DRACO RR Lyrae in the *g-r* vs *u-g* plane. In this case one has a large spread in *u-g* due in part to the significant photometric uncertainties ($\sigma(u-g) \sim 0.1$ mag and $\sigma(g-r) \sim 0.02$) affecting the data. In this case, the comparison with the theoretical loops does not allow us to discriminate a metallicity effect. However, the mean metallicity of this galaxy is generally considered poorer than Z=0.001 (see e.g. Mateo et al. 1998), so that it is quite strange that thus it is noteworty that a consistent fraction of the Draco RR Lyare is redder than our Z=0.006 models with an overdensity at *u-g* $> 1.25$. Possible sources for the discrepancies between theory and observations may result from observational uncertainties, including reddening and contamination effects, or theoretical biases, as for example the adopted model atmospheres and chemical mixture.

As for the reddening, a critical point is represented by the extinction law adopted to relate the measured E(B-V) to the extinctions in the SDSS filters (see e.g. Girardi et al. 2002). Assuming the coefficents tabulated by Girardi et al. (2004), an underestimation of the E(B-V) color excesses of the order of 0.02 mag would produce a final blue shift in u-g and g-r of about 0.02 and 0.03 respectively, in the direction of reducing the discrepancy between data and metal-poor predictions in Figs. 4.21.

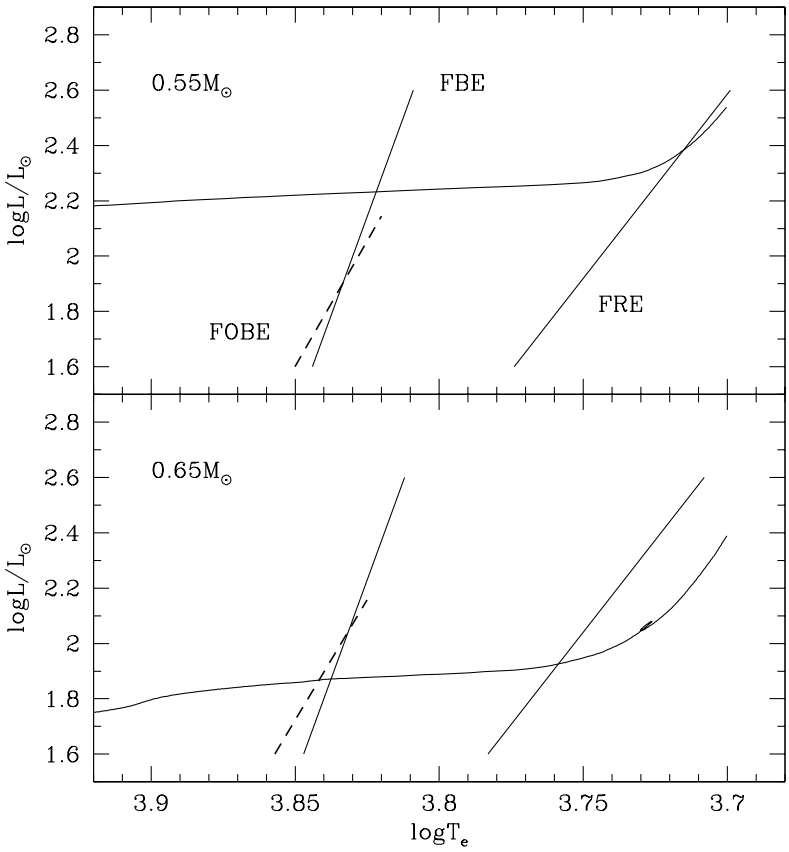


***Figure 4.23:*** *Selected evolutionary tracks with Z=0.0001 and [$\alpha$/Fe]=0.4 in comparison with the predicted FOBE, FBE and FRE. At luminosity levels brighter than the intersection between FOBE and FBE only the models pulsating in the fundamental mode are stable.*

## 4.2 BL Her stars (Di Criscienzo et al. 2006, A&A, submitted)

In this paragraph I compare the pulsational models of BL Herculis stars with observations. To this purpose I use the calculated syntethic models of BL Her stars by combining pulsational and evolutionary models. The pulsation models have been described in the previous chapter, while the adopted evolutionary framework is based on the models computed by Pietrinferni et al. (2004, 2006) for scaled solar and $\alpha$-enhanced ([$\alpha$/Fe]=0.4) metal distributions. The reader is referred to these papers[‡] for information on the physical inputs and numerical assumptions. Here, it is sufficient to note that this evolutionary framework

[‡]The whole set of stellar models can be retrieved at the following URL site: http://www.te.astro.it/BASTI/index.php.

***Table 4.8:*** *Luminosity $L_{FBE}$ at the fundamental blue edge of the models with the labeled metal content and [$\alpha$/Fe]=0.4, in comparison with the luminosity $L_{IP}$ at the intersection between FOBE and FBE. The models in bold face are the ones adopted for deriving the predicted relations (see text). The luminosity values are in solar units.*

| $M/M_{\odot}$ | $\log L_{FOBE}$ $Z$=0.0001 | $\log L_{FOBE}$ $Z$=0.001 | $\log L_{FOBE}$ $Z$=0.004 | $\log L_{IP}$ |
|---|---|---|---|---|
| 0.500 | – | – | 2.62 | 1.73 |
| 0.505 | – | – | **2.39** | 1.74 |
| 0.510 | – | 2.55 | **2.28** | 1.74 |
| 0.515 | 3.08 | 2.43 | **2.20** | 1.75 |
| 0.520 | 2.79 | **2.32** | **2.15** | 1.76 |
| 0.525 | 2.55 | **2.25** | **2.08** | 1.77 |
| 0.530 | 2.46 | **2.21** | **2.02** | 1.78 |
| 0.535 | **2.38** | **2.16** | **1.99** | 1.78 |
| 0.540 | **2.32** | **2.11** | **1.94** | 1.79 |
| 0.545 | **2.27** | **2.07** | **1.89** | 1.80 |
| 0.550 | **2.24** | **2.04** | **1.83** | 1.81 |
| 0.560 | **2.16** | **1.98** | – | 1.82 |
| 0.570 | **2.10** | **1.95** | – | 1.84 |
| 0.580 | **2.05** | **1.88** | – | 1.85 |
| 0.590 | **2.02** | **1.87** | – | 1.86 |
| 0.600 | **2.01** | – | – | 1.88 |
| 0.610 | **1.96** | – | – | 1.89 |
| 0.620 | **1.93** | – | – | 1.91 |

is based on the most updated physical scenario and its reliability and accuracy have already been tested by comparison with various empirical data sets (see also Riello et al. 2003, Salaris et al.2004, Recio-Blanco et al. 2005). The various stellar models present in the evolutionary database have been followed all along the main core H-burning phase and advanced core and shell He-burning evolutionary phases. All the He-burning models adopted in the present analysis have been computed by accounting for He-core mass and He-envelope abundance on the Zero Age Horizontal Branch (ZAHB) as obtained from a Red Giant Branch (RGB) progenitor with initial total mass equal to $\sim 0.8 M_{\odot}$, corresponding to an age at the RGB tip of the order of 13 Gyr. The procedure for deriving the

observational parameters of the predicted pulsators is in principle quite simple and has been described in several previous investigations (Bono, Caputo & Santolamazza 1997, Marconi et al. 2003, Fiorentino et al. 2006). As shown in Fig. 4.23, the relations of the predicted edges of the instability strip (eqs. 3.20 -3.21) give us the way to select the models evolving with a luminosity larger than $\log L_{IP}$ and showing FBE$\geq \log T_e \geq$ FRE. In this way, one derives that the mass range of the predicted fundamental pulsators varies from 0.515-0.62$M_{\odot}$ at [Fe/H]=$-$2.6 to 0.50-0.55$M_{\odot}$ at [Fe/H]=$-$0.7. These mass values are consistent with the mass range of the pulsating models listed in Table 3.7. However, as shown in Table 4.8, the average luminosity of the pulsators with a given mass increases as the metal content decreases, yielding that the [Fe/H]=$-$2.6 pulsators less massive than 0.53$M_{\odot}$ are more luminous than our brightest pulsating models. Since one cannot *a priori* be sure that the edge and period relations provided by the pulsation models listed in Table 3.7 can be extrapolated to higher luminosities, in the following I will use only the predicted pulsators whose mass and luminosity are consistent with those adopted for the pulsation models, as given in bold face in Table 4.8.

### 4.2.1 The connection between stellar evolution and pulsation

By calculating the fundamental period by means of equation 3.1 and adopting the magnitudes computed by Pietrinferni et al. (2004, 2006), I obtain the Period-Magnitude distribution plotted in Fig. 4.24 for the predicted fundamental pulsators with $Z$=0.0001 and [$\alpha$/Fe]=0.4. Note that the resulting periods are in the range from about 0.8 to 8 days, making our theoretical investigations quite appropriate for the analysis of observed BL Her stars.

As already found for other pulsating variables, the effect of the intrinsic width of the instability strip (see Fig. 4.23) is greatly reduced when moving from short to larg wavelengths. On this basis, it is quite clear that synthetic $PM_B$ to $PM_V$ relations will significantly depend on the actual distribution of the pulsators within the pulsation region, at variance with the case of the near-infrared magnitudes. effects in the case of the $JHK$ ones. A least square fit to all the fundamental models with [Fe/H]=$-$2.6 to $-$0.7 yields the linear relations listed in Table 4.9. As a result, one get that the apparent distance modulus $\mu_I$ of observed variables can be determined within $\pm$ 0.19 mag, whereas, thanks to the

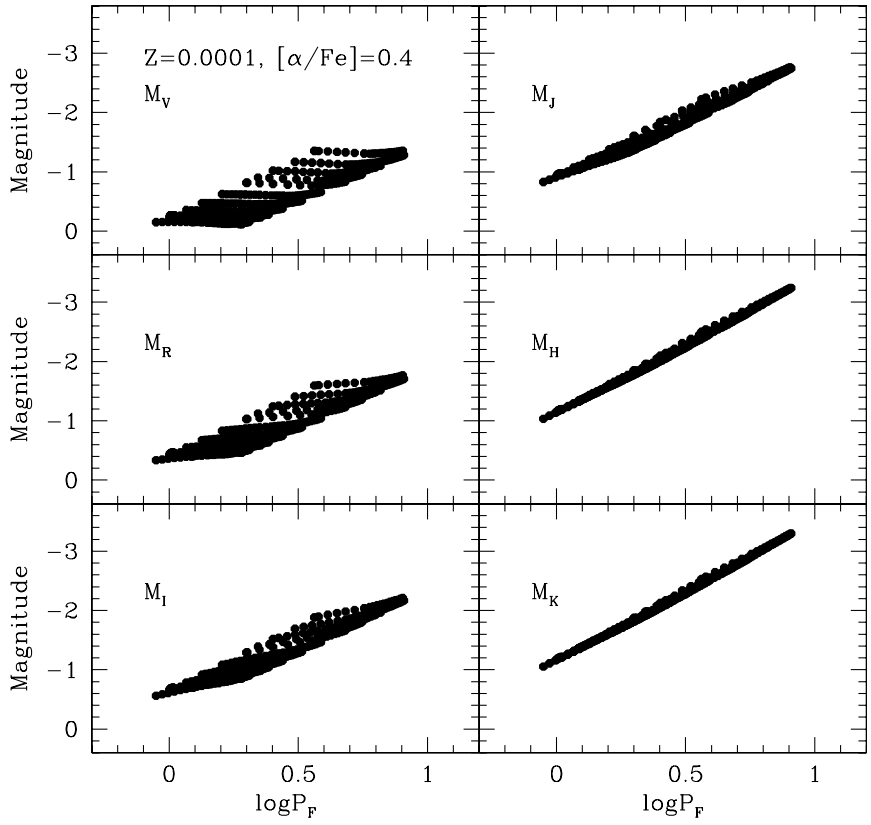


***Figure 4.24:*** *Period-Magnitude diagrams of fundamental pulsators with Z=0.0001 and [α/Fe]=0.4.*

quite tight $PM_H$ and $PM_K$ relations, either $\mu_H$ and $\mu_K$ can be determined with a formal accuracy of 0.06 mag, while the $PM_J$ relation, given the residual effect of the intrinsic width of the instability strip, yields $\mu_J$ within 0.14 mag. Concerning the scatter in optical magnitudes, it is well known that it can be removed if a Period-Magnitude-Color ($PMC$) is considered, i.e., if the pulsator magnitude is given as a function of the period and color. Several previous papers (see, e.g., Madore 1982, Madore & Freedman 1991, Tanvir 1999, Caputo et al. 2000, 2004) have already shown that the color coefficient of the various $PMC$ relations is not too different from the extinction-to-reddening ratio provided by optical and near-infrared reddening laws (see Dean et al. 1978, Caldwell & Coulson 1987, Cardelli, Clayton & Mathis 1989, Laney & Stobie 1993). On this basis, the adoption of the reddening insensitive Wesenheit functions, where the magnitude is corrected for the color according to the interstellar extinction, also removes

***Table 4.9:*** *Predicted $PM_J$, $PM_H$ and $PM_K$ relations for fundamental pulsators with iron content in the range of [Fe/H]=$-2.6$ to $-0.7$ and $P \leq 8$ days.*

| $M_i = a + blogP_F + c[Fe/H]$ | | | |
|---|---|---|---|
| $M_i$ | $a$ | $b$ | $c$ |
| $M_I$ | $-2.61 \pm 0.19$ | $-2.10 \pm 0.06$ | +0.04±0.01 |
| $M_J$ | $-0.64 \pm 0.14$ | $-2.29 \pm 0.04$ | +0.04±0.01 |
| $M_H$ | $-0.95 \pm 0.06$ | $-2.34 \pm 0.02$ | +0.06±0.01 |
| $M_K$ | $-0.97 \pm 0.06$ | $-2.38 \pm 0.02$ | +0.06±0.01 |

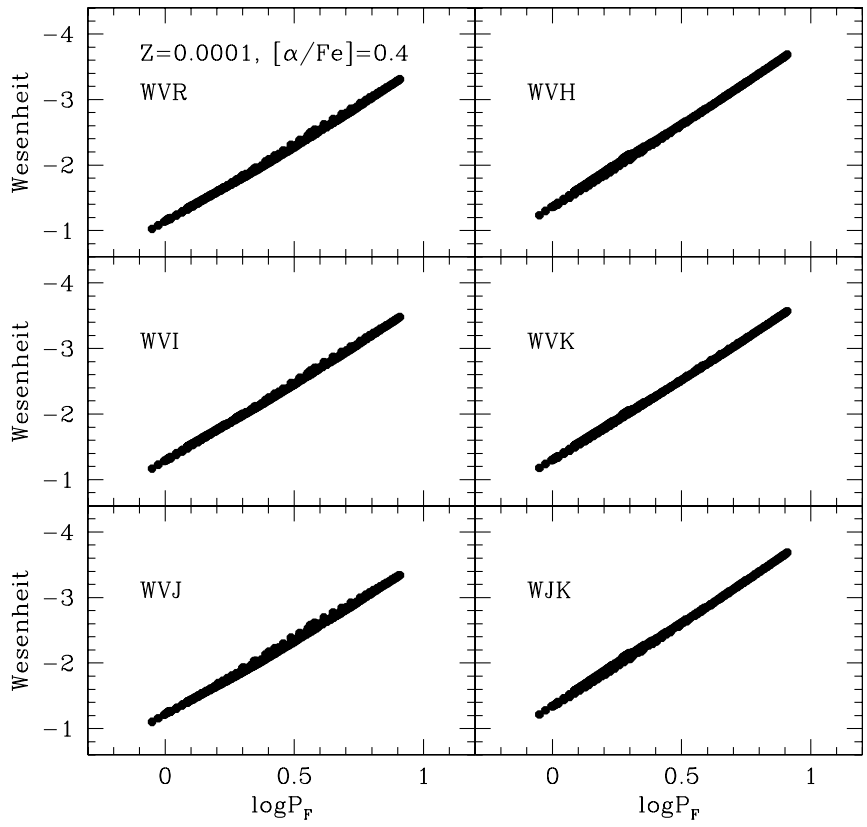


***Figure 4.25:*** *Selected Period-Wesenheit diagrams of fundamental pulsators with Z=0.0001 and [$\alpha$/Fe]=0.4.*

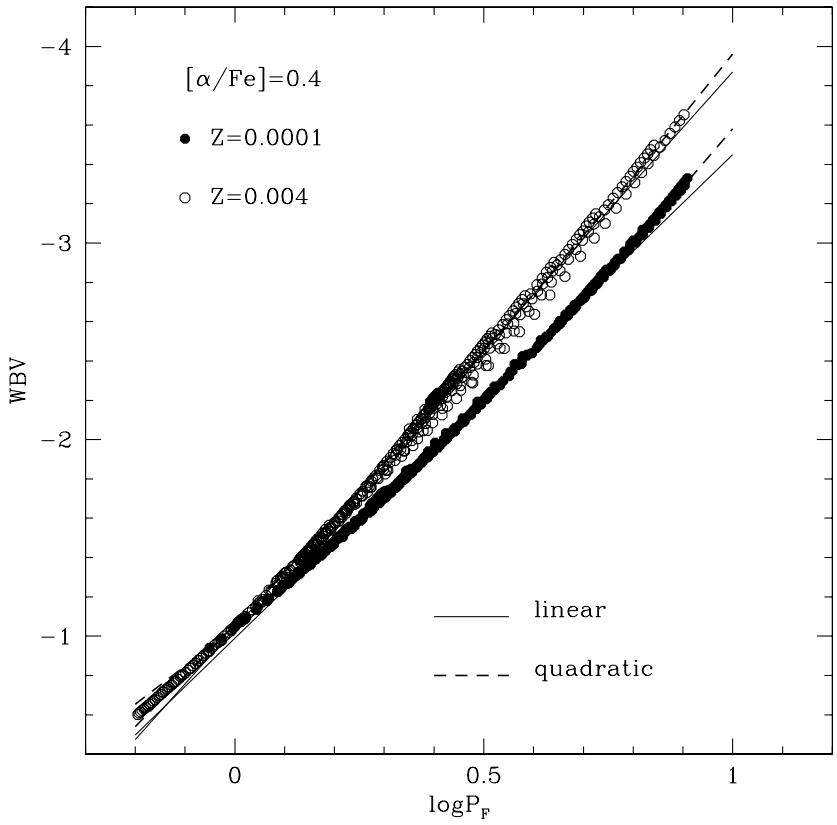


***Figure 4.26:*** *$W(BV)$ function versus period of selected fundamental pulsators. The solid and dashed lines are the linear and quadratic fit, respectively.*

larg part of the effect due to the dependence on effective temperature. In the following, adopting $A_V = 3.1E(B-V)$, $A_R = 2.45E(B-V)$, $A_I = 1.85E(B-V)$, $A_J = 0.897E(B-V)$, $A_H = 0.574E(B-V)$ and $A_K = 0.372E(B-V)$, I will refer to the Wesenheit functions $W(BV) = V - 3.1E(B-V)$, $W(VR) = V - 4.77(V-R)$, $W(VI) = V - 2.48(V-I)$, $W(VJ) = V - 1.407(V-J)$, $W(VH) = V - 1.227(V-H)$ and $W(VK) = V - 1.136(V-K)$. Moreover, since only near-infrared data are available for several P2Cs, I will consider also the function $W(JK)$=$K - 0.709(J-K)$. As shown in Fig. 4.25, where the fundamental pulsators with $Z$=0.0001 and [$\alpha$/Fe]=0.4 are plotted is some selected Period-Wesenheit diagrams, the magnitude dispersion at fixed period is indeed greatly reduced, leading to tight linear $PW$ relations. By a least square fit to all the fundamental pulsators with [Fe/H]=$-2.6$ to $-0.7$, I derive the coefficients listed in Table 4.10. These relations give us a quite safe way to estimate the intrinsic distance mod-

***Table 4.10:*** *Period-Wesenheit relations for fundamental pulsators with iron content in the range of [Fe/H]=−2.6 to −0.7 and period $P \leq 8$ days.*

| $W = a + blogP_F + c[Fe/H]$ | | | |
|---|---|---|---|
| $W$ | $a$ | $b$ | $c$ |
| $W(VR)$ | $-1.07\pm0.07$ | $-2.42\pm0.02$ | +0.01$\pm$0.01 |
| $W(VI)$ | $-1.16\pm0.07$ | $-2.43\pm0.02$ | +0.04$\pm$0.01 |
| $W(VJ)$ | $-1.04\pm0.06$ | $-2.37\pm0.02$ | +0.05$\pm$0.01 |
| $W(VH)$ | $-1.20\pm0.06$ | $-2.58\pm0.02$ | +0.06$\pm$0.01 |
| $W(VK)$ | $-1.13\pm0.06$ | $-2.52\pm0.02$ | +0.06$\pm$0.01 |
| $W(JK)$ | $-1.15\pm0.06$ | $-2.60\pm0.02$ | +0.06$\pm$0.01 |

ulus $\mu_0$ of observed variables with a formal accuracy of 0.06-0.07 mag, independently of the reddening. Concerning the $W(BV)$ function, I show in Fig. 4.26 that the pulsator distribution in the log$P_F$-$W(BV)$ plane is much better represented by a quadratic relation, i.e., $W(BV) = \alpha + \beta$log$P_F + \gamma$(log$P_F)^2$, in particular at the lowers metal contents. Note also that, at variance with the other Wesenheit functions, the $W(BV)$ function becomes brighter as the pulsator metal content increases, at fixed period, with the magnitude difference increasing towards the longer periods. As a whole, the least square fit to all the fundamental pulsators with [Fe/H]=−2.6 to −0.7 yields $\alpha = -1.06(\pm0.07)$, $\beta = -2.96(\pm0.08) - 0.36$[Fe/H] and $\gamma = -0.17(\pm0.05) + 0.13$[Fe/H].

### 4.2.2 Comparison with observations

The Galactic globular clusters with observed P2Cs are listed in Table 4.11 with their reddening $E(B-V)$, apparent visual magnitude $V$(HB) and HB type, as given by Harris (1996). For these variables, I will adopt the periods and the apparent magnitudes provided by Pritzl et al. (2003, $BVI$, hereafter Pr03) and Matsunaga et al. (2006, $JHK_s$, hereafter Ma06). In their investigations, Pr03 and Ma06 find quite tight linear correlations of the absolute magnitudes of P2Cs, as derived from RR Lyrae based distance moduli, with log$P$, without a clear evidence for a change in the slope between BL Her and W Vir stars. In particular, adopting $M_V$(RR)=0.89+0.22[Fe/H], Ma06 derive $\delta M_J/\delta$log$P = -2.23(\pm0.05)$, $\delta M_H/\delta$log$P = -2.34(\pm0.05)$ and $\delta M_{K_s}/\delta$log$P =$

***Table 4.11:*** *Galactic globular clusters with observed P2Cs listed with their reddening $E(B-V)$, iron content [Fe/H], apparent visual magnitude $V$(HB) and HB type, as given by Harris (1996). The last two columns give the numbers of BL Her and W Vir stars.*

| Name | $E(B-V)$ | [Fe/H] | $V$(HB) | HB type | $N_{BL}$ | $N_{WV}$ |
|---|---|---|---|---|---|---|
| HP1 | 1.19 | −1.55 | 18.60 | – | 0 | 2 |
| N1904 | 0.01 | −1.57 | 16.15 | +0.89 | 0 | 1 |
| N2419 | 0.11 | −2.12 | 20.45 | +0.86 | 1 | 0 |
| N2808 | 0.22 | −1.15 | 16.22 | −0.49 | 1 | 0 |
| N4372 | 0.39 | −2.09 | 15.50 | +1.00 | 2 | 0 |
| N5139-$\omega$ Cen | 0.12 | −1.62 | 14.53 | +0.94 | 9 | 2 |
| N5272-M3 | 0.01 | −1.57 | 15.68 | +0.08 | 0 | 1 |
| N5904-M5 | 0.03 | −1.27 | 15.07 | +0.31 | 0 | 2 |
| N5986 | 0.28 | −1.58 | 16.52 | +0.97 | 0 | 1 |
| N6093-M80 | 0.18 | −1.75 | 16.10 | +0.93 | 0 | 1 |
| N6205-M13 | 0.02 | −1.54 | 15.05 | +0.97 | 4 | 1 |
| N6218-M12 | 0.19 | −1.48 | 14.60 | +0.97 | 0 | 1 |
| N6229 | 0.01 | −1.43 | 18.03 | +0.24 | 0 | 1 |
| N6254-M10 | 0.28 | −1.52 | 14.65 | +0.98 | 1 | 2 |
| N6256 | 1.03 | −0.70 | 18.50 | – | 0 | 1 |
| N6266-M62 | 0.47 | −1.29 | 16.25 | +0.32 | 0 | 1 |
| N6273-M19 | 0.41 | −1.68 | 16.50 | – | 1 | 2 |
| N6284 | 0.28 | −1.32 | 17.40 | – | 2 | 0 |
| N6293 | 0.41 | −1.92 | 16.50 | +0.90 | 1 | 0 |
| N6325 | 0.89 | −1.17 | 17.90 | – | 0 | 2 |
| N6341-M92 | 0.02 | −2.28 | 15.10 | +0.91 | 1 | 0 |
| N6388 | 0.37 | −0.60 | 16.85 | – | 2 | 1 |
| N6402-M14 | 0.60 | −1.39 | 17.30 | +0.65 | 2 | 3 |
| N6441 | 0.47 | −0.53 | 17.51 | – | 2 | 5 |
| N6453 | 0.66 | −1.53 | 17.53 | – | 0 | 2 |
| N6569 | 0.55 | −0.86 | 17.52 | – | 0 | 1 |
| N6626-M28 | 0.40 | −1.45 | 15.55 | +0.90 | 0 | 2 |
| N6626-M28 | 0.40 | −1.45 | 15.55 | +0.90 | 0 | 1 |
| N6715-M54 | 0.15 | −1.58 | 18.17 | +0.75 | 2 | 0 |
| N6749 | 1.50 | −1.60 | 19.70 | +1.00 | 1 | 0 |
| N6752 | 0.04 | −1.56 | 13.70 | +1.00 | 1 | 0 |
| N6779-M56 | 0.20 | −1.94 | 16.16 | +1.00 | 1 | 1 |
| N7078-M15 | 0.10 | −2.26 | 15.83 | +0.67 | 2 | 1 |
| N7089-M2 | 0.06 | −1.62 | 16.05 | +0.96 | 0 | 4 |
| Ton1 | 2.28 | −1.30 | 21.40 | – | 0 | 1 |

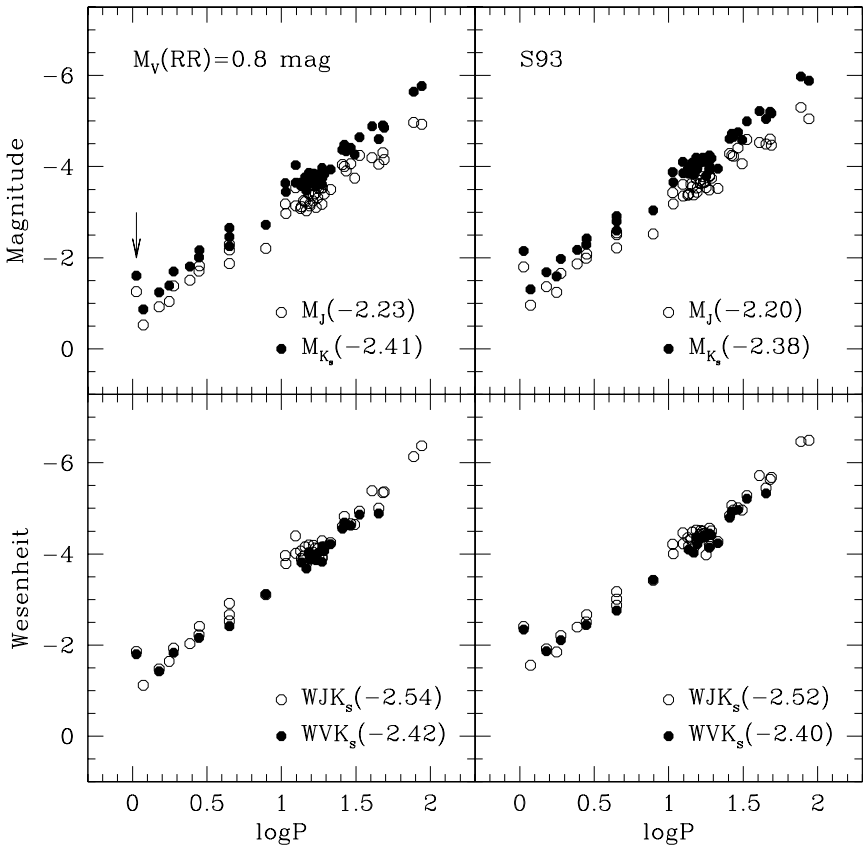


***Figure 4.27:*** *$PM$ and $PW$ distributions of observed P2Cs under two different assumptions on the absolute magnitude of RR Lyrae stars. The numbers in parentheses are the slopes of the relations, as derived by a linear regression to the data. The arrow indicates V7 in NGC 6341.*

$-2.41(\pm 0.05)$, which are in excellent agreement with the predicted slopes given in Table 4.9. In that study, it is also mentioned that the slope of the observed near-infrared $PM$ relations is not affected by different assumptions on the slope of the $M_V$(RR)-[Fe/H] relation. As a fact, by repeating the Ma06 procedure but adopting $M_V$(RR)=0.8 mag and $M_V$(RR)=0.94+0.30[Fe/H] (Sandage 1993: S93), the variation to the near-infrared $PM$ slopes is less than 2 percent (see the upper panels of Fig. 4.27). Here, I add that this holds also for the $PW$ relations based on $VJHK_s$ magnitudes (lower panels). Note that the arrow in this figure refers to NGC 6341 V7 (Del Principe et al. 2005) which will be discussed separately. Turning to the Pr03 optical magnitudes, some comments should be made to the data plotted in Fig. 4.28. Firstly, even removing the too faint outliers (i.e., the $BVI$ data of V24 and V28 in NGC 4372 and the $BV$ data of V12 and V32 in NGC

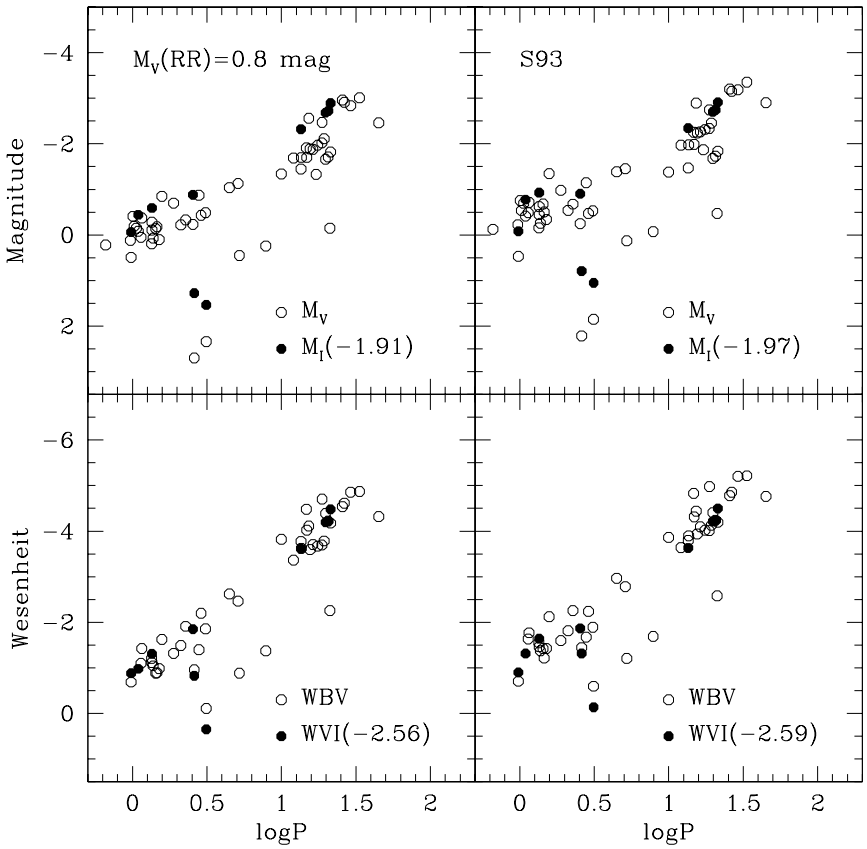


***Figure 4.28:*** *$PM$ and $PW$ distributions of observed P2Cs under two different assumptions on the absolute magnitude of RR Lyrae stars. The outliers are V24 and V28 in NGC 4372, V12 and V32 in NGC 6205 and V3 in NGC 6254.*

6205 and of V3 in NGC 6254, see also Pr03), there is a significant dispersion in the $PM_V$ and $PW(BV)$ planes as well as some evidence that the W Vir stars follow steeper $PM_V$ relations than the BL Her stars. As for the observed $PM_I$ and $PW(VI)$ relations, they appear linear and quite tight, with the slope independent of the adopted $M_V$(RR)-[Fe/H] relation and in good agreement with the predicted values. However, it should be mentioned that these results are based on a rather small number of data points (mostly, the variables in NGC 6441). In summary, all the observed P2Cs show linear near-infrared $PM$ relations and linear $PW$ relations, with the exclusion of $W(BV)$, independently of the adopted $M_V$(RR)-[Fe/H] relation. Moreover, the slopes of these relations are in close agreement with our predicted values for variables with $P \leq 8$ ys, supporting the hypothesis of similar relations for BL Her and W Vir stars. In addition, I wish to mention that the

[Fe/H] effect on the zero-point of the near-infrared $PM$ relations, as estimated by Ma06, is about 0.1 mag/dex$^{-1}$, again in agreement with the previous theoretical value.
On this ground, one can use the predicted relations derived in the previous section to derive the P2C distance moduli. To this purpose, since the Pietrinferni et al. (2004, 2006) magnitudes are in the Bessell & Brett (1988) near-infrared photometric system, the relations provided by Carpenter (2001) are used to transform the original 2MASS $JHK_s$ data given by Ma06 into standard $JHK$ magnitudes. For the P2C reddening and metal content, I adopt the values of the hosting globular cluster; however, for NGC 6388 and NGC 6441 I consider also [Fe/H]=$-$2.0, as adopted by Pr03 and Ma06. The resulting distance moduli are listed in Table 4.12, where the globular clusters with only W Vir stars are excluded. As for NGC 6341 V7, it will be discussed separately.
By inspection of the data in Table 4.12, the following points are worthy of mention:

- from the $BVI$ magnitudes of the NGC 6441 P2Cs, one finds an increasing discrepancy between the $\mu_{0,W(BV)}$ and $\mu_{0,W(VI)}$ values of a given variable when moving from short to long period stars. With [Fe/H]=$-$0.53, I get $\mu_{0,W(BV)} - \mu_{0,W(VI)} \sim$ 0.4 mag at log$P \sim$ 1.1 and $\sim$ 0.8 mag at log$P \sim$ 1.3. It is interesting to note that, if [Fe/H]=$-$2.0 is adopted, these differences are reduced to $\sim$ 0 and $\sim$0.3 mag, respectively. This would suggest that, despite the cluster high metallicity, the P2Cs may have a low metal content. However, I remind that the $\mu_{0,W(BV)}$ values are expected to be affected by large errors as a result of the older and less accurate photometry in these bands;

- For each given variable, the intrinsic distance modulus inferred by the near-infrared $W(JK)$ function is in a general agreement with the values based on the $W(VJ)$, $W(VH)$ and $W(VK)$ functions. No sure comparison can unfortunately be made with $\mu_{0,W(VI)}$, whereas we note significant discrepancies with the results based on $WBV$. This can be due to some old $BV$ data (see also Pr03), as well as, in the case of $\omega$ Cen variables, to the occurrence of a metallicity spread.

- Except the variables in $\omega$ Cen, the trend of the intrinsic and the apparent distance moduli, as determined by $JHK$ magnitudes, yields $A_J/E(B-V) \sim$ 0.85, $A_H/E(B-V) \sim$ 0.54 and $A_K/E(B-V) \sim$ 0.40, in reasonable agreement with

the extinction laws mentioned in section 4.2.1.

Eventually, by excluding the $\mu_{0,W(BV)}$ values, one derive the mean intrinsic distance moduli listed in Table 4.13 together with the estimated total uncertainty. As a matter of comparison, I give in the last column the cluster distance determined by adopting the relation $M_V$(RR)=0.89+0.22[Fe/H] and the reddening and HB visual magnitude in Table 4.11. As a whole, given the well known debate on the RR Lyrae distance scale (see Cacciari & Clementini 2003), we believe that the P2Cs distances agree with the RR Lyrae based values within the estimated uncertainty. As for a change in the $PM$ and $PW$ slopes around log$P \sim 1$, namely between BL Her and W Vir stars, the values listed in Table 4.13 show similar distances for the variables in $\omega$ Cen and NGC 6441, whereas for the remaining clusters there is a subtle discrepancy as the former distance moduli are shorter by $\sim 0.15$ mag than the latter ones.

We can now study NGC 6341 V7 which has a period log$P$=0.026 and is deviant from the near-infrared $PM$ relations (see arrow in Fig. 4.26). With $VJHK$ data taken from Del Principe et al. (2005), I would derive $\mu_0$=13.80$\pm$0.07 mag or 14.10$\pm$0.07 mag, depending on whether the variable is a fundamental or a first-overtone BL Her star (i.e, adopting log$P_F$=0.038). As a whole, these distances are too short with respect to $\mu_0(RR)$=14.65 mag, as derived by the relation $M_V$(RR)=0.89+0.22[Fe/H] using the values listed in Table 4.11. On the other hand, comparing the $K$ magnitudes of RR Lyrae stars from Del Principe et al. (2005) with the predicted $PM_K$ relations presented by Del Principe et al. (2006), one derive $\mu_0(RR)$=14.63$\pm$0.08 mag. Since the relations given in the present paper and those reported by Del Principe et al. (2006) are based on model computations which adopt homogeneous physics and numerical procedures, I can conclude that V7 is *not* a BL Her star but, due to the evidence that it is brighter than expected for its period, it may be an Anomalous Cepheid. Indeed, using for V7 the $PM_K$ relations determined by Fiorentino et al. (2006) from evolutionary and pulsation models of fundamental ACs, I derive $\mu_K$(AC)=14.69$\pm$0.15 mag.

Table 4.12: *Distance moduli (in magnitudes) for P2Cs in Galactic globular clusters, adopting the reddening and [Fe/H] values in Table 4.11. For NGC 6388 and NGC 6441, I adopt also [Fe/H]=−2.00. All the variables are taken as fundamental pulsators.*

| name | id | log$P$ | $\mu_{0,WBV}$ ±0.10 | $\mu_{0,WVI}$ ±0.06 | $\mu_{0,WVJ}$ ±0.06 | $\mu_{0,WVH}$ ±0.06 | $\mu_{0,WVK}$ ±0.06 | $\mu_{0,WJK}$ ±0.06 | $\mu_J$ ±0.15 | $\mu_H$ ±0.06 | $\mu_K$ ±0.06 |
|---|---|---|---|---|---|---|---|---|---|---|---|
| N2419 | 18 | 0.198 | 19.20 | – | – | – | – | – | – | – | – |
| N2808 | 10 | 0.247 | – | – | – | – | – | 14.99 | 15.21 | 15.15 | 15.10 |
| N5139 | 43 | 0.063 | 13.15 | – | – | – | – | – | – | – | – |
| N5139 | 92 | 0.129 | 13.53 | – | – | – | – | – | – | – | – |
| N5139 | 60 | 0.130 | 13.62 | – | – | – | – | – | – | – | – |
| N5139 | 61 | 0.357 | 13.40 | – | – | – | – | – | – | – | – |
| N5139 | 48 | 0.651 | 13.51 | – | 13.90 | 13.78 | 13.86 | 13.81 | 13.85 | 13.73 | 13.81 |
| N5139 | 29 | 1.168 | 13.23 | – | 13.85 | 13.95 | 13.89 | 13.89 | 13.88 | 13.83 | 13.82 |
| N5139 | 1 | 1.465 | – | – | 13.48 | 13.73 | 13.70 | 13.78 | 13.53 | 13.54 | 13.59 |
| N6205 | 1 | 0.164 | 14.76 | – | – | – | – | – | – | – | – |
| N6205 | 6 | 0.325 | 14.58 | – | – | – | – | – | – | – | – |
| N6205 | 2 | 0.709 | 14.68 | – | – | – | – | – | – | – | – |
| N6254 | 3 | 0.896 | – | – | 13.31 | 13.37 | 13.38 | 13.49 | 13.85 | 13.70 | 13.60 |
| N6254 | 2 | 1.272 | 14.01 | – | 13.56 | 13.70 | 13.63 | 13.63 | 13.73 | 13.64 | 13.60 |
| N6254 | 1 | 1.690 | – | – | – | – | – | 13.29 | 13.72 | 13.43 | 13.36 |
| N6273 | 4 | 0.386 | – | – | – | – | – | 14.69 | 14.94 | 14.82 | 14.80 |
| N6273 | 2 | 1.150 | – | – | – | – | – | 14.75 | 14.94 | 14.82 | 14.77 |
| N6273 | 1 | 1.228 | – | – | – | – | – | 14.78 | 14.96 | 14.82 | 14.79 |
| N6284 | 4 | 0.450 | – | – | – | – | – | 15.76 | 15.94 | 15.81 | 15.83 |
| N6284 | 1 | 0.651 | – | – | – | – | – | 15.77 | 15.93 | 15.81 | 15.82 |
| N6293 | 2 | 0.073 | – | – | – | – | – | 14.80 | 15.21 | 15.06 | 15.01 |
| N6388 | 18 | 0.461 | 15.08 | – | – | – | – | – | – | – | – |
| N6388 | 36 | 0.491 | 15.52 | – | – | – | – | – | – | – | – |
| N6388 | 37 | 1.000 | 15.14 | – | – | – | – | – | – | – | – |
| N6388mp | 18 | 0.461 | 14.89 | – | – | – | – | – | – | – | – |
| N6388mp | 36 | 0.491 | 15.31 | – | – | – | – | – | – | – | – |
| N6388mp | 37 | 1.000 | 14.81 | – | – | – | – | – | – | – | – |
| N6402 | 76 | 0.276 | 15.09 | – | 14.82 | 14.75 | 14.76 | 14.70 | 15.18 | 15.00 | 14.91 |
| N6402 | 2 | 0.446 | 15.47 | – | 14.83 | 14.83 | 14.86 | 14.84 | 15.24 | 15.07 | 15.01 |
| N6402 | 17 | 1.082 | 15.41 | – | – | – | – | – | – | – | – |
| N6402 | 7 | 1.134 | 15.32 | – | 14.82 | 14.93 | 14.93 | 14.96 | 15.41 | 15.16 | 15.09 |
| N6402 | 1 | 1.273 | 14.70 | – | 14.89 | 15.02 | 14.93 | 14.93 | 15.32 | 15.13 | 15.02 |
| N6441 | 118 | −0.009 | 15.60 | 15.53 | – | – | – | – | – | – | – |
| N6441 | 132 | 0.406 | – | 15.57 | – | – | – | – | – | – | – |
| N6441 | 128 | 1.131 | 15.98 | 15.57 | – | – | – | – | – | – | – |
| N6441 | 129 | 1.251 | – | – | – | – | – | 15.76 | 15.73 | 15.53 | 15.67 |
| .. | .. | .. | .. | .. | .. | .. | .. | .. | .. | .. | .. |

Table 4.12: (continued)

| name | id | log$P$ | $\mu_{0,WBV}$ ±0.10 | $\mu_{0,WVI}$ ±0.06 | $\mu_{0,WVJ}$ ±0.06 | $\mu_{0,WVH}$ ±0.06 | $\mu_{0,WVK}$ ±0.06 | $\mu_{0,WJK}$ ±0.06 | $\mu_J$ ±0.15 | $\mu_H$ ±0.06 | $\mu_K$ ±0.06 |
|---|---|---|---|---|---|---|---|---|---|---|---|
| N6441 | 127 | 1.296 | 15.92 | 15.39 | – | – | – | – | – | – | – |
| N6441 | 126 | 1.314 | 16.14 | 15.41 | – | – | – | – | – | – | – |
| N6441 | 6 | 1.330 | 16.24 | 15.19 | 15.37 | 15.59 | 15.59 | 15.68 | 15.94 | 15.75 | 15.70 |
| N6441mp | 118 | −0.009 | 15.60 | 15.59 | – | – | – | – | – | – | – |
| N6441mp | 132 | 0.406 | – | 15.63 | – | – | – | – | – | – | – |
| N6441mp | 128 | 1.131 | 15.62 | 15.63 | – | – | – | – | – | – | – |
| N6441mp | 129 | 1.251 | – | – | – | – | – | 15.89 | 15.79 | 15.62 | 15.76 |
| N6441mp | 127 | 1.296 | 15.55 | 15.65 | – | – | – | – | – | – | – |
| N6441mp | 126 | 1.314 | 15.78 | 15.47 | – | – | – | – | – | – | – |
| N6441mp | 6 | 1.330 | 15.88 | 15.25 | 15.44 | 15.67 | 15.68 | 15.77 | 16.00 | 15.84 | 15.79 |
| N6715 | 2 | 0.039 | – | 17.24 | – | – | – | – | – | – | – |
| N6715 | 1 | 0.130 | – | 17.14 | – | – | – | – | – | – | – |
| N6749 | 1 | 0.651 | – | – | – | – | – | 14.56 | 15.66 | 15.21 | 15.00 |
| N6752 | 1 | 0.139 | 13.13 | – | – | – | – | – | – | – | – |
| N6779 | 1 | 0.179 | 15.23 | – | 15.05 | 15.05 | 15.06 | 15.03 | 15.18 | 15.16 | 15.13 |
| N6779 | 6 | 1.653 | 16.37 | – | 15.19 | 15.40 | 15.31 | 15.34 | 15.44 | 15.32 | 15.27 |
| N7078 | 72 | 0.057 | 14.81 | – | – | – | – | – | – | – | – |
| N7078 | 1 | 0.157 | 15.24 | – | – | – | – | – | – | – | – |
| N7078 | 86 | 1.233 | – | – | 15.06 | 15.32 | 15.27 | 15.35 | 15.32 | 15.31 | 15.27 |

***Table 4.13:*** *Mean intrinsic distance moduli (in magnitudes), as derived by the Wesenheit functions of BL Her and W Vir stars. The quantity N is the number of averaged values. As a matter of comparison, in the last column is given the intrinsic distance moduli based on RR Lyrae stars (see text).*

| name | $\mu_0$(BLH) | N | $\mu_0$(WV) | N | $\mu_0$(RR) |
|---|---|---|---|---|---|
| N2808 | 14.99±0.06 | 1 | – | – | 14.90 |
| N5139 | 13.84±0.08 | 4 | 13.78±0.16 | 4 | 13.62 |
| N6254 | 13.39±0.20 | 4 | 13.56±0.16 | 2 | 13.23 |
| N6273 | 14.69±0.06 | 1 | 14.77±0.06 | 2 | 14.71 |
| N6284 | 15.77±0.06 | 2 | – | – | 15.93 |
| N6293 | 14.80±0.06 | 1 | – | – | 14.76 |
| N6402 | 14.80±0.08 | 8 | 14.93±0.09 | 8 | 14.86 |
| N6441 | 15.55±0.07 | 2 | 15.53±0.19 | 6 | 15.28 |
| N6441mp | 15.61±0.07 | 2 | 15.58±0.18 | 6 | 15.60 |
| N6715 | 17.19±0.10 | 2 | – | – | 17.16 |
| N6749 | 14.56±0.08 | 1 | – | – | 14.51 |
| N6779 | 15.05±0.06 | 4 | 15.31±0.11 | 4 | 15.08 |

# 5

# RR lyrae based calibration of Globular Clusters Luminosity Function

**(Di Criscienzo et al. 2006, MNRAS, 365)**

*RR Lyrae also provide an independent test of the Cepheid distance scale for nearby galaxies (Magellanic Clouds, M31), as well as a calibration of secondary distance indicators (in particular the globular clusters luminosity function, GCLF) in external galaxies, thus yielding relevant clues about the value of the Hubble constant. In this chapter I use various calibrations of the MV(RR)-[Fe/H] relations and several globular clusters catalogues to calculate the turnover magnitude of the Galactic GCLF, the first step to use the GCLF distance indicator. The application to external galaxies will show that the turnover magnitude of metal poor clusters in external galaxies is in excellent agreement with the value of both the Galactic and the M31 ones, as inferred fro an RR Lyrae distance scale referenced to the same LMC fiducial distance value.*

## 5.1 The method of GCLF

In several fields of modern astronomy, the determination of extragalactic distances is based on a ladder which is firmly anchored to Classical Cepheids and RR Lyrae stars, the "primary" standard candles for Population I and Population II stellar systems, respectively, with the properties of these variables used to calibrate "secondary" indicators which step-by-step lead us through the Local Group up to cosmologically significant distances. In this context, the Globular Clusters Luminosity Function is playing an ever increasing role to estimate the distance to galaxies within $\sim$ 30 Mpc, as witnessed by the huge amount of relevant papers published in the last decade. In the past, its use was hampered by the lack of observations of globular clusters beyond the Local Group but with the advent of modern telescopes, above all the Hubble Space Telescope (HST), it is now possible to resolve stellar populations in faraway galaxies, identify the GC candidates, measure their integrated magnitude and finally build the related luminosity function. The GCLF method is based on the assumption that within each galaxy hosting statistically significant numbers of GCs, the frequency of the cluster integrated magnitude $V(GC)$ exhibits a universal shape which can be fitted with a Gaussian distribution of type:

$$\frac{dN}{dV} = Ae^{-\frac{[V(GC)-V(TO)]^2}{2\sigma^2}} \tag{5.1}$$

where $dN$ is the number of clusters in the magnitude bin $dV$, $V(TO)$ is the magnitude of the peak or turnover, $\sigma$ is the Gaussian dispersion and $A$ the normalization factor. Once the turnover absolute value $M_V(TO)$ is known to be constant or varying in a predictable way, the distance to the parent galaxy follows immediately from the apparent (reddening corrected) magnitude of the GCLF peak. This relation is not universally accepted (see, *i.e.*, Richtler 2003 and references therein) and several authors prefer to use a $t$-distribution (see Secker 1992, Secker & Harris 1993, Barmby, Huchra & Brodie 2001, hereafter BHB), but with unimportant differences with the respect to the Gaussian turnover magnitude (Della Valle et al. 1998, BHB). Moreover, it should be noted that also the use of the GCLF for trustworthy distance determinations is argued because the absolute peak magnitudes suggested so far by the various authors show a scatter of about 0.5 mag (see Ferrarese et al. 2000). In any case, the only galaxy where globular clusters can be observed well over the turnover, down to the faintest integrated magnitudes, and where the cluster individual

distances are determined with a sufficiently high level of confidence, as inferred from the observed magnitude of the horizontal branch or the RR Lyrae stars, is the Milky Way. For these reasons, the absolute LF of Galactic Globular Clusters (GGCs) represents the first (obligatory) step to the calibration of extragalactic luminosity functions. Unfortunately, for the Milky Way itself current $M_V(TO)$ values show a large scatter, from $\sim -7.3$ mag (Secker 1992) to $\sim -7.6$ mag (Sandage & Tammann 1995), thus implying unpleasant uncertainties on the determination of the distance to external galaxies. In order to investigate the source of such a discrepancy, in the first part of section 5.2 I will estimate the effects on the Milky Way GCLF as due to the adopted metallicity calibration of the RR Lyrae absolute magnitude and to selective criteria of the GC sample, while section 5.3 deals with GCs in M31. As for other external galaxies, where no RR Lyrae stars are observed, in section 5.4 the apparent magnitude of the GCLF turnover is compared with the Surface Brightness Fluctuations measurements. In this way, is also possible to check the consistency between GCLF distances, which are based on the RR Lyrae luminosity scale, and those provided by the latter secondary distance indicator which is calibrated on Cepheid distances.

## 5.2 The Milky Way absolute GCLF

Almost all the recent papers dealing with the luminosity function of Galactic globular clusters adopt the data collected by Harris (1996). Using this catalog (2003 update, hereafter H96), and leaving out those for which all the required information are not available, Table 5.1 list the 144 clusters with measured metal content [Fe/H], apparent magnitude of the horizontal branch $V(HB)$ and apparent integrated magnitude $V(GC)$. In this table, I have excluded AM4 whose available photometry (Inman & Carney 1987) shows no stars brighter than the main-sequence turnoff. Moreover, following recent suggestions (see van den Bergh 2003, van den Bergh & Mackey 2004 and references therein), I have marked the clusters suspected to be not true members of the Galaxy but of the Sculptor dwarf galaxy (N6715(M54), Ter 7, Ter 8, Arp 2, Pal 12, N4147, and Pal 2) or of the Canis Major dwarf galaxy (N1851, N1904, N2298, and N2808). Let us also note that the same authors suggest that Pal 1, N5139 ($\omega$ Cen), and N2419 might have formed in now dis-

***Table 5.1:*** *Globular clusters in the Milky Way. Columns (1)-(4) are taken from Harris (1996, 2003 update). while columns (5)-(8) give the cluster absolute integrated magnitude according to the $M_V(RR)$-[Fe/H] relations discussed in the text. Clusters marked (a) and (b) are suspected to belong to the Sculptor and the Canis Major dwarf galaxy respectively, while Pal 1, N2419 and N5139 ($\omega$ Cen) might be associated with now not extant dwarf galaxies (the full table is reported at the end of this chapter)*

| Name (1) | [Fe/H] (2) | $M_V(GC)$ (3:H96) | $R_{GC}$ (4:H96) | $M_V(GC)$ (5:S93) | $M_V(GC)$ (6:F98) | $M_V(GC)$ (7:G03) | $M_V(GC)$ (8:B03) |
|---|---|---|---|---|---|---|---|
| N104 | $-0.76$ | $-9.42$ | 7.4 | $-9.40$ | $-9.28$ | $-9.39$ | $-9.36$ |
| N288 | $-1.24$ | $-6.74$ | 12.0 | $-6.78$ | $-6.62$ | $-6.73$ | $-6.76$ |
| N362 | $-1.16$ | $-8.41$ | 9.4 | $-8.45$ | $-8.29$ | $-8.41$ | $-8.42$ |
| N1261 | $-1.35$ | $-7.81$ | 18.2 | $-7.87$ | $-7.70$ | $-7.82$ | $-7.85$ |
| Pal 1 | $-0.60$ | $-2.47$ | 17.0 | $-2.42$ | $-2.32$ | $-2.42$ | $-2.37$ |
| AM 1 | $-1.80$ | $-4.71$ | 123.2 | $-4.84$ | $-4.62$ | $-4.75$ | $-4.81$ |
| Eridanus | $-1.46$ | $-5.14$ | 95.2 | $-5.22$ | $-5.03$ | $-5.15$ | $-5.20$ |
| Pal 2 | $-1.30$ | $-8.01$ | 35.4 | $-8.06$ | $-7.89$ | $-8.01$ | $-8.04$ |
| ... | ... | ... | ... | ... | ... | ... | ... |

trupted dwarf galaxies. The global features of the GGCs have been extensively studied (see, *i.e.*, van den Bergh & Mackey 2004, van den Bergh 2003 and references therein) and here is important only to draw attention to the cluster metallicity dichotomy at [Fe/H] $\sim -1.0$, with the metal-poor component containing about 3/4 of all clusters. Based on the H96 metal contents, Fig. 5.1 shows that the total distribution can be well described by two Gaussian curves peaked at [Fe/H] $\sim -1.55\pm0.04$ ($\sigma$=0.35$\pm$0.08) and $-0.55\pm0.06$ ($\sigma$=0.38$\pm$0.09). As a whole, no metal-rich cluster is observed at Galactocentric distances $R_{GC} > 8$ kpc, except the suspected peculiar (see above) clusters Pal 1, Pal 12, and Ter 7, while those located within 8 kpc span a metallicity range from [Fe/H]$\sim -2.3$ to $\sim 0$. As for the absolute integrated magnitude $M_V(GC)$ and the Galactocentric distances $R_{GC}$ listed in the Harris' catalog (columns (3) and (4) in Table 5.1), they rest on the cluster distance moduli determined by adopting $V(HB)$=$V(RR)$ and the H96 relation:

$$M_V(RR) = 0.80 + 0.15[Fe/H] \tag{5.2}$$

which provides a rather smooth luminosity decrease from metal-poor to metal-rich clusters. However, the review by Cacciari & Clementini (2003) shows that a general consen-

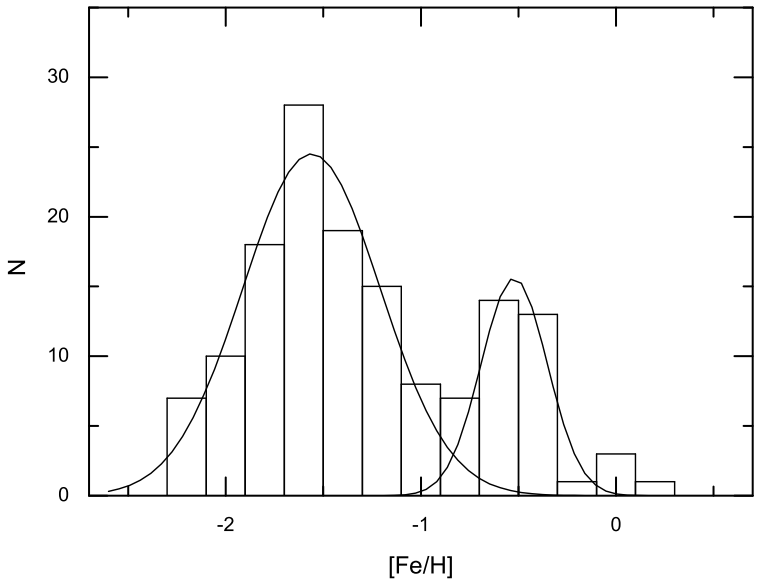


***Figure 5.1:*** *Frequency distribution of metallicity for GCs in the Milky Way. The data have been fitted with the two Gaussian curves shown in the figure.*

sus on the $M_V(RR)$-[Fe/H] calibration of RR Lyrae stars has not been achieved yet, with the longstanding debate concerning both the zero point and the slope of the calibration. Since the $M_V(GC)$ values depend on the cluster distance modulus, i.e. on the adopted $M_V(RR)$-[Fe/H] relation, I show in Fig. 5.2 the comparison between equation 5.2 and some relevant results presented in the recent literature. Specifically, I use the typical "long-scale" calibration by Sandage (1993, S93):

$$M_V(RR) = 0.94 + 0.30[Fe/H] \tag{5.3}$$

the revised Baade-Wesselink ("short-scale") one by Fernley et al. (1998, F98):

$$M_V(RR) = 0.98 + 0.20[Fe/H] \tag{5.4}$$

and the relation inferred by Gratton et al. (2003, G03):

$$M_V(HB) = 0.89 + 0.22[Fe/H] \tag{5.5}$$

on the basis of the main-sequence fitting procedure. Furthermore, since several observational and theoretical studies (see Bono et al. 2003, Di Criscienzo, Marconi & Caputo

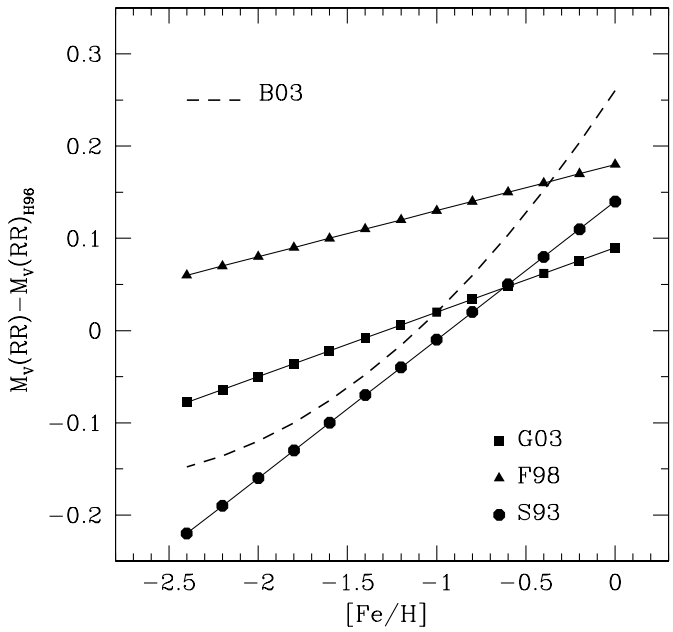


***Figure 5.2:*** *Comparison between the $M_V(RR)$-[Fe/H] relations discussed in the text.*

2004 and references therein) suggest that the $M_V(RR)$-[Fe/H] is not linear, becoming steeper when moving toward larger metal content, the two linear relations presented by Bono et al. (2003, B03) for GCs with [Fe/H] $< -1.6$ and $\geq -1.6$ have been approximated in the quadratic form:

$$M_V(RR) = 1.06 + 0.44[Fe/H] + 0.05[Fe/H]^2 \tag{5.6}$$

as shown in the figure with a dashed line. As irony of fate, all these relations yield for the "prototype" variable RR Lyr itself ([Fe/H]=$-1.39$) an absolute magnitude which is consistent with the value $M_V$=0.61$\pm$0.12 mag determined from the HST astrometric parallax $\pi_{HST}$=3.82$\pm$0.20 mas and current uncertainty on the extinction correction (see Benedict et al. 2002), thus hindering us from any a priori selection. This also in consideration of the fact that the absolute magnitude of RR Lyrae stars is expected to depend also on the HB morphology, becoming brighter up to $\sim 0.1$ mag, at fixed metal content, when the population of HB stars moves from red to blue (see, *i.e.*, Demarque et al. 2000, Cassisi et al. 2004

***Table 5.2:*** *RR Lyrae-based intrinsic distance moduli $\mu_0$ (mag) of LMC and M31. The errors in parenthesis take into account the uncertainty on [Fe/H] (Ref. Wa92: Walker (1992, Globular Clusters); Cl03: Clementini et al. (2003, Field); Da04: Dall' Ora et al. (2004, globular cluster, $K$ magnitudes); Bo04: Borissova et al. (2004, Field, $K$ magnitudes); Br04: Brown et al. (2004, field. The two measures refer to $ab$ and $c$-type variables). The original [Fe/H] values are increased by 0.1 dex to put the Zinn & West (1995) scale in agreement with the H96 scale).*

| Ref. | $V_0(RR)$ | [Fe/H] | $\mu_0$(H96) | $\mu_0$(S93) | $\mu_0$(F98) | $\mu_0$(G03) | $\mu_0$(B03) |
|---|---|---|---|---|---|---|---|
| *LMC* | | | | | | | |
| Wa92 | 18.95(0.04) | $-1.9$ | 18.44(0.05) | 18.58(0.07) | 18.35(0.09) | 18.48(0.09) | 18.55(0.06) |
| Cl03 | 19.06(0.06) | $-1.5$ | 18.49(0.08) | 18.57(0.11) | 18.38(0.09) | 18.50(0.09) | 18.55(0.11) |
| Da04 | | $-1.7$ | | | | | 18.52(0.12) |
| Bo04 | | $-1.5$ | | | | | 18.48(0.08) |
| *mean* | | | 18.47$\pm$0.08 | 18.58$\pm$0.11 | 18.37$\pm$0.11 | 18.49$\pm$0.13 | 18.53$\pm$0.11 |
| *M31* | | | | | | | |
| Br04 | 25.03(0.01) | $-1.6$ | 24.47(0.05) | 24.57(0.09) | 24.37(0.06) | 24.49(0.07) | 24.55(0.08) |
| Br04 | 25.06(0.01) | $-1.3$ | 24.46(0.05) | 24.51(0.09) | 24.34(0.06) | 24.46(0.07) | 24.49(0.08) |
| *mean* | | | 24.47$\pm$0.07 | 24.54$\pm$0.11 | 24.36$\pm$0.08 | 24.48$\pm$0.08 | 24.52$\pm$0.10 |

and references therein). On this ground, I estimate that the zero-point of all the $M_V(RR)$-[Fe/H] relations has an intrinsic uncertainty of about 0.05 mag. However, with everything else being constant, inspection of data in Fig. 5.2 discloses that the effects of the adopted $M_V(RR)$-[Fe/H] relation on the $M_V(GC)$ magnitude of individual clusters may amount to quite significant values. Therefore I have used all the $M_V(GC)$ values listed in Table 5.1 to construct the LFs generated by the various $M_V(RR)$-[Fe/H] calibrations adopted in this paper. Before proceeding, in Table 5.2 are given the RR Lyrae-based intrinsic distance moduli $\mu_0$ of the Large Magellanic Cloud (LMC) and M31, as inferred by these $M_V(RR)$-[Fe/H] relations. In the same table are also listed the results provided by recent near-infrared observations of LMC RR Lyrae stars and theoretical predictions discussed in B03. According to the data in Table 5.2, the adopted $M_V(RR)$ calibration modifies the RR Lyrae distance to LMC and M31, but without effect on the relative distance of the two galaxies which turns out to be $\mu_0$(M31)$-\mu_0$(LMC)=6.0$\pm$0.1 mag. Concerning the absolute distance to LMC, which is a benchmark to the Cepheid distance scale, it is important to recall the wide range spanned by current estimates (see Caputo et al. 2000; Gibson et al. 2000, Clementini et al., 2003), including those provided by SN1987A ($\mu_0$=18.50$\pm$0.05

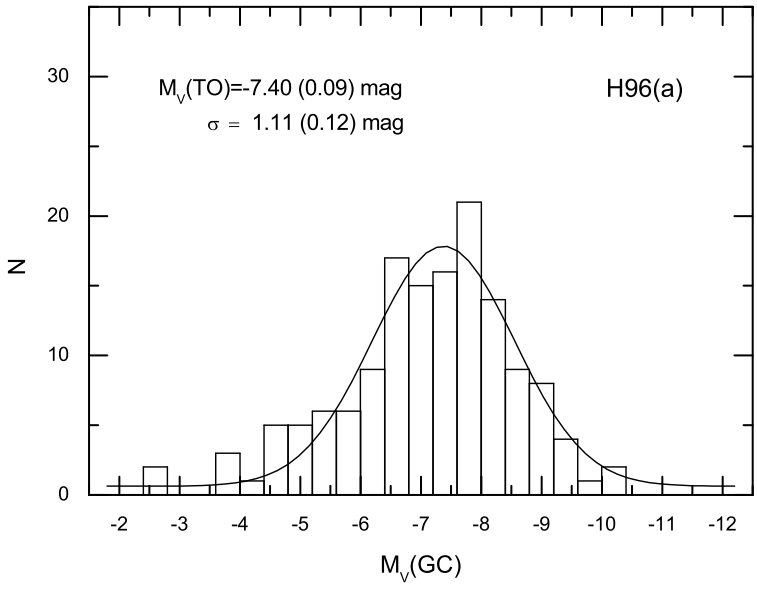


***Figure 5.3:*** *GCLF for Galactic clusters in the full sample H96(a).*

mag, Panagia 1998) and eclipsing binaries ($\mu_0$=18.23-18.53 mag, Fitzpatrick et al. 2003). Fig. 5.3 shows the luminosity function of the GGC full sample (hereafter H96(a)) using the absolute integrated magnitudes listed by H96 (column (3) in Table 5.3). The data have been fitted with a two-parameter (turnover and dispersion) Gaussian curve varying the width (0.2, 0.3, 0.4 mag) and the center of the magnitude bins. The resulting averaged values of $M_V(TO)$ and $\sigma$ are reported in the figure. This procedure should allow us to take into account the intrinsic dispersion of the $M_V(RR)$-[Fe/H] relation as well as the additional effects due to the uncertainty of the apparent integrated visual magnitude $V(GC)$ and the adopted metallicity scale. It is important to stress that accurate integrated photometry of Galactic GCs is difficult, especially for those located in crowded regions toward the Galactic Center, at large distances or with low luminosity. However, most of the $V(GC)$ values reported in the Harris catalog, as obtained from consistent original databases and based on concentric-aperture photometry of the clusters, are accurate till $\sim$ 0.1 mag and only for a small number of sparse and/or faint clusters the accuracy is worse than 0.1 mag. On the other side, the scale from Zinn & West (1984) used by H96 and the one from Carretta & Gratton (1997) adopted by G03 show a maximum discrepancy of $\sim$

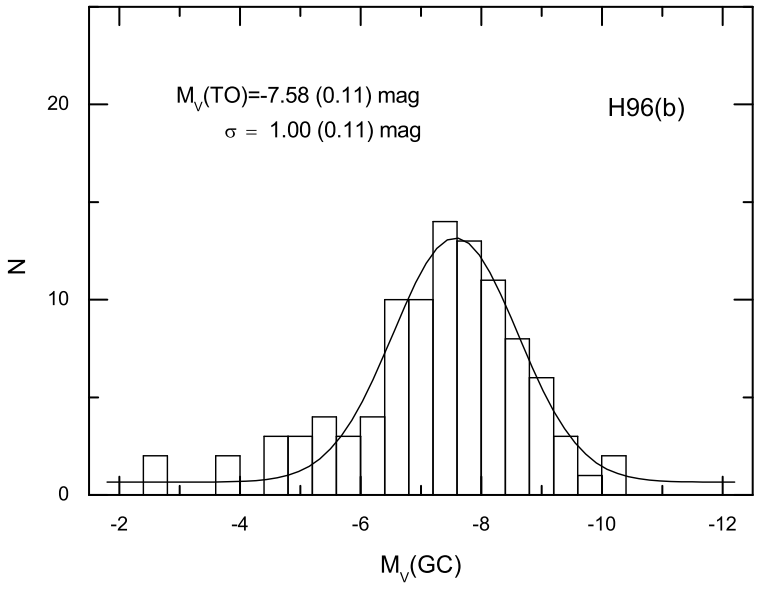


***Figure 5.4:*** *As in Fig. 5.3, but for the selected sample H96(b).*

0.2 dex at intermediate metal deficiency ($-1.0\leq$ [Fe/H] $\leq -1.9$, see Kraft & Ivans, 2003), thus introducing a maximum uncertainty of the order of 0.03 mag on $M_V(RR)$. The resulting peak magnitude$M_V(TO)$=$-$7.40$\pm$0.09 mag is fully consistent with $-$7.44$\pm$0.15 mag and $-$7.40$\pm$0.11 mag, as obtained by Kavelaars & Hanes (1997) and Harris (2001), respectively, on the basis of H96 catalog and $M_V(RR)$calibration. Therefore I repeat the procedure adopting the$M_V(GC)$ values given in columns (5)-(8) of Table 5.1, with the numerical results labelled H96(a) in the first part of Table 5.3. Quite surprisingly, I derive that, in spite of the different zero points and slopes, the adopted dependence of $M_V(RR)$ on metallicity does not modify significantly the peak magnitude, with the exception of the F98 relation which gives a value fainter by $\sim$ 0.15 mag with respect to the average $M_V(TO)$=$-$7.42$\pm$0.11 mag of the other calibrations. In this, the turnover magnitude $M_V(TO)$=$-$7.26$\pm$0.08 mag based on the F98 calibration agrees with$-$7.29$\pm$0.13 mag, as determined by Secker (1992) using a previous GC catalog (Harris et al. 1991) and $M_V(RR)$=1.00+0.20[Fe/H], which is only 0.02 mag fainter than equation 5.4.

However, at variance with the above agreement with the quoted studies, the results in this way are fainter than $M_V(TO)$=$-$7.60$\pm$0.11 mag, the peak magnitude obtained by

***Table 5.3:*** *$M_V(TO)$ and $\sigma$ values of GGCs as based on the $M_V(RR)$-[Fe/H] relations discussed in the text. The results are based on the H96 catalog of GGCs with (a) denoting the full sample and (b) the Secker (1992) selection (see text).*

| Sample | $\langle$[Fe/H]$\rangle$ | $M_V(RR)$ | $M_V(TO)$ | $\sigma$ |
|---|---|---|---|---|
| H96(a) | $-1.29\pm0.57$ | H96 | $-7.40\pm0.09$ | $1.11\pm0.12$ |
| N=144 | | S93 | $-7.46\pm0.11$ | $1.14\pm0.13$ |
| | | F98 | $-7.26\pm0.08$ | $1.11\pm0.10$ |
| | | G03 | $-7.40\pm0.11$ | $1.14\pm0.12$ |
| | | B03 | $-7.40\pm0.09$ | $1.14\pm0.11$ |
| H96(b) | $-1.39\pm0.51$ | H96 | $-7.58\pm0.11$ | $1.00\pm0.11$ |
| N=100 | | S93 | $-7.66\pm0.11$ | $1.04\pm0.12$ |
| | | F98 | $-7.47\pm0.10$ | $1.00\pm0.11$ |
| | | G03 | $-7.62\pm0.11$ | $1.02\pm0.12$ |
| | | B03 | $-7.64\pm0.12$ | $1.00\pm0.11$ |

Sandage & Tammann (1995) with the S93 relation, and than $-7.55\pm0.14$ mag, as determined by Larsen et al. (2001, hereafter L01) from the H96 absolute integrated magnitudes. Those two results deal with the selected GGC subset as earlier adopted in the Secker (1992) study, namely holding for GCs with $E(B\text{-}V)$ $\leq$1.0 mag and $2 \leq R_{GC} \leq$35 kpc. For this reason, I have repeated my analysis by applying this selection to all the clusters in Table 5.1. In this way I derive, (see Fig. 5.4 and the H96(b) values listed in the second part of Table 5.3), that the peak magnitudes are now brighter by $\sim 0.2$ mag with respect to those of the full sample H96(a). As shown in Fig. **??**, where the two GC samples are plotted in the $M_V(GC)$-log$R_{GC}$ plane, the reason of such a variation is the fact that Secker's selection removes a larger number of clusters fainter than $-7.40$ mag (the peak magnitude of the H96(a) sample, see dashed line) with respect to a the brighter ones, leading to the systematic increase of the peak luminosity. Consequently, H96(b) magnitudes $M_V(TO)$=$-7.66\pm0.11$ mag and $-7.58\pm0.11$ mag, as based on equations 5.3 and 5.4, are now in agreement with the Sandage & Tammann (1995) and L01 results, respectively, but the value based on equation 5.4, increased by 0.02 mag to account for the small difference with the relation adopted by Secker (1992), turns out to be significantly brighter ($\sim 0.16$ mag) than the Secker's value. Of importance for the following discussion is the evidence that the constraints to select the GC sample have an effect on the peak magnitude which

***Table 5.4:*** *As in Table 5.3. but for metal-rich (MR: [Fe/H]$>-1.0$) and metal-poor (MP: [Fe/H] $<-1.0$) GGCs.*

| H96(a) | MR: N=44 $\langle$[Fe/H]$\rangle=-0.57\pm0.26$ | MP: N=100 $\langle$[Fe/H]$\rangle=-1.61\pm0.30$ |
|---|---|---|
| $M_V(RR)$ | $M_V(TO)(\sigma)$ | $M_V(TO)(\sigma)$ |
| H96 | $-7.20\pm0.18(1.08\pm0.23)$ | $-7.49\pm0.09(1.09\pm0.11)$ |
| S93 | $-7.17\pm0.19(1.08\pm0.23)$ | $-7.56\pm0.10(1.12\pm0.12)$ |
| F98 | $-7.04\pm0.14(1.09\pm0.19)$ | $-7.35\pm0.08(1.10\pm0.10)$ |
| G03 | $-7.18\pm0.20(1.07\pm0.25)$ | $-7.50\pm0.09(1.10\pm0.10)$ |
| B03 | $-7.08\pm0.19(0.99\pm0.23)$ | $-7.55\pm0.09(1.12\pm0.12)$ |
| H96(b) | MR: N=26 $\langle$[Fe/H]$\rangle=-0.67\pm0.21$ | MP: N=74 $\langle$[Fe/H]$\rangle=-1.64\pm0.31$ |
| $M_V(RR)$ | | $M_V(TO)(\sigma)$ |
| H96 | $\sim -7.4$ | $-7.63\pm0.09(1.00\pm0.10)$ |
| S93 | $\sim -7.3$ | $-7.72\pm0.10(1.02\pm0.12)$ |
| F98 | $\sim -7.2$ | $-7.52\pm0.12(1.00\pm0.11)$ |
| G03 | $\sim -7.3$ | $-7.65\pm0.11(1.00\pm0.12)$ |
| B03 | $\sim -7.3$ | $-7.70\pm0.11(1.00\pm0.11)$ |

may be larger than that introduced by the adopted RR Lyrae distance scale. This is a crucial point in view of the comparison of the Milky Way GCLF with one in another galaxy. In particular, the fact that many external galaxies show a bimodal metallicity distribution, as inferred from the color behavior, and that several studies present extragalactic GCLFs selected by the cluster metallicity or distance from the galaxy center, lead us to analyze the dependence of the Galactic GCLF on both [Fe/H] and $R_{GC}$.

**Dependence on metallicity**

According to Fig. 5.1, I split at [Fe/H]$=-1.0$ the GC full sample and give in the first part of Table 5.4 the resulting peak magnitudes and $\sigma$ values for the metal-poor (MP) and the metal-rich (MR) groups (see Fig. 5.5 which deals with absolute integrated magnitudes based on the H96 relation). As a whole, the peak magnitude of the MP clusters ($\langle$[Fe/H]$\rangle=-1.61$) is brighter by about 0.10 mag than that of the combined sample ($\langle$[Fe/H]$\rangle=-1.29$) listed in the first part of Table 5.3, independently of the adopted $M_V(RR)$ calibration. Moreover, even though the number of MR clusters is slightly smaller than that required to measure the Gaussian parameters with reasonable precision

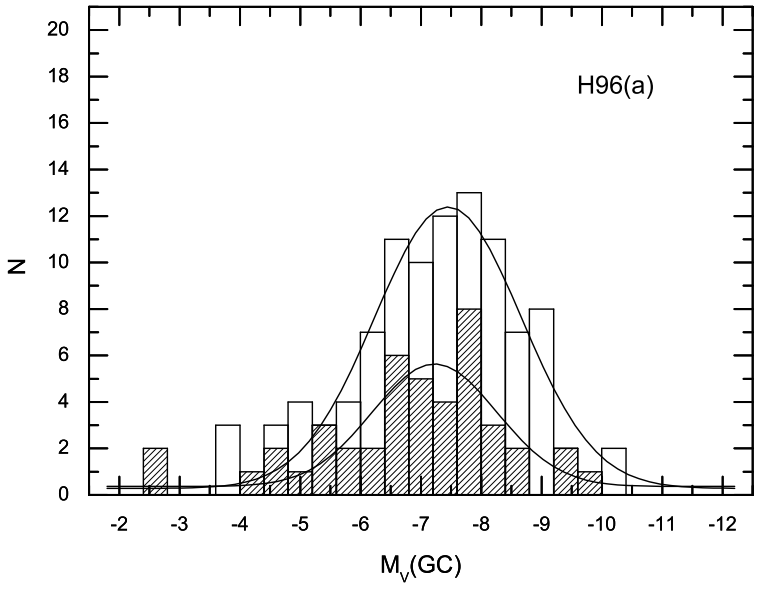


***Figure 5.5:*** *GCLFs for metal-poor (white area) and metal-rich (dashed area) Galactic clusters in the full sample H96(a).*

(N$\geq$ 50, according to BHB), the TO magnitude of the metal-rich ($\langle$[Fe/H]$\rangle$=$-$0.57) sample is fainter by about 0.36 mag than the value of the metal-poor one, again independently of the adopted $M_V(RR)$ calibration. As for the Secker's selection (i.e., H96(b) sample), I derive quite similar results, with the peak magnitude of MP clusters ($\langle$[Fe/H]$\rangle$=$-$1.64) brighter by about 0.34 mag and 0.05 mag than that of the few MR ones ($\langle$[Fe/H]$\rangle$=$-$0.67) and the combined sample ($\langle$[Fe/H]$\rangle$=$-$1.39), respectively.

It is worth noticing that such an empirical evidence is consistent, also on a quantitative way, with the theoretical calculations by Ashman, Conti & Zepf (1995, hereafter ACZ) who suggest a metallicity effect $\Delta M_V(TO)$=0.32$\Delta$[Fe/H], as inferred by synthetic cluster populations with different metallicity and constant age and mass function. Furthermore, the above results are in agreement with previous observations by Whitmore et al. (1995: M87), Kundu & Whitmore (1998: NGC3115), and Puzia et al. (1999: NGC 4472*) who find a difference between the LFs of blue (metal-poor) and red (metal-rich) GCs in a given

*For this galaxy, Lee, Kim & Geisler (1998) and Lee & Kim (2000) find little, if any, difference in the peak luminosities of blue and red clusters.

galaxy in the sense that the peak visual magnitude of the former clusters is $\sim 0.13$, $\sim 0.16$, and $\sim 0.51$ mag, respectively, brighter than that of the red ones. Moreover, L01 in their study of relatively nearby early-type galaxies which exhibit a clear dichotomy between blue and red GCs show that, fitting the luminosity functions of the two populations separately, the $V$-band turnover of the blue GCs is brighter by about 0.55 mag and 0.26 mag than that of the red ones and of the combined samples, respectively (see the data listed in the following Table 5.6). In summary, also GCs in external galaxies showing well distinct red and blue GC populations suggest that the peak magnitude becomes fainter with increasing the metal content of the GC sample, apparently following the ACZ theoretical metallicity effect. I will come back on this issue in the following section.

**Dependence on Galactocentric distance**

Concerning the dependence of $M_V(TO)$ on the cluster distance from the Galactic center, a subdivision of metal-poor clusters into inner halo ($R_{GC} \leq 8$ kpc) and outer halo ($R_{GC} > 8$ kpc) discloses that the shape of the GCLF varies (it is broader for the outer halo), but with no significant variation on the peak luminosity with respect to the value of the combined sample. In this, my result agrees with that obtained by Kavelaars & Hanes (1997) who use an older version of Harris catalog. For the sake of the following discussion, I have also adopted a dividing line at 3.8 kpc for the metal-poor sample, but again without finding significant variation between the peak magnitude of innermost and outermost clusters.

## 5.3 Globular clusters in M31

In the field of distance determinations, the Andromeda galaxy plays a role of great importance because it contains either Classical Cepheids and RR Lyrae stars which provide independent distances and consequently a valuable test for consistency between these primary distance scales. I have shown in Table 5.2 that the RR Lyrae-based distance to M31 depends on the adopted $M_V(RR)$-[Fe/H] calibration but, for each given relation, the relative distance with respect to LMC is constant, i.e., $\mu_0$(M31)$-\mu_0$(LMC)= 6.0$\pm$0.1 mag. It follows that the M31 Cepheid distance $\mu_0$=24.44$\pm$0.1 mag (Freedman & Madore 1990) calibrated on $\mu_0$(LMC)=18.50 mag agrees with the RR Lyrae-based value, thus providing

***Table 5.5:*** *$M_V(TO)$ for metal-poor ([Fe/H]=−1.57) GCs in M31.(1): $M_V(RR)$-[Fe/H] relations discussed in section 5.2; (2): RR Lyrae-based intrinsic distance moduli from Table 5.2; (3) $M_V(TO)$ without metallicity correction; (4) metallicity corrected $M_V(TO)$ for $\Delta$[Fe/H] $\sim -0.3$ dex with respect to the average metallicity of the H96(a) sample of GCs in the Milky Way. Errors as in column (3); (5) as in column (4), but for $\Delta$[Fe/H] $\sim -0.2$ dex with respect to the average metallicity of the H96(b) sample.*

| $M_V(RR)$ | $\mu_0(RR)$ | $M_V(TO)$ | $M_V(TO)_Z$ | $M_V(TO)_Z$ |
|---|---|---|---|---|
| (1) | (2) | (3) | (4) | (5) |
| H96 | 24.47 | −7.63±0.17 | −7.54 | −7.57 |
| S93 | 24.54 | −7.70±0.19 | −7.61 | −7.64 |
| F98 | 24.36 | −7.52±0.18 | −7.43 | −7.46 |
| G03 | 24.48 | −7.64±0.18 | −7.55 | −7.58 |
| B03 | 24.52 | −7.68±0.19 | −7.59 | −7.62 |

a first evidence about the internal consistency of the two distance scales. As for the GCLF method, the published values of $M_V(TO)$ span a rather discomforting range, as reported by BHB in their recent analysis of M31 GCs. According to these authors, who study several subsamples of the cluster population, for the halo and disk clusters the peak magnitude is $V_0(TO)$=16.84±0.11 mag and 16.67±0.16 mag, respectively. On the other hand, when full sample at the metallicity [Fe/H]=−1.0, the metal-poor ($\langle$[Fe/H]$\rangle$=−1.57) and metal-rich ($\langle$[Fe/H]$\rangle$=−0.61) groups show $V_0(TO)$=16.84±0.16 mag and 16.43 ±0.27 mag, respectively. Moreover, a quite significant dependence of $V(TO)$ on the projected galactocentric distance is observed: adopting a dividing line at $R_{gc} \sim$ 3.8 kpc the innermost and outermost clusters of the whole sample show $V_0(TO)$=16.37±0.21 mag and 16.80±0.14 mag, while using only metal-poor clusters the peak magnitude is 16.32±0.21 mag (inner) and 17.02±0.22 mag (outer), with almost no difference in the mean metallicity of the two subsets. As a whole, such variations of the GCLF parameters with either $R_{gc}$ or [Fe/H] appear at odds with the GGC behavior presented above, neither have been reported for other galaxies. As stated by BHB, a definitive answer on this issue will require better and less contaminated data on the M31 clusters and for this reason I prefer to use in the following discussion only the results concerning the full sample of metal-poor clusters. Using $V_0(TO)$=16.84±0.16 mag together with the distance moduli given in Table 5.2, I derive the $M_V(TO)$ values listed in column (3) of Table 5.5. The comparison with

the Galactic values listed in the previous Table 5.3 shows that the M31 absolute peak magnitudes are brighter by about 0.25 mag and 0.04 mag than the results based on the H96(a) and H96(b) sample, respectively. By accounting for the metallicity correction suggested by ACZ (see values in columns (4) and (5) of Table 5.5), the difference with the H96(a) results decreases to $\sim$ 0.16 mag, while that with the H96(b) ones is almost zero. On the other hand, I can keep away from any metallicity effect by directly comparing the metal-poor clusters in M31 with those in the Milky Way. From data in Table 5.4 and in column (3) of Table 5.5, one derives that the M31 peak magnitudes are 0.14 mag systematically brighter than the H96(a) ones, but almost coincident with those inferred from the H96(b) sample. To give a reason for these results, I note that the full sample in the BHB study is composed by clusters out of $R_{gc} \sim 1$ kpc from the center of M31 and that the median galactocentric distance of the metal-poor set is 5.5 kpc, in fair agreement with the constraints of Secker' selection which indeed was originally thought to simulate the Galaxy as if it were viewed from the outside and for this reason provides a better agreement with observations of GCs in external galaxies. However, it should be mentioned that the M31 distance moduli given in Table 5.2 refer to a field population of RR Lyrae stars and that the M31 GCs are expected at a variety of distances. In summary, no firm conclusion can be given, although I find evidence that the LFs of Galactic and M31 Globular Clusters suggest quite similar $M_V(TO)$ magnitudes, provided that the same $M_V(RR)$ calibration and internally consistent constraints to select the GC samples are adopted.

## 5.4 External galaxies

In their paper, ACZ show that the theoretical metallicity correction on the peak magnitude helps to remove the discrepancy between the GCLF and the Surface Brightness Fluctuations (SBF) distance scales. Following a different approach, I say that in the case of galaxies for which both types of methods are possible the GCLF universality can straightway be tested by considering the difference between $V(TO)$ and $m^*$, the SBF magnitude adjusted to a fiducial color (see later). Since the $m^*$ absolute calibration is assumed to depend only on a zero-point, such a difference provides information for or against the constancy of the GCLF peak absolute magnitude, independently of the galaxy distance.

***Table 5.6:*** *Turnover magnitude and metallicity for GCLFs in Larsen et al. (2001) galaxies.*

| galaxy | $V(TO)_{all}$ | [Fe/H]$_a$ | $V(TO)_{blue}$ | [Fe/H]$_b$ | $V(TO)_{red}$ | [Fe/H]$_r$ |
|---|---|---|---|---|---|---|
| N0524 | 24.51 (0.09) | −0.79 | 24.34 (0.12) | −1.26 | 24.68 (0.14) | −0.28 |
| N1023 | 23.53 (0.31) | −0.99 | 22.82 (0.47) | −1.59 | 23.92 (0.39) | −0.40 |
| N3115 | 22.55 (0.21) | −1.06 | 22.45 (0.27) | −1.54 | 22.66 (0.33) | −0.45 |
| N3379 | 22.78 (0.22) | −0.80 | 22.57 (0.30) | −1.34 | 23.02 (0.32) | −0.38 |
| N3384 | 23.30 (0.12) | −0.88 | 22.98 (0.12) | −1.44 | 24.37 (0.30) | −0.19 |
| N4365 | 24.37 (0.16) | −0.86 | 24.01 (0.14) | −1.26 | 24.83 (0.23) | −0.30 |
| N4406 | 23.38 (0.11) | −0.91 | 23.28 (0.14) | −1.24 | 23.52 (0.17) | −0.49 |
| N4472 | 23.78 (0.13) | −0.73 | 23.38 (0.15) | −1.44 | 24.21 (0.23) | −0.19 |
| N4473 | 23.66 (0.12) | −0.96 | 23.46 (0.15) | −1.47 | 23.86 (0.15) | −0.43 |
| N4486 | 23.50 (0.06) | −0.69 | 23.36 (0.10) | −1.40 | 23.58 (0.07) | −0.24 |
| N4494 | 23.40 (0.11) | −1.24 | 23.24 (0.13) | −1.64 | 23.76 (0.22) | −0.69 |
| N4552 | 23.32 (0.16) | −0.93 | 23.01 (0.21) | −1.39 | 23.61 (0.24) | −0.36 |
| N4594 | 22.09 (0.10) | −0.73 | 21.80 (0.19) | −1.46 | 22.22 (0.12) | −0.30 |
| N4649 | 23.58 (0.08) | −0.76 | 23.46 (0.13) | −1.39 | 23.66 (0.11) | −0.20 |

With such a purpose, in the following I adopt the $V(TO)$ magnitudes measured by L01 by two-parameters fits to GCLFs in early-type galaxies together with the correspondent $I$-band SBF measurements by Tonry et al. (2001, hereafter T01) as adjusted to the fiducial color $(V-I)_0$=1.15 mag according to the T01 relation:

$$m_I^* = m_I - 4.5[(V-I)_0 - 1.15] \tag{5.7}$$

where $(V-I)_0$ is the galaxy color. All the galaxies studied by L01 exhibit clear bimodal color distribution and for such a reason the peak magnitude was measured for either the blue and the red populations, as well as for the combined samples. These magnitudes are reported in Table 5.6 together with the mean metallicity of the combined, blue, and red samples, as determined using the L01 intrinsic $(V-I)_0$ colors and the relation of Kundu & Whitmore (1998), while Table 5.7 gives the T01 $m_I^*$ values. As shown in the upper panel of Fig. 5.6 , which deals with the combined samples and where open circles refer to measured peak magnitudes, while filled ones depict the metallicity corrected values scaled to the average value [Fe/H]=−1.3 of all the GGCs (see Table 5.3), the difference between the two magnitudes is $m_I^* - V(TO)$=5.67±0.31 mag (no metallicity correction, dashed line) and 5.81±0.31 mag (metallicity corrected, solid line), thus suggesting for the GCLFs in these galaxies a reasonably similar absolute peak magnitude.

***Table 5.7:*** *SBF magnitudes and differences with the GCLF turnover magnitudes for Larsen et al. (2001) galaxies.*

| galaxy | $m_i^*$ | $m_I^* - V(TO)_{all}$ | $m_I^* - V(TO)_{blue}$ | $m_I^* - V(TO)_{red}$ |
|---|---|---|---|---|
| N0524 | 30.16 (0.20) | 5.65 (0.22) | 5.82 (0.23) | 5.48 (0.24) |
| N1023 | 28.55 (0.15) | 5.02 (0.34) | 5.73 (0.49) | 4.63 (0.42) |
| N3115 | 28.19 (0.08) | 5.64 (0.22) | 5.74 (0.28) | 5.53 (0.34) |
| N3379 | 28.38 (0.10) | 5.60 (0.24) | 5.81 (0.32) | 5.36 (0.33) |
| N3384 | 28.59 (0.13) | 5.29 (0.18) | 5.61 (0.18) | 4.22 (0.33) |
| N4365 | 29.82 (0.16) | 5.45 (0.23) | 5.81 (0.21) | 4.99 (0.28) |
| N4406 | 29.43 (0.13) | 6.05 (0.17) | 6.15 (0.19) | 5.91 (0.21) |
| N4472 | 29.31 (0.09) | 5.53 (0.16) | 5.93 (0.17) | 5.10 (0.25) |
| N4473 | 29.24 (0.12) | 5.58 (0.17) | 5.78 (0.19) | 5.38 (0.19) |
| N4486 | 29.30 (0.15) | 5.80 (0.16) | 5.94 (0.18) | 5.72 (0.17) |
| N4494 | 29.43 (0.09) | 6.03 (0.14) | 6.19 (0.16) | 5.67 (0.24) |
| N4552 | 29.19 (0.13) | 5.87 (0.21) | 6.18 (0.25) | 5.58 (0.27) |
| N4594 | 28.21 (0.17) | 6.12 (0.20) | 6.41 (0.26) | 5.99 (0.21) |
| N4649 | 29.39 (0.14) | 5.81 (0.16) | 5.93 (0.19) | 5.73 (0.18) |
| *mean* | | 5.67 (0.31) | 5.93 (0.21) | 5.38 (0.50) |

Moreover, by considering the blue clusters separately, in the lower panel in the same figure it is shown that the peak magnitudes scale even better with the SBF measurements yielding a difference $m_I^* - V(TO)$=5.93$\pm$0.21 mag (no metallicity correction, dashed line) and 5.99$\pm$0.22 mag (solid line), with a correction that accounts for the difference between the [Fe/H] values of the blue clusters (see data in column (5) of Table 5.6) and the average metallicity of the Galactic metal-poor clusters ([Fe/H]=$-$1.6, see Table 5.4). As for the red clusters, one find that the two magnitudes are poorly correlated for one derive $m_I^* - V(TO)$=5.38$\pm$0.50 mag (no metallicity correction) and 5.46$\pm$0.48 mag (metallicity corrected to the average metal content [Fe/H]=$-$0.6 of metal-rich GGCs (see Table 5.4)).

In summary, provided that the $m_I^*$ absolute calibration is assumed to rest on a zero-point, the L01 data for galaxies showing a bimodal distribution in the GC colors suggest that the luminosity functions of the blue (metal-poor) clusters peak at the same absolute magnitude within $\sim$ 0.2 mag, while for the GCLFs of the combined samples the constancy is attained within $\sim$ 0.3 mag as a result of the quite scattered peak magnitudes of the red (metal-rich) globular clusters. This behavior holds even if the ACZ theoretical metallicity

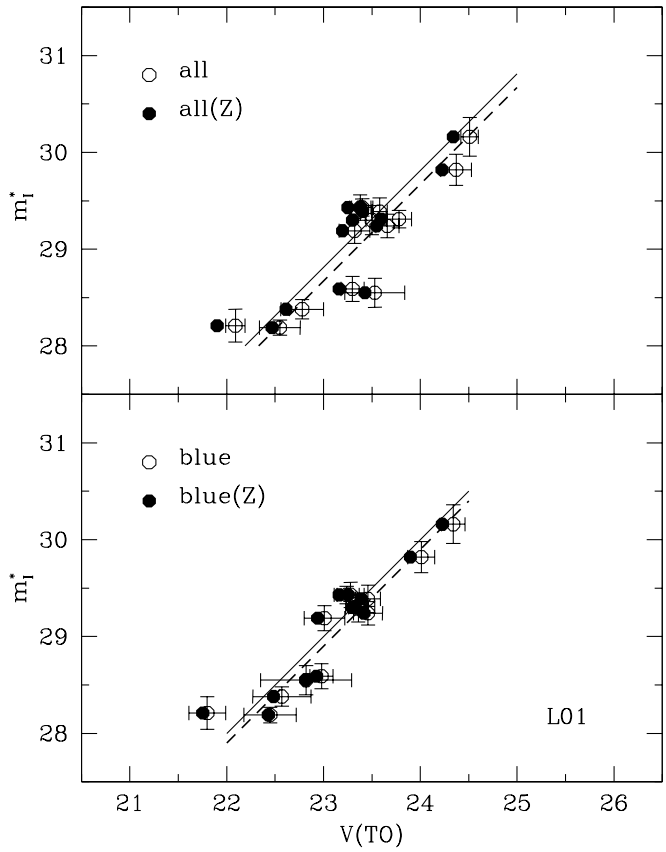


***Figure 5.6:*** *SBF measurements versus GCLF peak magnitudes for the external galaxies studied by Larsen et al. (2001). The upper panel refers to the combined samples of GCs, while the lower one deals with blue (metal-poor) clusters. Open and filled circles depict observed and metallicity corrected peak magnitudes, respectively (see text).*

correction is taken into account, likely suggesting that in external galaxies the metal-rich GCs may have different ages and/or mass distributions than the metal-poor component. Apparently, this result disagrees with Kundu & Whitmore (2001a, b) whose sample contains few galaxies which show evidence of bi-modality in the GC color distribution, but for which they find agreement between the GCLF and the SBF distances, considering the metal content and peak magnitude of the GC full samples. However, by inspection of Table 5.6 of Kundu & Whitmore (2001a) one note that the difference $\Delta\mu_0$(GCLF-SBF[†]) varies from $-0.27$ to +0.67 mag, while from Table 5.3 in Kundu & Whitmore (2001b) one has that the difference between the GCLF distance moduli and those from the literature

[†]SBF data from Neilsen 1999

ranges from $-0.70$ to +0.38 mag, depending on the galaxy.

I want to stress again that all the above discussion relies on the assumption that the absolute calibration of the SBF $m_I^*$ magnitudes depends only on a zero-point. In this case, the differences $m_I^* - V(TO)_{blue}$ given in Table 5.7 would yield that the absolute peak magnitudes for the metal-poor clusters in the L01 galaxies have a scatter of about 0.2-0.3 mag, which means 2-3 Mpc at Virgo distances. As a matter of the fact, looking at the $M_I^*$ magnitudes given by Tonry et al. (1999) for six calibrating galaxies (see their Table 5.2) one finds a range of $\sim$ 0.5 mag, with even the best SBF measurements giving $M_I^* = -1.77 \pm 0.12$ (NGC224) and $-2.04 \pm 0.19$ mag (NGC7331). On this ground, it is quite difficult to distinguish whether the scatter in the $m_I^* - V(TO)_{blue}$ differences reflects a real scatter of the absolute peak magnitudes or is due to the intrinsic uncertainty of the SBF calibration. Concerning the latter point, Tonry et al. (1999), using the Ferrarese et al. (2000) HST Cepheid distances to the six calibrating galaxies, prefer to adopt the median value $M_I^* = -1.74 \pm 0.08$ mag rather than the weighted mean $-1.80 \pm 0.08$ mag, given the wide range in the errors in the SBF measurement. Accordingly, for all the blue clusters in the L01 galaxies I derive $M_V(TO) = -7.67 \pm 0.23$ mag and $-7.73 \pm 0.23$ mag, depending on whether the ACZ metallicity correction is neglected or used, respectively, *within a Cepheid distance scale calibrated on $\mu_0$(LMC)=18.50 mag.*

This is a crucial point to be considered before comparing these peak absolute magnitudes with those of metal-poor clusters in the Milky Way since the values listed in Table 5.4 are correlated to the LMC distance moduli given in Table 5.2 for the various $M_V(RR)$-[Fe/H] relations. In other words, if I adopt $\mu_0$(LMC)=18.50 mag, then the peak absolute magnitude of Galactic metal-poor clusters is $M_V(TO) = -7.50 \pm 0.10$ mag and $-7.66 \pm 0.11$ mag for the H96(a) and H96(b) samples, respectively. On this basis, as already presented for the metal-poor GCs in M31, one find a better agreement with the Galactic peak magnitude dealing with the Secker's selection of GCs. However, as discussed in Jensen et al. (2003), the zero-point of the SBF calibration follows the uncertainties of the Cepheid scale: indeed, I show in Table 5.8 that the revised HST Cepheid distances determined by Freedman et al. (2001, $KP_n$) for the SBF calibrating galaxies[‡] would lead to the slightly fainter median value $M_I^* = -1.63 \pm 0.05$ mag and weighted mean

[‡]For N224 (M31) ground observations by Freedman & Madore (1990) were used.

***Table 5.8:*** *SBF calibration from Cepheid distances.*

| galaxy | [O/H] | $m_I^*$ | $\mu_0$(KP$_n$) | $\mu_0$(KP$_{n,Z}$) | $\mu_0$(F02) |
|---|---|---|---|---|---|
| LMC | $-0.40$ | | 18.50 | 18.50 | 18.50 |
| N7331 | $-0.23$ | 28.86 (0.14) | 30.81 (0.09) | 30.84 (0.09) | 30.71 (0.09) |
| N3031 | $-0.15$ | 26.21 (0.25) | 27.75 (0.08) | 27.80 (0.08) | 27.63 (0.09) |
| N4258 | $-0.05$ | 27.57 (0.08) | 29.44 (0.07) | 29.51 (0.07) | 29.32 (0.06) |
| N4725 | +0.02 | 28.87 (0.32) | 30.38 (0.06) | 30.46 (0.06) | 30.28 (0.07) |
| N0224 | +0.08 | 22.67 (0.05) | 24.38 (0.05) | 24.48 (0.05) | 24.30 (0.08) |
| N3368 | +0.30 | 28.34 (0.20) | 29.97 (0.06) | 30.11 (0.06) | 30.09 (0.10) |
| N4548 | +0.44 | 29.68 (0.53) | 30.88 (0.05) | 31.05 (0.05) | 31.20 (0.05) |
| galaxy | | | $M_I^*$ | $M_I^*$ | $M_I$ |
| N7331 | | | $-1.96$ (0.17) | $-1.99$ (0.17) | $-1.86$ (0.17) |
| N3031 | | | $-1.54$ (0.26) | $-1.59$ (0.26) | $-1.42$ (0.26) |
| N4258 | | | $-1.87$ (0.11) | $-1.94$ (0.11) | $-1.75$ (0.10) |
| N4725 | | | $-1.51$ (0.33) | $-1.59$ (0.33) | $-1.40$ (0.33) |
| N0224 | | | $-1.71$ (0.07) | $-1.81$ (0.07) | $-1.64$ (0.09) |
| N3368 | | | $-1.63$ (0.21) | $-1.77$ (0.21) | $-1.75$ (0.22) |
| N4548 | | | $-1.20$ (0.53) | $-1.37$ (0.53) | $-1.52$ (0.53) |
| *median* | | | $-1.63$ (0.05) | $-1.77$ (0.05) | $-1.64$ (0.05) |
| *w-mean* | | | $-1.75$ (0.05) | $-1.84$ (0.05) | $-1.68$ (0.05) |

$-1.75\pm0.05$ mag. Furthermore, one should also consider the occurrence of a metallicity effect on the Cepheid distance scale. Using the empirical relation adopted by Freedman et al. (2001), namely $\Delta\mu_0 = -0.2\Delta$[O/H] where $\Delta$[O/H] is the difference between the oxygen abundance of the galaxy and that of LMC, the metallicity corrected distance moduli (KP$_{n,Z}$) yield a median value and a weighted mean as $M_I^* = -1.77\pm0.05$ mag and $-1.84\pm0.05$ mag, respectively. In several papers, the occurrence of a metallicity effect on the Cepheid distance scale is rejected also in consideration of a mistakenly believed disagreement between the empirical correction adopted by Freedman et al. (2001) and the predicted one $\Delta\mu_0$=+0.27$\Delta\log Z$, as based on nonlinear convective models of Cepheid structures (see Caputo, Marconi & Musella 2002 and references therein) with $Z$ in the range of 0.004 (Small Magellanic Cloud) to 0.02 (roughly solar chemical composition). As a matter of fact, it should firstly be clear that the empirical correction holds with the oxygen abundance of the parent galaxy, whereas the theoretical one is based on the chemical composition of the Cepheids. Moreover, it has been shown (Fiorentino

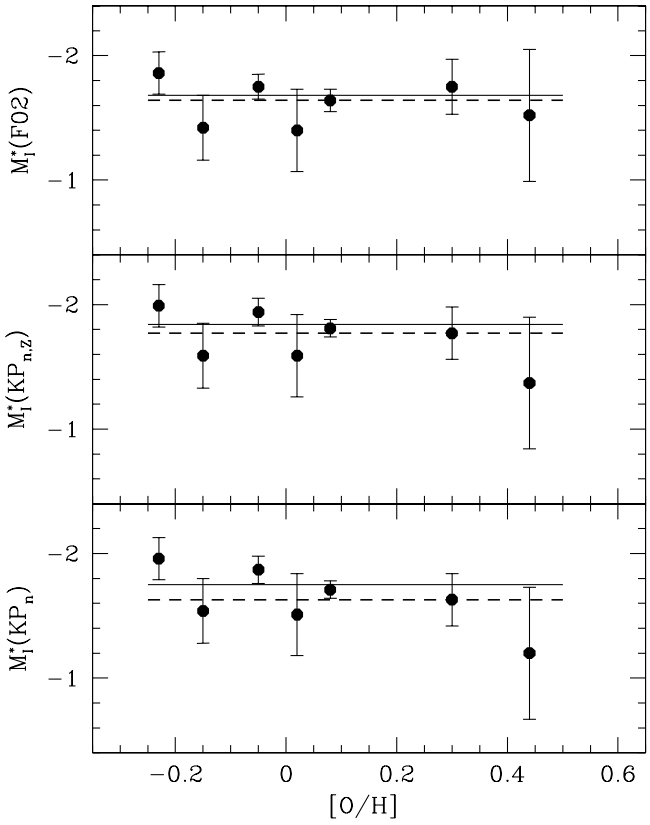


***Figure 5.7:*** *SBF absolute magnitudes of calibrating galaxies as a function of the galaxy oxygen abundance. The three panels deal with the revised Cepheid distances by Freedman et al. (2001) without metallicity correction ($KP_n$) and adopting either the empirical correction ($KP_{n,Z}$) or the theoretical one (F02). Dashed and solid lines show the median value and the weighted mean, respectively.*

et al. 2002, F02) that the theoretical correction is not linear over the whole metallicity range covered by galaxies hosting Cepheids, with a turnover at about solar chemical composition and with sign and amount of the correction depending on both the helium and metal content of the Cepheid. On this basis, F02 showed that the empirical metallicity correction suggested by Cepheid observations in two fields of the galaxy M101 may be accounted for adopting a helium-to-metal enrichment ratio $\Delta Y/\Delta Z \sim 3.5$, as also confirmed on the basis of an updated extended model set (Marconi, Musella & Fiorentino 2005). It is also of interest to note that recent high-resolution spectroscopic abundances for Galactic and Magellanic Cloud Cepheids (Romaniello et al. 2005) show that the

Cepheid luminosities are incompatible with the empirical linear correction, whereas are fairly described by the F02 non-monotonic theoretical behavior with a helium-to-metal enrichment ratio $\Delta Y/\Delta Z$=2.5-3.5. As for the effects on the SBF calibration, I show in Fig. 5.7 the absolute $M_I^*$ values of the calibrating galaxies as a function of the [O/H] abundance of the galaxies (see also Table 5.8). The three panels refer to the HST revised distance moduli by Freedman et al. (2001) without metallicity correction (KP$_n$) and using both the empirical (KP$_{n,Z}$) and the theoretical correction (F02) with $\Delta Y/\Delta Z$=3.5. With reference to the median values (dashed line) and the weighted means (solid line), one has that a metallicity correction to the measured Cepheid distances is *needed* to remove the trend of $M_I^*$ with the oxygen abundance, and that the theoretical relation seems to work better than the empirical one to give a fairly constant SBF zero-point. Eventually, is important to note that using the weighted mean $M_I^*$=$-$1.68$\pm$0.05 mag provided by the theoretically corrected distance moduli to the SBF calibrating galaxies together with the ACZ metallicity correction yields that the peak absolute magnitude of the L01 blue GCs is $M_V(TO) = -7.67\pm0.23$ mag which is astonishingly coincident with the values $-7.66\pm0.11$ mag and $-7.65\pm0.19$ mag inferred by metal-poor clusters in the Milky Way and M31, respectively, *at $\mu_0$(LMC)=18.50 mag.* In closure, I wish to mention that a recent theoretical SBF calibration (Cantiello et al. 2003) yields $M_I^*$=$-$1.74$\pm$0.23 mag, as determined using stellar evolutionary tracks computed with the same input physics adopted for our pulsation models of RR Lyrae and Cepheid structures, in particular for those computed by B03 and F02. On these grounds, I should adopt $\mu_0$(LMC)=18.53 mag and the weighted mean provided by the SBF calibrating galaxies becomes $M_I^*$=$-$1.71$\pm$0.05 mag, that is practically coincident with the theoretical value, with the above $M_V(TO)$ luminosities increased by 0.03 mag.

Table 5.9: *Here is reported Table 5.1 entirely*

| Name (1) | [Fe/H] (2) | $M_V(GC)$ (3:H96) | $R_{GC}$ (4:H96) | $M_V(GC)$ (5:S93) | $M_V(GC)$ (6:F98) | $M_V(GC)$ (7:G03) | $M_V(GC)$ (8:B03) |
|---|---|---|---|---|---|---|---|
| NGC 104 | −0.76 | −9.42 | 7.4 | −9.40 | −9.28 | −9.39 | −9.36 |
| NGC 288 | −1.24 | −6.74 | 12.0 | −6.78 | −6.62 | −6.73 | −6.76 |
| NGC 362 | −1.16 | −8.41 | 9.4 | −8.45 | −8.29 | −8.41 | −8.42 |
| NGC 1261 | −1.35 | −7.81 | 18.2 | −7.88 | −7.70 | −7.82 | −7.85 |
| Pal 1 | −0.60 | −2.47 | 17.0 | −2.42 | −2.32 | −2.42 | −2.37 |
| AM 1 | −1.80 | −4.71 | 123.2 | −4.84 | −4.62 | −4.75 | −4.81 |
| Eridanus | −1.46 | −5.14 | 95.2 | −5.22 | −5.03 | −5.15 | −5.20 |
| Pal 2 | −1.30 | −8.01 | 35.4 | −8.06 | −7.89 | −8.01 | −8.04 |
| NGC 1851b | −1.22 | −8.33 | 16.7 | −8.38 | −8.21 | −8.33 | −8.35 |
| NGC 1904b | −1.57 | −7.86 | 18.8 | −7.95 | −7.75 | −7.88 | −7.93 |
| NGC 2298b | −1.85 | −6.30 | 15.7 | −6.44 | −6.21 | −6.34 | −6.40 |
| NGC 2419 | −2.12 | −9.58 | 91.5 | −9.76 | −9.50 | −9.64 | −9.71 |
| Pyxis | −1.30 | −5.75 | 41.7 | −5.80 | −5.63 | −5.75 | −5.78 |
| NGC 2808b | −1.15 | −9.39 | 11.1 | −9.43 | −9.27 | −9.38 | −9.40 |
| E 3 | −0.80 | −2.77 | 7.6 | −2.75 | −2.63 | −2.74 | −2.71 |
| Pal 3 | −1.66 | −5.70 | 95.9 | −5.81 | −5.60 | −5.73 | −5.78 |
| NGC 3201 | −1.58 | −7.46 | 8.9 | −7.55 | −7.36 | −7.48 | −7.53 |
| Pal 4 | −1.48 | −6.02 | 111.8 | −6.10 | −5.92 | −6.04 | −6.08 |
| NGC 4147a | −1.83 | −6.16 | 21.3 | −6.30 | −6.08 | −6.20 | −6.27 |
| NGC 4372 | −2.09 | −7.77 | 7.1 | −7.95 | −7.70 | −7.83 | −7.90 |
| Rup 106 | −1.67 | −6.35 | 18.5 | −6.46 | −6.25 | −6.38 | −6.44 |
| NGC 4590 | −2.06 | −7.35 | 10.1 | −7.52 | −7.27 | −7.40 | −7.47 |
| NGC 4833 | −1.80 | −8.16 | 7.0 | −8.29 | −8.07 | −8.20 | −8.26 |
| NGC 5024 | −1.99 | −8.70 | 18.3 | −8.86 | −8.62 | −8.75 | −8.82 |
| NGC 5053 | −2.29 | −6.72 | 16.9 | −6.93 | −6.66 | −6.79 | −6.87 |
| NGC 5139 | −1.62 | −10.29 | 6.4 | −10.40 | −10.19 | −10.32 | −10.37 |
| NGC 5272 | −1.57 | −8.93 | 12.2 | −9.02 | −8.82 | −8.95 | −9.00 |
| NGC 5286 | −1.67 | −8.61 | 8.4 | −8.72 | −8.51 | −8.64 | −8.70 |
| NGC 5466 | −2.22 | −6.96 | 16.2 | −7.16 | −6.89 | −7.03 | −7.10 |
| NGC 5634a | −1.88 | −7.69 | 21.2 | −7.83 | −7.61 | −7.73 | −7.80 |
| NGC 5694 | −1.86 | −7.81 | 29.1 | −7.95 | −7.72 | −7.85 | −7.92 |
| IC 4499 | −1.60 | −7.33 | 15.7 | −7.43 | −7.23 | −7.35 | −7.41 |
| NGC 5824 | −1.85 | −8.84 | 25.8 | −8.98 | −8.75 | −8.88 | −8.94 |
| Pal 5 | −1.41 | −5.17 | 18.6 | −5.24 | −5.06 | −5.18 | −5.22 |
| NGC 5897 | −1.80 | −7.21 | 7.3 | −7.34 | −7.12 | −7.25 | −7.31 |
| .. | .. | .. | .. | .. | .. | .. | .. |

Table 5.9: (continued)

| Name (1) | [Fe/H] (2) | $M_V(GC)$ (3:H96) | $R_{GC}$ (4:H96) | $M_V(GC)$ (5:S93) | $M_VGC)$ (6:F98) | $M_V(GC)$ (7:G03) | $M_V(GC)$ (8:B03) |
|---|---|---|---|---|---|---|---|
| NGC 5904 | −1.27 | −8.81 | 6.2 | −8.86 | −8.69 | −8.81 | −8.84 |
| NGC 5927 | −0.37 | −7.80 | 4.5 | −7.71 | −7.63 | −7.73 | −7.64 |
| NGC 5946 | −1.38 | −7.20 | 5.8 | −7.26 | −7.09 | −7.20 | −7.24 |
| NGC 5986 | −1.58 | −8.44 | 4.8 | −8.53 | −8.34 | −8.46 | −8.51 |
| Pal 14 | −1.52 | −4.73 | 69.0 | −4.82 | −4.62 | −4.74 | −4.79 |
| NGC 6093 | −1.75 | −8.23 | 3.8 | −8.36 | −8.14 | −8.27 | −8.33 |
| NGC 6121 | −1.20 | −7.20 | 5.9 | −7.24 | −7.08 | −7.19 | −7.22 |
| NGC 6101 | −1.82 | −6.91 | 11.1 | −7.05 | −6.82 | −6.95 | −7.02 |
| NGC 6144 | −1.75 | −6.75 | 2.6 | −6.88 | −6.66 | −6.79 | −6.85 |
| NGC 6139 | −1.68 | −8.36 | 3.6 | −8.47 | −8.27 | −8.39 | −8.45 |
| Terzan 3 | −0.73 | −4.61 | 2.4 | −4.58 | −4.47 | −4.57 | −4.53 |
| NGC 6171 | −1.04 | −7.13 | 3.3 | −7.14 | −7.00 | −7.11 | −7.11 |
| 1636−283 | −1.50 | −3.97 | 2.0 | −4.06 | −3.87 | −3.99 | −4.04 |
| NGC 6205 | −1.54 | −8.70 | 8.7 | −8.79 | −8.60 | −8.72 | −8.77 |
| NGC 6229 | −1.43 | −8.05 | 29.7 | −8.13 | −7.95 | −8.06 | −8.11 |
| NGC 6218 | −1.48 | −7.32 | 4.5 | −7.40 | −7.22 | −7.34 | −7.38 |
| NGC 6235 | −1.40 | −6.44 | 4.1 | −6.51 | −6.33 | −6.45 | −6.49 |
| NGC 6254 | −1.52 | −7.48 | 4.6 | −7.57 | −7.37 | −7.49 | −7.54 |
| NGC 6256 | −0.70 | −6.52 | 1.8 | −6.48 | −6.37 | −6.47 | −6.43 |
| Pal 15 | −1.90 | −5.49 | 37.9 | −5.63 | −5.40 | −5.53 | −5.60 |
| NGC 6266 | −1.29 | −9.19 | 1.7 | −9.25 | −9.08 | −9.19 | −9.22 |
| NGC 6273 | −1.68 | −9.18 | 1.6 | −9.29 | −9.09 | −9.21 | −9.27 |
| NGC 6284 | −1.32 | −7.97 | 7.6 | −8.03 | −7.85 | −7.97 | −8.00 |
| NGC 6287 | −2.05 | −7.36 | 2.1 | −7.53 | −7.28 | −7.41 | −7.48 |
| NGC 6293 | −1.92 | −7.77 | 1.4 | −7.92 | −7.68 | −7.81 | −7.88 |
| NGC 6304 | −0.59 | −7.32 | 2.2 | −7.27 | −7.17 | −7.27 | −7.21 |
| NGC 6316 | −0.55 | −8.35 | 3.2 | −8.30 | −8.20 | −8.30 | −8.24 |
| NGC 6341 | −2.28 | −8.20 | 9.6 | −8.40 | −8.14 | −8.27 | −8.34 |
| NGC 6325 | −1.17 | −6.95 | 1.1 | −6.98 | −6.82 | −6.94 | −6.96 |
| NGC 6333 | −1.75 | −7.94 | 1.7 | −8.07 | −7.85 | −7.98 | −8.04 |
| NGC 6342 | −0.65 | −6.44 | 1.7 | −6.40 | −6.29 | −6.39 | −6.34 |
| NGC 6356 | −0.50 | −8.52 | 7.6 | −8.46 | −8.37 | −8.47 | −8.40 |
| NGC 6355 | −1.50 | −8.08 | 1.8 | −8.17 | −7.98 | −8.10 | −8.15 |
| NGC 6352 | −0.70 | −6.48 | 3.3 | −6.44 | −6.33 | −6.43 | −6.39 |
| IC 1257 | −1.70 | −6.15 | 17.9 | −6.27 | −6.06 | −6.18 | −6.24 |
| .. | .. | .. | .. | .. | .. | .. | .. |

Table 5.9: (continued)

| Name (1) | [Fe/H] (2) | $M_V(GC)$ (3:H96) | $R_{GC}$ (4:H96) | $M_V(GC)$ (5:S93) | $M_VGC)$ (6:F98) | $M_V(GC)$ (7:G03) | $M_V(GC)$ (8:B03) |
|---|---|---|---|---|---|---|---|
| Terzan 2 | −0.40 | −5.27 | 0.9 | −5.19 | −5.11 | −5.21 | −5.12 |
| NGC 6366 | −0.82 | −5.77 | 5.0 | −5.76 | −5.63 | −5.74 | −5.72 |
| Terzan 4 | −1.60 | −6.09 | 1.3 | −6.19 | −5.99 | −6.11 | −6.17 |
| HP 1 | −1.55 | −6.44 | 6.1 | −6.54 | −6.34 | −6.46 | −6.51 |
| NGC 6362 | −0.95 | −6.94 | 5.1 | −6.95 | −6.81 | −6.92 | −6.91 |
| Liller 1 | 0.22 | −7.63 | 1.8 | −7.45 | −7.44 | −7.52 | −7.30 |
| NGC 6380 | −0.50 | −7.46 | 3.2 | −7.40 | −7.31 | −7.41 | −7.34 |
| Terzan 1 | −1.30 | −4.90 | 2.5 | −4.95 | −4.78 | −4.90 | −4.93 |
| Ton 2 | −0.50 | −6.14 | 1.4 | −6.07 | −5.98 | −6.08 | −6.01 |
| NGC 6388 | −0.60 | −9.42 | 3.2 | −9.37 | −9.27 | −9.37 | −9.32 |
| NGC 6402 | −1.39 | −9.12 | 4.1 | −9.19 | −9.01 | −9.13 | −9.16 |
| NGC 6401 | −0.98 | −7.90 | 2.7 | −7.90 | −7.77 | −7.88 | −7.87 |
| NGC 6397 | −1.95 | −6.63 | 6.0 | −6.79 | −6.55 | −6.68 | −6.75 |
| Pal 6 | −1.09 | −6.81 | 2.2 | −6.84 | −6.69 | −6.80 | −6.81 |
| NGC 6426 | −2.26 | −6.69 | 14.6 | −6.89 | −6.62 | −6.76 | −6.83 |
| Djorg 1 | −2.00 | −6.26 | 4.1 | −6.42 | −6.18 | −6.31 | −6.38 |
| Terzan 5 | 0.00 | −7.87 | 2.4 | −7.73 | −7.69 | −7.78 | −7.61 |
| NGC 6440 | −0.34 | −8.75 | 1.3 | −8.66 | −8.59 | −8.68 | −8.58 |
| NGC 6441 | −0.53 | −9.64 | 3.9 | −9.58 | −9.49 | −9.59 | −9.52 |
| Terzan 6 | −0.50 | −7.67 | 1.6 | −7.61 | −7.52 | −7.62 | −7.55 |
| NGC 6453 | −1.53 | −6.88 | 1.8 | −6.97 | −6.78 | −6.90 | −6.95 |
| UKS 1 | −0.50 | −6.88 | 0.8 | −6.82 | −6.73 | −6.83 | −6.76 |
| NGC 6496 | −0.64 | −7.23 | 4.3 | −7.18 | −7.08 | −7.18 | −7.13 |
| Terzan 9 | −2.00 | −3.85 | 1.6 | −4.01 | −3.77 | −3.90 | −3.97 |
| Djorg 2 | −0.50 | −6.98 | 1.4 | −6.91 | −6.82 | −6.92 | −6.85 |
| NGC 6517 | −1.37 | −8.28 | 4.3 | −8.34 | −8.16 | −8.28 | −8.32 |
| Terzan10 | −0.70 | −6.31 | 2.4 | −6.27 | −6.16 | −6.26 | −6.22 |
| NGC 6522 | −1.44 | −7.67 | 0.6 | −7.74 | −7.56 | −7.68 | −7.72 |
| NGC 6535 | −1.80 | −4.75 | 3.9 | −4.88 | −4.66 | −4.79 | −4.85 |
| NGC 6528 | −0.04 | −6.56 | 0.6 | −6.42 | −6.38 | −6.47 | −6.31 |
| NGC 6539 | −0.66 | −8.30 | 3.1 | −8.26 | −8.15 | −8.26 | −8.21 |
| NGC 6540 | −1.20 | −5.38 | 4.4 | −5.42 | −5.26 | −5.37 | −5.40 |
| NGC 6544 | −1.56 | −6.66 | 5.3 | −6.76 | −6.56 | −6.68 | −6.73 |
| NGC 6541 | −1.83 | −8.37 | 2.2 | −8.51 | −8.29 | −8.41 | −8.48 |
| NGC 6553 | −0.21 | −7.77 | 2.2 | −7.66 | −7.60 | −7.70 | −7.57 |
| .. | .. | .. | .. | .. | .. | .. | .. |

Table 5.9: (continued)

| Name (1) | [Fe/H] (2) | $M_V(GC)$ (3:H96) | $R_{GC}$ (4:H96) | $M_V(GC)$ (5:S93) | $M_VGC)$ (6:F98) | $M_V(GC)$ (7:G03) | $M_V(GC)$ (8:B03) |
|---|---|---|---|---|---|---|---|
| NGC 6558 | −1.44 | −6.46 | 1.0 | −6.53 | −6.35 | −6.47 | −6.51 |
| IC 1276 | −0.73 | −6.67 | 3.7 | −6.64 | −6.53 | −6.63 | −6.59 |
| Terzan12 | −0.50 | −4.14 | 3.4 | −4.08 | −3.99 | −4.09 | −4.02 |
| NGC 6569 | −0.86 | −8.30 | 2.9 | −8.29 | −8.16 | −8.27 | −8.25 |
| NGC 6584 | −1.49 | −7.68 | 7.0 | −7.77 | −7.58 | −7.70 | −7.74 |
| NGC 6624 | −0.44 | −7.49 | 1.2 | −7.41 | −7.33 | −7.43 | −7.34 |
| NGC 6626 | −1.45 | −8.18 | 2.7 | −8.26 | −8.07 | −8.19 | −8.23 |
| NGC 6638 | −0.99 | −7.13 | 2.3 | −7.14 | −7.00 | −7.11 | −7.11 |
| NGC 6637 | −0.70 | −7.64 | 1.9 | −7.61 | −7.50 | −7.60 | −7.56 |
| NGC 6642 | −1.35 | −6.77 | 1.7 | −6.84 | −6.66 | −6.78 | −6.81 |
| NGC 6652 | −0.96 | −6.68 | 2.8 | −6.69 | −6.55 | −6.66 | −6.66 |
| NGC 6656 | −1.64 | −8.50 | 4.9 | −8.60 | −8.40 | −8.52 | −8.58 |
| Pal 8 | −0.48 | −5.52 | 5.6 | −5.45 | −5.37 | −5.47 | −5.39 |
| NGC 6681 | −1.51 | −7.11 | 2.1 | −7.19 | −7.00 | −7.12 | −7.17 |
| NGC 6712 | −1.01 | −7.50 | 3.5 | −7.51 | −7.37 | −7.48 | −7.48 |
| NGC 6715a | −1.58 | −10.01 | 19.2 | −10.10 | −9.91 | −10.03 | −10.08 |
| NGC 6717 | −1.29 | −5.66 | 2.4 | −5.72 | −5.55 | −5.66 | −5.69 |
| NGC 6723 | −1.12 | −7.84 | 2.6 | −7.87 | −7.71 | −7.83 | −7.84 |
| NGC 6749 | −1.60 | −6.70 | 5.0 | −6.80 | −6.60 | −6.72 | −6.78 |
| NGC 6752 | −1.56 | −7.73 | 5.2 | −7.83 | −7.63 | −7.75 | −7.80 |
| NGC 6760 | −0.52 | −7.86 | 4.8 | −7.80 | −7.70 | −7.80 | −7.74 |
| NGC 6779 | −1.94 | −7.38 | 9.7 | −7.53 | −7.30 | −7.43 | −7.50 |
| Terzan 7a | −0.58 | −5.05 | 16.0 | −4.99 | −4.90 | −5.00 | −4.94 |
| Pal 10 | −0.10 | −5.79 | 6.4 | −5.67 | −5.62 | −5.71 | −5.56 |
| Arp 2a | −1.76 | −5.29 | 21.4 | −5.42 | −5.20 | −5.33 | −5.39 |
| NGC 6809 | −1.81 | −7.55 | 3.9 | −7.68 | −7.46 | −7.59 | −7.65 |
| Terzan 8a | −2.00 | −5.05 | 19.1 | −5.21 | −4.97 | −5.10 | −5.17 |
| Pal 11 | −0.39 | −6.86 | 7.9 | −6.78 | −6.70 | −6.80 | −6.70 |
| NGC 6838 | −0.73 | −5.60 | 6.7 | −5.57 | −5.46 | −5.56 | −5.52 |
| NGC 6864 | −1.16 | −8.55 | 14.6 | −8.59 | −8.43 | −8.55 | −8.56 |
| NGC 6934 | −1.54 | −7.46 | 12.8 | −7.55 | −7.36 | −7.48 | −7.53 |
| NGC 6981 | −1.40 | −7.04 | 12.9 | −7.11 | −6.93 | −7.05 | −7.09 |
| NGC 7006 | −1.63 | −7.68 | 38.8 | −7.79 | −7.59 | −7.71 | −7.76 |
| NGC 7078 | −2.26 | −9.17 | 10.4 | −9.37 | −9.10 | −9.24 | −9.31 |
| NGC 7089 | −1.62 | −9.02 | 10.4 | −9.13 | −8.92 | −9.05 | −9.10 |
| .. | .. | .. | .. | .. | .. | .. | .. |

Table 5.9: (continued)

| Name (1) | [Fe/H] (2) | $M_V(GC)$ (3:H96) | $R_{GC}$ (4:H96) | $M_V(GC)$ (5:S93) | $M_VGC)$ (6:F98) | $M_V(GC)$ (7:G03) | $M_V(GC)$ (8:B03) |
|---|---|---|---|---|---|---|---|
| NGC 7099 | $-2.12$ | $-7.43$ | 7.1 | $-7.61$ | $-7.35$ | $-7.49$ | $-7.56$ |
| Pal 12a | $-0.94$ | $-4.48$ | 15.9 | $-4.48$ | $-4.35$ | $-4.46$ | $-4.45$ |
| Pal 13 | $-1.74$ | $-3.74$ | 26.7 | $-3.86$ | $-3.65$ | $-3.77$ | $-3.83$ |
| NGC 7492 | $-1.51$ | $-5.77$ | 24.9 | $-5.85$ | $-5.66$ | $-5.78$ | $-5.83$ |

# 6

# Summary of principal results

## 6.1 Distance scales for RR Lyrae stars

On the basis of updated nonlinear pulsation models which have been computed including a nonlocal time-dependent treatment of convection, I have produced a new theoretical scenario for RR Lyrae stars with different chemical compositions typical of Galactic globular clusters ($0.0001 < Z < 0.006$ and $Y = 0.24, 0.26$) (see section 3.1). All the computed models have been trasformed in the Johnson-Cousins photometric bands, and relevant relations connecting pulsation observables, such as the period and the amplitude of the oscillation, to the intrinsic stellar parameters, have been derived. The dependence of theoretical predictions on the adopted efficiency of convection in the star external layers has also been investigated in detail.

The comparison with variables in selected Galactic globular clusters (see sections 4.1) shows that the slope of the predicted relations is in good agreement with the observed distributions, allowing us to derive the true distance modulus, as well the reddening under two assumptions for the mixing-length parameter. Adopting recent suggestions, that the value of such a parameter may increase from the blue to the red edge of the pulsation region, I have obtained a close agreement among the distance moduli inferred by the various approaches, supporting the self-consistency of the pulsational scenario. Moreover,

I have shown that the relative distance moduli, both apparent and intrinsic, match well those inferred by empirical relations (see Kovacs & Walker 2001).
As for the absolute values, I have emphasized that they depend on the adopted evolutionary mass of the variables which, in turn, mainly depends on the adopted ratio between $\alpha$ and heavy elements, decreasing when passing from solar-scaled to $\alpha$-enriched chemical mixtures, for fixed [Fe/H]. On this issue, it is worth mentioning that empirical results suggest [$\alpha$/Fe]$\sim$ 0.3 (Carney 1996, Lee & Carney 2002) and that such a value is consistent with the global features of color-magnitude diagrams (Caputo & Cassisi 2002).
I have also transformed the predicted scenario for RR Lyrae stars into the SDSS photometric system (see section 3.1.4), providing theoretical tools for the interpretation of modern large RR Lyrae surveys in these bands. Mean magnitudes and colors and the pulsation amplitudes have been used to derive multiband analytical relations that can be used to constrain both the distances and the stellar masses. Rather constant amplitude ratios are found for *r, i, z* with respect to the *g* band, suggesting that only few points along the light curves in these filters will be required, if the g curve is accurately sampled. The theoretical *g-r* vs *u-g* and *r-i* vs *g-r* plots have been compared in section 4.1.3 with available data in the literature. In particular, for field RR Lyrae stars from the QUEST survey the comparison seems to suggest a higher mean metallicity than usually assumed. In order to understand this occurrence several sources of systematic errors have been discussed.

## 6.2 BL Herculis stars

In section 3.2 new pulsational models of BL Herculis stars (a sub-class of Population II Cepheids) are described and analytical relations for the boundaries of the instability strip as a function of the adopted stellar physical parameters, as well as the pulsation equation for these bright objects, are derived. I have confirmed earlier suggestions that for each given mass and helium content there exists an "intersection" luminosity, as given by the intersection between the first overtone blue edge and the fundamental red edge, above which only the fundamental mode is stable. By combining the pulsational results with the predictions of the evolutionary models by Pietrinferni et al. (2004, 2006), in

section 4.2 I have selected models brighter than the "intersection" luminosity and therefore pulsating only in the fundamental mode, with periods longer than $\sim 0.8$ d and stellar masses $\leq 0.62\ M_{\odot}$. For the evolutionary models that have masses and luminosities consistent with the physical parameters adopted in the pulsation models, I have derived the predicted Period-Magnitude ($PM$) and Period-Wesenheit ($PW$) relations at the various photometric bands. I have shown that the predicted slopes are in close agreement with the empirical ones, quite independently of the slope in the adopted $M_V$(RR)-[Fe/H] relation. The predicted $PM$ and $PW$ relations have been applied to all the known BL Her stars in Galactic globular clusters and the resulting distance moduli are in statistical agreement with the RR Lyrae based values. The use of BL Herculis stars to evaluate the distance of globular clusters is very important especially in the case of clusters with blue HB and with the consequent lack or low number of RR Lyrae stars. It is worth mentioning that a comparison between the distances obtained for RR Lyrae stars and the ones for BL Her stars has shown a good agreement, supporting the reliability and the internal consistency of the adopted theoretical scenario at the various mass and luminosity values.
Of importance, is to note that the application of the predicted relations to NGC6341 V7 provides evidence that this variable is not a Population II Cepheids. Conversely, using the results presented by Fiorentino et al. (2006) for Anomalous Cepheids, as based on homogeneous stellar and pulsational codes, I have confirmed the earlier suggestion by Matsunaga et al (2006) that this star can be the second Anomalous Cepheid observed in Galactic globular clusters.

## 6.3 One step beyond: RR Lyrae-based calibration of GCLF

In the last chapter I have investigated the universality of the Globular Cluster Luminosity Function (GCLF) and the use of its peak magnitude for reliable distance determinations to external galaxies. The main results may be summarized as follows:

- concerning the dependence of the Milky Way GCLF on the adopted $M_V$-[Fe/H] relation to get the cluster distances, I find no significant effects on the absolute

peak magnitude $M_V(TO)$. Moreover, I show that the selection of the GC sample may influence the peak magnitude: in particular, for each given $M_V(RR)$-[Fe/H] relation, using only GCs with reddenings $E(B-V) \leq 1.0$ mag and Galactocentric distances $2 \leq R_{GC} \leq 35$ kpc, as earlier suggested by Secker (1992) to treat the Galaxy as if it were viewed from the outside, yields that the peak magnitude becomes systematically brighter by about 0.2 mag. As a whole, I have founded that the combined effects of the adopted $M_V(RR)$ calibration and selective criteria are the main reasons for the discordant Galactic peak magnitudes presented in the relevant literature.

- Grouping the Galactic clusters by metallicity, the peak magnitude of the metal-poor ([Fe/H]$< -1.0$) subsample is brighter than that of the metal-rich ([Fe/H]$> -1.0$) one by about 0.36 mag. This empirical result meets, also in a quantitative way, the theoretical metallicity effect suggested by Ashman, Conti & Zepf (1995) on the basis of synthetic GC populations with similar age and mass-function. As for the dependence on the Galactocentric distance, I found that the shape of the GCLF is broader for the outer halo ($R_{GC} > 8$ kpc) than for the inner one, but with no significant effect on the peak luminosity.

- Using BHB data for metal-poor GCs in M31, I find a close agreement with the metal-poor Galactic sample results, as obtained according to the Secker's selection and using the same $M_V(RR)$ calibration to get cluster distances.

- Concerning external galaxies with available deep photometry and close enough to have apparent GCLF extending below the turnover, I have used the sample provided by Larsen et al. (2001) which contains galaxies showing a bimodal distribution of the GC color (and consequently of the metallicity). Given the absence of RR Lyrae stars to measure the galaxy distances, I have used the $I$-band SBF measurements (Tonry et al. 2001) to evaluate the difference between the apparent peak magnitude $V(TO)$ and the SBF magnitude $m_I^*$, as adjusted to the fiducial color $(V-I)_0 = 1.15$ mag. In this way, I have shown that the blue (metal-poor) cluster component peaks at the same luminosity within $\sim 0.2$ mag, while the GCLFs of the full samples show constant values within $\sim 0.3$ mag as a consequence of the quite scattered peak

magnitudes of the red globular clusters.

The adoption of the theoretical metallicity correction by ACZ does not significantly modify these results, thus suggesting that in external galaxies blue and red globular clusters may have different ages and/or mass distributions.

- Finally, within a Cepheid and RR Lyrae distance scale calibrated on $\mu_0$(LMC)=18.50 mag, the three sets of metal-poor GCs give $M_V(TO)$=$-$7.66$\pm$0.11 mag (Milky Way), $-$7.65$\pm$0.19 mag (M31), and $-$7.67$\pm$0.23 mag (extragalactic clusters). This would suggest a value of $-$7.66$\pm$0.09 mag (weighted mean), with any modification of the LMC distance modulus producing a similar variation of the GCLF peak luminosity.

# A

# The equations of stellar pulsation

The equation of stellar pulsation are the fundamental equations of hydrodynamics and heat transport. There are two possible mathematical descriptions of a fluid behaviour: the Eulerian one and the Lagrangian one. In the Eulerian description the gas is treated as a continuum, so that its properties, such as the local density $\rho(\mathbf{r}, t)$ and the local pressure $p(\mathbf{r}, t)$, as well as the local instantaneous velocity **u**(t, **r**), can be specified as functions of position (**r**) and time (*t*). Here **r** denotes the position vector to a given point in space, and the description therefore corresponds to what is seen by a stationary observer. Otherwise, the Lagrangian description is that of an oserver who follows the motion of the gas. A given element of gas can be labelled, *i.e.*, by its initial position $\mathbf{r_o}$ and its motion is specified by giving its position **r**(t, $\mathbf{r_o}$) as a function of time. Its velocity **u**(t, **r**)=*d***r** / *dt*, at fixed $\mathbf{r_o}$, is equivalent to the Eulerian velocity mentioned above. It is often convenient to use the Lagrangian description because of its more direct physical interpretation. The Lagrangian time derivative observed when following the pulsational motion, D / D *t*=$\partial$ / $\partial t$ + **u** $\cdot \bigtriangledown$), is also known as the material time derivative or Stokes derivative; in contrast $\partial$ / $\partial t$ is the local time derivative, *i.e.* the time derivative at a fixet point.

The fundamental hydrodynamical conservation equation are:

$$(\frac{\partial}{\partial t} + \mathbf{u}\cdot \bigtriangledown)\rho + \rho \bigtriangledown \cdot \mathbf{u} = 0 \qquad (\textbf{Continuity eq.})(A.1)$$

$$(\frac{\partial}{\partial t} + \mathbf{u}\cdot \bigtriangledown)\mathbf{u} = -\frac{1}{\rho} \bigtriangledown P - \bigtriangledown \phi \qquad (\textbf{Momentum eq.})(A.2)$$

$$(\frac{\partial}{\partial t} + \mathbf{u}\cdot \bigtriangledown)E + P(\frac{\partial}{\partial t} + \mathbf{u}\cdot \bigtriangledown)V = -\frac{1}{\rho}\bigtriangledown \cdot \mathbf{F} \qquad (\textbf{Thermal energy eq.})(A.3)$$

where $P$ is the thermodynamic pressure, $\phi$ is the gravitational potential, $E$ is the internal energy per unit mass, $V = 1/\rho$ is the specific volume, and $F$ denotes the total heat flux vector due to all transport mechanism that might be operative (radiation, conduction, convection, neutrino losses, mass loss, etc. ).

The most important contributions to the total heat flux $\mathbf{F}$ are the radiative and convective fluxes, rather than the thermal conduction (because of the low density typical of stellar envelopes). Usually, all time derivatives are ignored when dealing with the radiative flux, and the approximations valid in deep stellar interiors are used. Therefore, it is usually adequate to compute the integrated radiative flux from a formula based on the "diffusion approximation":

$$\mathbf{F} \approx -\frac{4\pi}{3\kappa\rho}(\frac{dB(T)}{dT}) \bigtriangledown T, \qquad (A.4)$$

where $B(T)$ is the integrated Plank function and $\kappa$ is the opacity. In the pulsation envelope models, the "diffusion approximation", that neglects the effects of frequency, is usually adopted throughout the envelope, even in optically thin regions, in both radiative and convective transport equations.

The convective contribution to $\mathbf{F}$ poses severe theoretical problems emerged many times in applications to pulsatig stars. A *time-dependent* treatment of convection results as a necessary theory, since in some parts of a pulsating star the characteristic time scales associated with convective motions are shorter than the pulsation period. A successfully theoretical framework has been elaborated by Stellingwerf (1974, 1975, 1982). This approach is discussed in section 2.3.

# References


Adelman-McCarthy J.K. et al., 2006, ApJS, 162, 38

Alcalá J.M. et al., 2006, MmSAI, in press.

Alcock, C.,Allsman, R., Alves, D., Axelrod, T., Becker, A.,Bennett, D., Cook, K., Freeman, K., Griest, K., Lawson, W., Lehner, M.,Marshall, S., Minn

Ashman, K., Conti, A., Zepf, S., 1995, AJ, 110, 1164 (ACZ)

Asplund M., Grevesse N., & Sauval, A.J. 2005, in "Cosmic Abundances as Records of Stellar Evolution and Nucleosynthesis", eds. F.N. Bash & T.J. Barnes, ASP Conf. Series, 336, 25

Backer, N. H. & Kippenhahn, R., 1962,Zs. f. Astrophys., 54 114

Baker, N. H. & Gouth, D. O., 1979, ApJ, 234, 232

Backer, N. H. & Kippenhahn, R., 1965, ApJ, 142, 862

Barmby, P., Huchra, J., Brodie, J., 2001, AJ, 121, 1482 (BHB)

Benedict, G. F., et al. 2002, AJ, 123, 473

Bessell, M.S. & Brett, J.M., 1988, PASP, 100, 1134B

Bohm-Vitense, E., 1958, Zeitschrift fur Astrophysik, 46, 108

Bonanos A.Z., Stanek K.Z., Szentgyorgyi A.H., Sasselov D.D., Bakos G.A., 2004, AJ, 127, 861

Bono G., Caputo F., Castellani V., Marconi M., 1997, A&AS, 121, 327

Bono G., Caputo F., Castellani V., Marconi M., Storm J., Degl'Innocenti S., 2003, MNRAS, 344, 1097

Bono G., Stellingwerf R. F., 1994, ApJS, 93, 233

Bono, G., Caputo, F., Castellani, V., Marconi, M., Storm, J., Degl'Innocenti, S., 2003, MNRAS., 344, 1097 (B03)

Bono, G., Caputo, F., Santolamazza, P., 1997, A&A, 317, 171

Bono, G., Caputo, F., Castellani, V., & Marconi, M. 1997, A&AS, 121, 327

Bono, G., Caputo, F., Castellani, V., Marconi, M, & Storm, J. 2001, MNRAS, 326, 1183

Bono, G., Caputo, F., Castellani, V., Marconi, M, Storm, J., &

Bono, G., Caputo, F., Cassisi, S., Castellani, V., Marconi, M., 1997, ApJ, 489, 822

Bono, G., Caputo, F., Cassisi, S., Incerpi, R., Marconi, M., 1997, ApJ, 483,811

Bono, G., Caputo, F., Cassisi, S., Castellani, V., Marconi, M., 1997, ApJ, 479, 279

Bono, G., Caputo, F. & Di Criscienzo, MNRAS, submitted (Paper VI)

Bono, G., Castellani, V., & Stellingwerf, R.F., 1995, ApJ., 445, 145

Bono, G., Castellani, V., & Marconi, M. 2000, ApJ, 532, L129

Bono, G., Franois, P, 2005, A & A, 429, 37

Bono, G., Marconi, M., Stellingwerf, R. F.2000,ApJ, 532, 129

Bono, G., & Stellingwerf, R. F. 1994, ApJS, 93, 233

Bono, G.; Caputo, F., Castellani, V., Marconi, M., 1997, A&AS, 121, 327

Borissova, J., Minniti, D., Rejkuba, M., Alves, D., Cook, H., Freeman, K., 2004, A&A, 423, 97

Brown, T., Ferguson, H., Smith, E., Kimble, R., Sweigart, A., Renzini, A., Rich, R.,2004, AJ, 127, 2738

Buchler, J. R. & Moskalik, P., 1994, A&A, 292,450

Buchler,J. R. & Buchler, N. E. G.,1994,A&A,285, 213

Burki, G.& Meylan, G.,1986,A&A, 159, 255

Cacciari C.,2003, in G. Piotto, G. Meylan, S. G. Djorgovski, M. Riello, eds. "New Horizons in Globular Cluster Astronomy", ASP Conference Proceedings, Vol. 296,329

Cacciari, C., & Clementini, G. 2003, in "Stellar Candles for the Extragalactic Distance Scale", Eds. D. Alloin and W. Gieren, Lecture Notes in Physics, 635, 105

Caldwell,J. A. R.& Coulson, I. M.,1987,AJ, 93, 1090

Cantiello, M., Raimondo, G., Brocato, E., Capaccioli, M., 2003, AJ, 125, 2783

Caputo F., Bono, G., Fiorentino, G., Marconi, M., Musella, I., 2005, ApJ, 629, 1021

Caputo, F., & Cassisi, S. 2002, MNRAS, 333, 825

Caputo F., Castellani V., Degl'Innocenti S., Fiorentino G., Marconi M., 2004, A&A, 424, 927C

Caputo F., Castellani V., Marconi M., Ripepi V., 2000, MNRAS, 316, 819

Caputo, F., Castellani, V., Marconi, M., Ripepi, V., 2000, MNRAS, 316, 819

Caputo, F., Castellani, V., Marconi, M., Ripepi, V. 1999, MNRAS, 306, 815

Caputo, F., Castellani, V., Degl'Innocenti, S., Fiorentino, G., Marconi, M.,2004, A&A, 424, 927

Caputo, F., degl'Innocenti, S. & Marconi, M., 2002, ASPC, 265, 185

Caputo, F., Marconi, M., Musella, I., Santolamazza, P., 2000, A&A, 359, 1059

Caputo, F., Marconi, M.; Musella, I.,2000, A&A, 354, 610

Caputo, F., Marconi, M., Musella, I., 2002, ApJ, 566, 833

Caputo, F., Santolamazza, P., & Marconi, M. 1998, MNRAS, 293, 364

Caputo,F., 1998, A&ARv, 9,33

Cardelli, J.A., Clayton, G.C., & Mathis, J.S., 1989, ApJ, 345, 245

Carney, B. W. 1996, PASP, 108, 900

Carpenter, J., 2001, AJ, 121, 2851

Carretta, E., & Gratton, R., 1997, A&AS, 121, 95

Carretta, E., Gratton, R. G., Clementini, G., Fusi Pecci, F. 2000, ApJ, 533

Cassisi, S., Castellani, M., Caputo,F., Castellani, V., 2004, A&A, 426 ,641(Paper IV)

Cassisi, S., Salaris, M., Castelli, F., Pietrinferni, A., 2004,ApJ, 616, 498

Castellani, M., Caputo, F., & Castellani, V. 2003, A&A, 410, 871 (Paper I)

Castellani, V., Degl'Innocenti, S., & Marconi, M. 2002, in ASP Conf. Ser. 265, Omega Centauri: A Unique Window into Astrophysics, ed. F. van

Castelli F., Kurucz R. L., 2003, IAU Symp. 210, Modeling of Stellar Atmospheres, ed. N. E. Piskunov, W. W. Weiss, & D. F. Gray (San Francisco: ASP)

Castelli, F., Gratton, R. G., & Kurucz, R. L. 1997a, A&A, 318, 841 (CGKa)

Castelli, F., Gratton, R. G., & Kurucz, R. L. 1997b, A&A, 324, 432 (CGKb)

Castor, J. I., 1968, ApJ, 154, 793

Catelan M., 2004, ApJ, 600, 409

Catelan M., Pritzl B. J., Smith H. A., 2004, ApJS, 154, 633

Christy , R. F., 1966, ApJ, 144, 108

Christy , R. F., 1967, "Aerodynamic Phenomena in Stellar Atmospheres" (IAU Symposium No. 28), ed. R. N. Thomas, p. 105

Christy , R. F., 1968,Q. J. R. Astron. Soc., 9, 13

Clement, C. M., & Sheldon, L. 1999, ApJ, 515, L85

Clement, C. M., et al. 2001, AJ, 122, 2587

Clementini, G., Gratton, R., Bragaglia, A., Carretta, E., Di Fabrizio, L., Maio, M., 2003, AJ, 125,1309

Clementini, G., Gratton, R. G., Bragaglia, A., Ripepi, V., Fiorenzano, A. F. M., Held, E. V., Carretta, E. 2005, ApJ, 630, L14

Clement, C. M. & Rowe, J. 2000, AJ, 120, 2579

Corwin, T. M., Carney, B. W., & Nifong, B. C. 1999, AJ, 118, 2875

Cox, J. P. 1955, ApJ, 122, 286

Cox, J. P. 1963, ApJ, 138, 487

Cox, J. P. 1973, Rep. Prog. Phys.,37, 563

Cox, J. P. 1980, "Thoery of Stellar Pulsation" (Princeton: Princeton University Press)

Dall'Ora, M. et al., 2004, ApJ, 610, 269

Dean, J. F.; Warren, P. R.; Cousins, A. W. J., 1978, MNRAS, 183, 569

Degl'Innocenti, S. 2003, MNRAS, 344, 1097

Del Principe, M. et al., 2006, ApJ,(in press,astro-ph/0608052)

Del Principe, M., Piersimoni, A. M., Bono, G., Di Paola, A., Dolci, M., Marconi, M., 2005, AJ,.129, 2714

Della Valle, M., Kissler-Patig, M., Danziger, J., Storm, J., 1998, MNRAS, 299, 267

Deupree, R. G., 1977, ApJ, 215, 620

Deupree, R. G., 1979, ApJ, 234, 228

Demarque, P., Zinn, R., Lee, Y., Yi, S, 2000, AJ, 119,1398

Di Criscienzo M., Caputo F., Marconi M., Musella I., 2006, MNRAS, 365, 1357

Di Criscienzo, M., Marconi, M. & Caputo, F.,2004, ApJ, 612, 1092 (Paper III)

Di Criscienzo, M. 2002, Ph.D. thesis, Univ. Naples

Di Criscienzo, M., Marconi, M., & Caputo, F. 2003, Mem. Soc. Astron.Italiana, 75, 190

Di Criscienzo, M., Caputo, F., Marconi, M., Cassisi, S., 2006, A&A, submitted (D06)

Dickens, R. J., & Saunders, J. 1965, Royal Obs. Bull., 101, 101

Dinescu D.I.,

Fernley, J., Skillen, I., Carney, B. W., Cacciari, C., Janes, K., 1998, MNRAS, 293, 61 (F98)

Ferrarese, L., Ford, H., Huchra, J., et al, 2000, ApJS, 128, 431

Feuchtinger, M. U., 1999, A&A, 351, 103

Feuchtinger, M. U. & Dorfi, E. A.,1998, in “A Half Centuty of Stellar Pulastion Interpretation: A Tribute to Arthur Cox” (ASP Conference Series No. 135), ed P. A. Bradley and J. A. Guzik, p. 297

Fiorentino, G., Caputo, F.,Marconi, M., Musella, I., 2002, ApJ, 76, 402 (F02)

Fiorentino, G.,Limongi,M., Marconi, M., Caputo, F., 2006, A&A, (in press)

Fiorentino,G., Marconi,M. & Musella, I.,2006 (in preparation)

Fiorentino,G., Marconi,M., Limongi,M., Caputo,F., A&A, in press Desidera, S. Fitzpatrick, E. L., Ribas, I., Guinan, E. F., Maloney, F. P., Claret, A., 2003, ApJ, 587, 685

Freedman, W. et al., 2001, ApJ, 553, 47

Freedman, W., Madore, B., 1990, AJ, 335, L35

Fukugita M. et al., 1996, AJ, 111, 1748

Gehmeyer, M. & Winkler, K. H. A., 1992a, A&A, 253, 92

Gehmeyer, M. & Winkler, K. H. A., 1992b, A&A, 253, 101

Gibson, B.K., 2000, MmSAI, Vol. 71, p. 693

Gingold, R. A.,1985, MmSAI, 56, 169

Girardi L., Grebel E. K., Odenkirchen M., Chiosi C., 2004, A&A, 422, 205

Girardi et al., 2002, A&A, 391, 195

Gratton R.G., Carretta E., Desidera S., Lucatello S., Mazzei P., Barbieri M., 2003, A&A, 406, 131

Gratton, R., Bragaglia, A., Carretta, E., Clementini, G., Desidera, S., Grundahl, F., Lucatello, S., 2003, A&A, 408, 529

Grevesse N., Sauval A. J., 1998, Space Science Reviews, 85, 161

Gonczi, G. & Osaki, Y. 1980, A&A, 84, 304

Gouth, D. O. 1977, ApJ,214, 196

Harris, H. C., 1985, AJ, 90, 756

Harris, W., 1996, AJ, 112 (update 2003 avaible on http://physun.physics.mcmaster.ca)

Harris, W., 2001, stcl.conf., 223

Inman, R. & Carney, B., 1987, AJ, 93,1166

Ivezic Z., Vivas A.K., Lupton R.H., Zinn R., 2005, AJ, 129, 1096

Ivezic Z., et al., 2000, AJ, 120, 963

Jensen, J., Tonry, J., Barris, B., Thompson, R., Liu, M., Rieke, M., Ajhar, E., Blakeslee, J., 2003, ApJ, 583, 712

Kaluzny, J., Olech, A., Thompson, I. B., Pych, W., Krzeminski, W., & Shwarzenberg-Czerny, A. 2000, A&AS, 143, 215

Kaluzny, J., Thompson, I., Krzeminski, W., Olech, A., Pych, W., Mochejska, B. 2002, in “ASP Conf. Ser. 265, Centauri, A Unique Window into Astrophysics”, ed. F. van Leeuwen, J. D. Hughes, & G. Piotto (San Francisco: ASP), 155

Keeney B.A., Majewski S.R., Girard T.M., 2004, AJ, 128, 687

Kovacs, G., & Jurcsik, J. 1997, A&A, 322, 218

Kovacs, G., & Walker, A. R. 2001, A&A, 374, 264

Kraft, R. & Evans, I.,2003, PASP, 115, 143

Kubiak, M.& Udalski, A., 2003, AcA, 53, 117

Kucinskas A. et al. 2005, A&A, 442, 281

Kucinskas A. et al., 2006, astro-ph/0603416

Kuhfub, R., 1986, A&A, 160, 116

Kundu, A., Whitmore, B., 1998, AJ, 116, 2841

Kundu, A., Whitmore, B., 2001a, AJ, 121, 2950

Kundu, A., Whitmore, B., 2001b, AJ, 122, 1251

Kurucz R. L., 1990, Stellar Atmospheres: Beyond Classical Models, NATO Asi Ser., ed. L. Crivellari et al., 441

Laney, C. & Stobie, R. S., 1993,MNRAS,263,921L

Larsen, S., Forbes, D., Brodie, J., Huchra, J.,Forbes, D., Grillmair, C., 2001, AJ, 121, 2974 (L01)

Lastennet, E., Fernandes, J., Valls-Gabaud, D., & Oblak, E. 2003, A&A, 409, 611

Ledoux, P., Simon, R., Paturel, G., Petit,C., Rousseau, J., di nella-Courtois, H. 1999, Astron. Nachrichten, vol. 320, no. 1, p. 21

Lee, J. W., & Carney, B. W. 1999, AJ, 117, 2868

Lee, J. W., & Carney, B. W. 2002, AJ, 124, 1511

Lee, M., Kim, E., 2000, AJ, 120, 260L

Lee, M., Kim, E., Geisler, D., 1998, AJ, 115, 947L

Leeuwen, J. P. Hughes, & G. Piotto (San Francisco: ASP), 193

Lynden-Bell D., 1982, Observatory, 102, 202

Madore, B. F. 1982, ApJ, 253, 575

Madore, B. F., & Freedman, W. L. 1991, PASP, 103, 933

Madore, B. F., 1982, ApJ, 253, 575

Marconi M., et al.. 2006, MmSAI, in press

Marconi, M., Caputo, F., Di Criscienzo, M., & Castellani, M. 2003, ApJ, 596, 299 (Paper II)

Marconi, M. & Di Criscienzo, 2006, A&A,(in press, astro-ph/0701256)

Marconi, M., Fiorentino, G., & Caputo, F. 2004, A&A, 417, 1101

Marconi, M., Musella, I., & Fiorentino, G. 2005, ApJ, 632, 590

Marconi,M., Fiorentino,G. &Caputo,F.,2004, A&A, 417, 1101

Mateo M. L., 1998, ARA&A, 36, 435

Matsunaga,N. et al., 2006, MNRAS, 370, 1979

McNamara, D. H., 1995, AJ, 109, 2134

Moskalik, P. & Buchler, J. R., 1993 ApJ, 406,190

Neilsen, E., 1999, PhD thesis

Nemec, J.M., Nemec, A.F.L. & Lutz, T.E., 1994, AJ, 108

Oke J. B., Schild R. E., 1970, ApJ, 161, 1015

Olech, A., Kaluzny, J., Thompson, I. B., Pych, W., Krzeminski, W., & Shwarzenberg-Czerny, A. 1999, AJ, 118, 442

Palmieri, R., Piotto, G., Saviane, I., Girardi, I., & Castellani, V. 2002, A&A, 392, 115

Panagia, N.,1998, MmSAI, 69, 225 Desidera, S. Piersimoni, A., Bono, G., & Ripepi, V. 2002, AJ, 124, 1528

Pietrinferni, A, Cassisi, S., Salaris, M., & Castelli, F., 2006, ApJ, 642, 797

Pietrinferni, A, Cassisi, S., Salaris, M., & Castelli, F., 2004, ApJ, 612, 168

Pritzl, B., Smith, H., Stetson, P., Catelan, M., Sweigart, A., Layden, A., Rich, R., 2003, AJ, 126, 1381

Puzia, T., Kissler-Patig, M., Brodie, J., Huchra, J., 1999, AJ, 118, 2734

Recio-Blanco, A.; Piotto, G.; de Angeli, F.; Cassisi, S.; Riello, M.; Salaris, M.; Pietrinferni, A.; Zoccali, M.; Aparicio, A.2005, A&A, 432, 851R

Rey S.-C., Lee Y.-W., Joo J.-M., Walker A., Baird S., 2000, AJ, 119, 1824

Rich, R. M., et al. 1997, ApJ, 484, L25

Richtler, T., 2003, LNP, 635, 281

Riello, M., Cassisi, S., Piotto, G., Recio-Blanco, A., De Angeli, F., Salaris, M., Pietrinferni, A., Bono, G., Zoccali, M.,2003,A&A,410,553

Romaniello, M., Primas, F., Mottini, M., Groenewegen, M.,

Salaris M., Chieffi A., Straniero O., 1993, ApJ, 414, 580

Salaris, M., Riello, M., Cassisi, S., Piotto, G.,2004A&A,420,911S

Sandage A., 1993, AJ, 316, 719 (S03)

Sandage, A. & Tammann, G., 2006, ARA&A, 44. 93

Sandage, A., 1993 ,AJ, 106, 687S

Sandage, A., Diethelm, R., Tammann, G., 1994,A&A, 283, 111

Sandage, A., Tammann, G., 1995, ApJ, 415

Schlegel D. J., Finkbeiner D. P., Davis M. 1998, ApJ, 500, 525

Secker, J., 1992, AJ, 104, 1472

Secker, J., Harris, W., 1993, AJ, 105, 135

Sollima A., Pancino E., Ferraro F. R., Bellazzini M., Straniero O., Pasquini L., 2005, ApJ, 634, 332

Soszynski, I., et al. 2003, Acta Astron., 53, 93

Stellingwerf, R.F., 1974, ApJ, 192, 139

Stellingwerf, R.F., 1975, ApJ, 195, 441

Stellingwerf, R.F., 1982, ApJ, 262, 330S

Thompson I. B., Kaluzny J., Pych W., Burley G., Krzeminski W., Paczynski, B., Persson S., Preston G. W., 2001, AJ, 121, 3089

Tonry, J., Ajhar, E., Blakeslee, J., Dressler, A., 1999, A&AS, 194

Tonry, J., Dressler, A., Blakeslee, J., Ajhar, E., Fletcher, A., Luppino, G., Metzger, M., Moore, C., 2001., ApJ, 546, 681

Tuggle, R. & Iben, I., 1972, ApJ, 8, 5

Udalski, A., Soszynski, I., Szymanski, M., Kubiak, M., Pietrzynski, G., Wozniak, P., Zebrun, K.,1999, AcA, 49, 223

Unno, W., 1967, Pub. Astr. Soc. Japan, 19, 140

Van Albada T.S., Baker N., 1971, ApJ, 169, 311

Vivas A.K., Zinn R., 2006, astro-ph/0604359

Vivas A.K., et al., 2001, ApJ, 554, 33

Vivas A.K., et al., 2004, AJ, 127, 1158

Walker, A. R. 1994, AJ, 108, 555

Walker, A., 1992, ApJ, 390, 81

Wallerstein, G.,2002, PASP, 114, 689

Wallerstein, G. 1990, ASPC, 11, 56

Wallerstein, G.& Cox, A. N., 1984, PASP, 96, 677

Whitmore, B., Sparks, W., Lucas, R., Macchetto, F., Biretta, J., 1995, ApJ, 454, 73

Wu C., Qiu Y.L., Deng J.S., Hu J.Y., Zhao Y.H., 2005, AJ, 130, 1640

Zinn, R. & West, M., 1984, ApJS, 55,45

van den Bergh, S., 2003, ApJ, 590

van den Bergh, S., Mackey, A., 2004, MNRAS, 354

Zhevakin, S. A., 1953, Russian A. J., 30, 161

Zhevakin, S. A., 1954a, Russian A. J., 31, 141

Zhevakin, S. A., 1954b, Russian A. J., 31, 335